UNCLASSIFIED

AD NUMBER

AD819581

LIMITATION CHANGES

TO:

Approved for public release; distribution is unlimited.

FROM:

Distribution authorized to U.S. Gov't. agencies and their contractors; Critical Technology; JUL 1967. Other requests shall be referred to Air Force Materials Laboratory, Wright-Patterson AFB, OH 45433.

AUTHORITY

AFSC ltr dtd 2 Mar 1972

THIS PAGE IS UNCLASSIFIED

AD0819581

AFML-TR-66-335

DEVELOPMENT AND UTILIZATION OF A COMBINATION CRYOGENIC AND ELEVATED TEMPERATURE COMPLIANCE GAGE FOR DETERMINATION OF FRACTURE TOUGHNESS OF HIGH STRENGTH METALLIC MATERIALS

SIDNEY O. DAVIS

TECHNICAL REPORT AFML-TR-66-335

JULY 1967

This document is subject to special export controls and each transmittal to foreign governments or foreign nationals may be made only with prior approval of MAAM, Air Force Materials Laboratory.

20080815 264

AIR FORCE MATERIALS LABORATORY
DIRECTORATE OF LABORATORIES
AIR FORCE SYSTEMS COMMAND
WRIGHT-PATTERSON AIR FORCE BASE, OHIO



NOTICE

When Government drawings, specifications, or other data are used for any purpose other than in connection with a definitely related Government procurement operation, the United States Government thereby incurs no responsibility nor any obligation whatsoever; and the fact that the Government may have formulated, furnished, or in any way supplied the said drawings, specifications, or other data, is not to be regarded by implication or otherwise as in any manner licensing the holder or any other person or corporation, or conveying any rights or permission to manufacture, use, or sell any patented invention that may in any way be related thereto.

Copies of this report should not be returned unless return is required by security considerations, contractual obligations, or notice on a specific document.

1300 - August 1967 - CO455 - 4-69

AFML-TR-66-335

DEVELOPMENT AND UTILIZATION OF A COMBINATION CRYOGENIC AND ELEVATED TEMPERATURE COMPLIANCE GAGE FOR DETERMINATION OF FRACTURE TOUGHNESS OF HIGH STRENGTH METALLIC MATERIALS

SIDNEY O. DAVIS

AD819581

This document is subject to special export controls and each transmittal to foreign governments or foreign nationals may be made only with prior approval of MAAM, Air Force Materials Laboratory.

FOREWORD

This report was prepared by Mr. Sidney O. Davis of the Materials Information Branch, Materials Applications Division, Air Force Materials Laboratory, Research and Technology Division, Air Force Systems Command, Wright-Patterson AFB, Ohio. The work described was performed by Mr. Davis under the direction of Dr. J. W. Spretnak, Department of Metallurgical Engineering, Ohio State University. This program was conducted under Project No. 7381, "Materials Applications," Task 738106, "Design Information Development."

This report covers work accomplished from 21 June to 14 December 1965 and was submitted by Mr. Davis in fulfillment of requirements for Metallurgical Engineering Course 710 (Metallurgical Investigations) at the Ohio State University Graduate Center under the Ohio State University Graduate Study Program, Wright-Patterson AFB, Ohio. The accomplishment of this work also provides the government and private concerns with needed technical information in the application of fracture mechanics concepts. The manuscript was released by the author in October 1966 for publication as an RTD technical report.

All (or any) of the items compared in this report were commercial items that were not developed or manufactured to meet any Government specification, to withstand the tests to which they were subjected, or to operate as applied during this study. Any failure to meet the objectives of this study is no reflection on any of the commercial items discussed herein or on any manufacturer.

The author expresses his appreciation to Dr. Spretnak of the Ohio State University for his guidance and counsel during the course of the investigation. Appreciation is also expressed to Materials Information Branch, Materials Applications Division, Air Force Materials Laboratory, for supplying the materials, fabrication facilities, test samples, and laboratory test facilities.

It is also a pleasure to acknowledge the cooperation and support of Mr. Philip E. Doepker and Mr. Dale Opela of the University of Dayton who assisted with the cryogenic testing. With gratitude the author expresses his appreciation to Mr. Roger Niemi and Mr. Richard Olt of Monsanto Corporation who fabricated the author's conceptual ideas into experimental hardware.

This technical report has been reviewed and is approved.



D. A. SHINN
Chief, Materials Information Branch
Materials Applications Division
Air Force Materials Laboratory

ABSTRACT

The Fracture Mechanics approach and its limitations are discussed based upon a literature survey. A workable compliance gage enabling the measurement of plane strain K_{Ic} pop-in stress or load level and plane stress K_c failure load as a function of compliance (deflection) from -320° to 600°F in an air environment has been developed, designed, and constructed. The load-deflection readout instrumentation is compatible with commercially available X-Y recorders.

The gage was calibrated at -320°, 75°, and 350°F in an air environment. This was performed and accomplished by comparing experimentally determined results on 2024-T3 aluminum alloy with the Westergaard-Irwin theoretically derived compliance parameters that reflect compliance at the edges of a centrally cracked sheet or plate specimen. The compliance gage was used to determine the fracture toughness of 2024-T3 aluminum alloy at -320°, 75°, and 350°F.

The experimentally obtained compliance results were in agreement with the Westergaard-Irwin theoretically derived hypothesis involving a mathematical model and general theory of elasticity (Reference 2). It was also established from experimental test data and fracture mechanics analytical concepts that 2024-T3 aluminum alloy data at 75° and 350°F (short time) use can be based on the evidences of gross plastic flow before failure. However, at -320°F and below the design criteria with this alloy should be based upon the fracture toughness of the material and the severity of defects to avoid catastrophic failure under cryogenic service conditions.

TABLE OF CONTENTS

SECTION		PAGE
I	INTRODUCTION	1
II	FRACTURE MECHANICS APPROACH, BACKGROUND INFORMATION	2
III	COMPLIANCE ANALYSIS THEORY FOR WESTERGAARD-IRWIN'S CENTRALLY CRACKED SPECIMENS	12
IV	BOYLE'S COMPLIANCE EXPERIMENTAL ANALYSIS OF A CENTRALLY CRACKED SPECIMEN AT ROOM TEMPERATURE	20
V	DEVELOPMENT OF A CRYOGENIC, ELEVATED TEMPERATURE COMPLIANCE GAGE	26
VI	CRYOGENIC, ELEVATED TEMPERATURE COMPLIANCE GAGE CALIBRATION EXPERIMENTAL RESULTS AND DISCUSSION	40
VII	CRYOGENIC, ELEVATED TEMPERATURE EXPERIMENTAL FRACTURE TOUGHNESS RESULTS AND DISCUSSION	77
VIII	CONCLUSIONS	83
REFERENCES		85
APPENDIX: CURVE PLOTTED DATA		89
A.	Tensile Test Curves of Raw Data	90
B.	Calibration Load-Deflection Curves of Raw Data for Variable-Crack-Length Centrally Notched Specimens	103
C.	Load-Deflection Curves of Raw Data for Fractured Centrally Notched Specimens	110

LIST OF ILLUSTRATIONS

FIGURE		PAGE
1.	General Limits for Fracture Toughness Analysis (Reference 3)	5
2.	Fracture Transition as Determined by Net Fracture Stress and Yield Stress Data (Reference 3)	6
3.	Fracture Surface of 0.10-Inch-Thick Brittle Fracture Specimen (Reference 3)	7
4.	Correlation of σ_{net}/σ_{YS} Ratio to Percent Shear-Lip in Steel Alloys 0.060 to 0.130 Inch Thick (Reference 3)	8
5.	Correlation of σ_{net}/σ_{YS} Ratio to Percent Shear-Lip in Aluminum and Titanium Alloys 0.060 to 0.130 Inch Thick (Reference 3)	9
6.	Ratio of Experimental (Plastic) to Theoretical (Elastic + Plastic) Stress Intensity Factors as a Function of σ_{net}/σ_{YS} (Reference 3)	10
7.	Centrally Cracked Panel Configuration With Infinite and Finite Widths.	19
8.	Typical Load-Deflection Curve for Centrally Cracked Sheet Specimens Showing Pop-In (Reference 41)	21
9.	Calibration Curve Derived From Compliance Measurements on a Series of Specimens Having Various Slot Lengths (Reference 41)	21
10.	Symmetrical Centrally Cracked Tensile Specimen For Sheet and Plate (Reference 43)	22
11.	Boyle Room Temperature Compliance Gage Load-Extension System Combined With a Load-Acoustical Measurement System	24
12.	Detail View of Boyle Compliance Gage and Acoustical Pickup Crystal	25
13.	Modified Compliance Gage	31
14.	Initial Compliance Gage Performance	32
15.	Clamp-On Head Assembly	33
16.	Exploded View of Clamp-On Head Assembly	34
17.	Baldwin Model PS-5M Releasable Extensometer Mounted on the Compliance Gage	35
18.	Modified Compliance Gage Performance With a Baldwin Extensometer	36
19.	Modified Compliance Gage Performance With a Riehle Extersometer	37

LIST OF ILLUSTIONS (CONT'D)

FIGURE		PAGE
20.	Load Compliance System and X-Y Recorder for Cryogenic, Elevated Temperature Compliance Gage	38
21.	Detail View of Cryogenic, Elevated Temperature Compliance Gage	39
22.	Flat Hot-Test Specimen	41
23.	Fatigue-Cracked Centrally Notched 3-Inch-Wide Tensile Specimen	42
24.	Fractograph of Fractured Surfaces of 2024-T3 Tensile Test Specimens	51
25.	Three-Inch Wide Centrally Notched Specimens With Fracture Toughness Varying in 2a Crack Length From 0.6 to 1.4 Inches	52
26.	Cryogenic Tensile Testing Compliance Calibration and Fracture Toughness Apparatus	53
27.	Derived Load-Deflection Curves for Centrally Notched Specimens, -320°F, Longitudinal	55
28.	Derived Load-Deflection Curves for Centrally Notched Specimens, -320°F, Transverse	56
29.	Derived Load-Deflection Curves for Centrally Notched Specimens, 75°F, Longitudinal	57
30.	Derived Load-Deflection Curves for Centrally Notched Specimens, 75°F, Transverse	58
31.	Derived Load-Deflection Curves for Centrally Notched Specimens, 350°F, Longitudinal	59
32.	Derived Load-Deflection Curves for Centrally Notched Specimens, 350°F, Transverse	60
33.	Averaged Transverse and Longitudinal Load-Deflection Curves for Centrally Notched Specimens, -320°F	61
34.	Averaged Transverse and Longitudinal Load-Deflection Curves for Centrally Notched Specimens, 75°F	62
35.	Averaged Transverse and Longitudinal Load-Deflection Curves for Centrally Notched Specimens, 350°F	63
36.	Averaged Transverse and Longitudinal Load-Deflection Curves for Centrally Notched Specimens, 2a = 0	64
37.	Averaged Transverse and Longitudinal Load-Deflection Curves for Centrally Notched Specimens, 2a = 0.6	65

LIST OF ILLUSTRATION (CONT'D)

FIGURE		PAGE
38.	Averaged Transverse and Longitudinal Load-Deflection Curves for Centrally Notched Specimens, 2a = 0.8	66
39.	Averaged Transverse and Longitudinal Load-Deflection Curves for Centrally Notched Specimens, 2a = 1.0	67
40.	Averaged Transverse and Longitudinal Load-Deflection Curves for Centrally Notched Specimens, 2a = 1.4	68
41.	Theoretical and Experimental Compliance as a Function of Crack Length	70
42.	Example Theoretical and Experimental (-320°F) Compliance as a Function of Crack Length	73
43.	Example Theoretical and Experimental (75°F) Compliance as a Function of Crack Length	74
44.	Example Theoretical and Experimental (350°F) Compliance as a Function of Crack Length	75
45.	Summary of Load-Deflection Curves	78
46.	Fractographs of Fractured Surfaces of 2024-T3 Centrally Notched Fracture Toughness Specimens	79
47.	Tensile Test Data at Room Temperature, Specimen Number L-7	91
48.	Tensile Test Data at Room Temperature, Specimen Number L-8	92
49.	Tensile Test Data at Room Temperature, Specimen Number T-7	93
50.	Tensile Test Data at Room Temperature, Specimen Number T-8	94
51.	Tensile Test Data at 200°F, Specimen Number L-3	95
52.	Tensile Test Data at 200°F, Specimen Number L-4	96
53.	Tensile Test Data at 200°F, Specimen Number T-3	97
54.	Tensile Test Data at 200°F, Specimen Number T-4	98
55.	Tensile Test Data at 350°F, Specimen Number L-5	99
56.	Tensile Test Data at 350°F, Specimen Number L-6	100
57.	Tensile Test Data at 350°F, Specimen Number T-5	101
58.	Tensile Test Data at 350°F, Specimen Number T-6	102

LIST OF ILLUSTRATION (CONT'D)

FIGURE		PAGE
59.	Load-Deflection Curves for Centrally Notched Specimens -320°F (Longitudinal)	104
60.	Load-Deflection Curves for Centrally Notched Specimens -320°F (Transverse)	105
61.	Load-Deflection Curves for Centrally Notched Fracture Specimens, 75°F, (Longitudinal)	106
62.	Load-Deflection Curves for Centrally Notched Fracture Specimens, 75°F, (Transverse)	107
63.	Load-Deflection Curves for Centrally Notched Fracture Specimens, 350°F, (Longitudinal)	108
64.	Load-Deflection Curves for Centrally Notched Fracture Specimens, 350°F, (Transverse)	109
65.	Original Load-Deflection Curve to Fracture, Longitudinal Centrally Notched Specimen at -320°F	111
66.	Original Load-Deflection Curve to Fracture, Transverse Centrally Notched Specimen at -320°F	112
67.	Original Load-Deflection Curve to Fracture, Longitudinal Centrally Notched Specimen at 75°F	113
68.	Original Load-Deflection Curve to Fracture, Transverse Centrally Notched Specimen at 75°F	114
69.	Original Load-Deflection Curve to Fracture, Longitudinal Centrally Notched Specimen at 350°F	115
70.	Original Load-Deflection Curve to Fracture, Transverse Centrally Notched Specimen at 350°F	116

LIST OF TABLES

TABLE		PAGE
I	Material Information	40
II	2024-T3 Calibration Test Specimen Schedule	43
III	Detail Calibration Test Specimen Schedule	44
IV	Revised Detail Calibration Test Specimen Schedule	46
V	Tensile Test Data of 2024-T3 Al Alloy at Room Temperature (75°F)	47
VI	Tensile Test Data of 2024-T3 Al Alloy at 200°F	48
VII	Tensile Test Data of 2024-T3 Al Alloy at 350°F	49
VIII	Average Tensile Data of 2024-T3 Al Alloy at -320°, 75°, and 350°F	50
IX	Compliance Gage Experimental Data	69
X	Elastic Compliance Gage Experimental Data	71
XI	Tabulated Results From Fracture Toughness Tests of 2024-T3 Al Alloy	80
XII	Tabulated Comparative Data From Fracture Tests of 2024-T3 Al Alloy	82

SECTION I

INTRODUCTION

The performance requirements for modern airborne systems have resulted in needs for high strength metallic structural materials (Reference 1). The requirements of the minimum possible weight in solid-propellant rocket casings has led to the use of very high strength materials, for example, steels with yield strengths greater than 200,000 psi and both ferrous and nonferrous materials having a strength-to-density ratio greater than or equal to 700,000 psi/lb per cu in. At these strength levels, many structural engineering metallic materials have exhibited brittleness in the presence of small flaws, which may be present in the material or may arise during fabrication of thin or thick-walled pressure vessels or structural components. As a result, service failure often occurs by brittle cataclysmic fracture rather than by gross yielding and distortion and at stresses well below the design stresses, usually based on the engineering 0.2 percent offset yield strength of the material (Reference 2).

At present, there are generally accepted test methods but no standardized tests for evaluating the resistance of high strength engineering structural materials to brittle fracture, especially the resistance of a sheet or plate material to crack initiation or propagation. Early in 1959, at the suggestion of the United States Department of Defense, the ASTM organized an ad hoc committee (presently ASTM E-24 Committee) to review testing methods available and, ultimately, to recommend to the ASTM a standard method for evaluating high strength sheet materials with respect to their resistance to brittle fracture. Early in the discussion of this problem it became apparent that probably two types of tests would be required to handle the macrocrack initiation and propagation problem. It was highly desirable to have a method for measuring the resistance to crack propagation of a sheet material in such a way that the result of this measurement could be used quantitatively to assist in the design of pressure vessels and in the analysis of service failures. Since the indications were that such a test method would probably be somewhat complex and time-consuming, there also appeared to be a need for a simpler and more rapid screening test, capable of qualitatively ranking many materials with respect to their resistance to brittle fracture (Reference 2). The fatigue-crack sharp-notch test has served this purpose successfully. But to this date, no test has been standardized to measure quantitatively the brittle fracture resistance of high strength materials. However, the ASTM E-24 Fracture Testing Committe has made several recommendations.

In principle, there are two approaches used to prove a test method. The first approach depends on the availability of a large body of service performance data, particularly service failure data. With this information, a correlation can be attempted between test results and service performance to determine if the test method is measuring the material characteristics that govern performance.

In the absence of adequate service performance data, it may still be possible to establish a test method if a suitable method of analysis is available by which it may be shown that the test method is measuring the significant quantities governing performance and the test results may be generalized to the more complex condition existing in an actual structure. It is the view of the experts in the specialized field of "Brittle Fracture" that, at present, the second approach must be taken with respect to high-strength structural materials (Reference 2). The validity of the analytical methods of "Fracture Mechanics" is sufficiently well established to justify the analytical approach.

SECTION II

FRACTURE MECHANICS APPROACH, BACKGROUND INFORMATION

What is the role of fracture mechanics in engineering today? The fracture mechanics concept combines the metallurgist's knowledge of materials with the stress analyses applied by mechanics personnel to offer the design engineer a tool with which to build reliability into his structure. In the past two decades, with each instance of catastrophic failure of ships, jet airliners, and missile cases, the fracture mechanics field has assumed a greater importance and responsibility in the field of engineering. It is the purpose of this discussion to outline briefly some of the pertinent areas covered by fracture mechanics and discuss the current status of each.

Two specific cases are generally considered to fit all problems, one of plane stress for thin sections and one of plane strain for thick sections. For these two cases, a single fracture toughness parameter, K_c for plane stress and K_{Ic} for plane strain, may be evaluated for a particular material. For any specific design problem, an estimate or exact solution of the crack conditions that prevail may be made through elastic stress analyses. An estimate of either the flaw size (assuming an operating stress) or an operating stress (assuming a minimum flaw size) may then be made and the design can be tailor-made accordingly. This design may actually incorporate "material design," "structural design," or a combination of both; that is, for a desired structure, the material will have to be optimized and for a desired material, the structure will have to be optimized.

It is immediately evident that the field dealing with fracture toughness is becoming increasingly complex. It would be of value if some guidelines could be attached to fracture toughness parameters so that the materials researcher would know when a particular value of toughness is valid and the designer would know when a particular toughness parameter is applicable. It would also be of value to the materials specialists and to the fabricators to know where to look for materials with exceptional combinations of strength and toughness. Although this subject matter is too broad to be covered in detail, some of the more pertinent points are reviewed in this report.

PLANE STRESS

Plane stress deals with the crack conditions found in thin sections such as missile skins or thin pressure vessels. The formula generally used was derived from the Westergaard-Irwin analysis (Reference 2) for finite width sections, and is as follows:

$$K_c = \sigma_o \left[W \tan \frac{\pi a}{W} \right]^{1/2} \qquad (1)$$

which means that a crack of length 2a will propagate when the toughness, K_c, and applied stress, σ_o, are such that Equation 1 is fulfilled. Thus, the toughness of a material may be described by K_c if σ_o and $\underline{a}$ are measured accurately in a test. Fracture toughness testing has assumed a considerable role in evaluating the potential of high strength materials. To meet the need of evaluating ductile-brittle metals as well as very brittle ones, a plasticity correction (Reference 2) was added to Equation 1, giving

$$K_c = \sigma_o \left[qW \right]^{1/2} \; ; \; q = \tan \left[\frac{\pi a}{W} + \frac{K_c^2}{2W\sigma_{YS}^2} \right] \tag{2}$$

where a graphical method is used to determine q for various values of (σ_o/σ_{YS}) and $\pi a/W$. This analysis has become an accepted standard for measuring the fracture toughness of thin-gage material.

It is pertinent to both the metallurgist and the designer to know what limitations there are, if any, to Equation 2. Gerberich (Reference 3) obtained the numerical solution for Equation 2 and found that there is an upper bound beyond which the theory is not applicable. This boundary is given by

$$q = \left[\frac{2}{(\sigma_o/\sigma_{YS})^2} - 1 \right]^{1/2} \; ; \; (\sigma_o/\sigma_{YS})^2 = \text{constant} \tag{3}$$

which means that for a particular value of $(\sigma_o/\sigma_{YS})^2$, there is a maximum value of q given by Equation 3. In terms of crack length, the theoretical limit states that for a particular value of $(\sigma_o/\sigma_{YS})^2$ the crack length must be small enough such that

$$\frac{\pi a}{W} \leq \tan^{-1} q - \frac{1}{2} q (\sigma_o/\sigma_{YS})^2 \tag{4}$$

where q is defined by Equation 3. Near this upper bound, the test specimen will have undergone gross plastic deformation since the ratio of net fracture stress to yield strength, σ_{net}/σ_{YS}, is approximately 1.15. Therefore, to be more realistic, some investigators have chosen an airbitrary limit of $\sigma_{net} \leq \sigma_{YS}$ to define the usable limits of the fracture toughness equation. This limit is given by

$$\frac{a}{W} \leq \frac{1}{2} (1 - \sigma_o/\sigma_{YS}) \tag{5}$$

The upper bounds of these two limits are depicted in Figure 1. Within the hatched area, quantitative measurement of K_c can be made; but such data may not result in practical answers toward the upper limits. The obvious question is how experimental evidence agrees with these two limits.

In a fracture toughness test, the net section stress at failure is a relatively good measure of resistance to fracture. In Figure 2, the ratio σ_{net}/σ_{YS} is plotted versus σ_{YS}/E for steel, aluminum, and titanium alloys with gage sections from 0.060 to 0.130 inch thick. Two types of information may be extracted from this plot. First, there is a change in slope for each particular class of alloys at different values of σ_{YS}/E. This occurs at a σ_{net}/σ_{YS} value of about 0.75 for aluminum alloys, 0.92 for steel alloys, and 1.0 for titanium alloys. The corresponding values of σ_{YS}/E are about 6 for aluminum, 7 for steel, and 8 for titanium. These transition points suggest that for values of σ_{YS}/E greater than those indicated, the K_c value obtained is probably good quantitative information (Reference 3).

Secondly, for a value of σ_{YS}/E less than 5, 6, or 7 for the respective alloy systems, the fracture toughness value obtained is probably not quantitatively correct and provides only relative information. It should be noted that the values of σ_{YS}/E correspond to σ_{net}/σ_{YS} values of about 1.0 to 1.12 for these materials. They are toward the upper bound of the theoretical analysis (Reference 3).

Further verification of the first point is provided by studying the fracture appearance of brittle fracture coupons (Reference 3). In Figure 3 the fracture surface of a 3-inch-wide specimen is shown. An Elox notch which was subsequently fatigue-cracked is shown as the first two areas. At a critical stress, a plane strain "pop-in" occurred which resulted in the flat transverse triangle shown in the next area. Further cracking was in a plane stress mode as indicated by the shear failure. For more brittle specimens, the flat transverse fracture will extend all the way to the end of the specimen. Thus, the fracture appearance may range from 0 to 100 percent shear. A considerable amount of fracture appearance data were plotted in Figures 4 and 5 versus the ratio σ_{net}/σ_{YS} (Reference 3). As the ratio of σ_{net}/σ_{YS} approaches 1, a 100 percent shear failure is approached. And, the transition point from partial shear to complete shear failures occurs at σ_{net}/σ_{YS} ratios of 0.79, 0.90, and 1.0, which are very similar to the ratios obtained in Figure 2. This suggests that for values of σ_{net}/σ_{YS} less than approximately 0.75 for aluminum, 0.90 for steel, and 1.0 for titanium, the fracture toughness approach is very useful (Reference 3).

What about measuring fracture toughness when σ_{net}/σ_{YS} is greater than these values? As the plastic zone size at the tip of the crack starts to become significantly large, the plastic energy dissipation becomes large compared to the value estimated by Irwin's extension of the elastic analysis. Direct experimental evidence of this was obtained by Swedlow and Gerberich (Reference 14) using an experimental stress analysis technique. Analyzing the plastic strains at the tips of the cracks they found the plastic energy release rate from

$$G_p = \frac{1}{t} \frac{\delta U_p}{\delta a} \tag{6}$$

where t is the plate thickness, U_p is the plastic strain energy, and a is the half crack length. This converted to an Irwin type of stress intensity factor by

$$K_p = \left[E G_p \right]^{1/2} \tag{7}$$

The ratio of K_p/K_c thus indicates when the plastic energy release rate becomes large compared to the Griffith-Irwin energy release rate. As shown in Figure 6 (Reference 3), the plastic energy release rate becomes excessively large for these materials at a value of σ_{net}/σ_{YS} somewhere between 0.8 and 1.0. Thus, it is fairly indicative that the fracture toughness value, K_c, is not quantitatively valid at values of σ_{net}/σ_{YS} greater than 1.0 for aluminum and steel alloys. Although indications are that the value of σ_{net}/σ_{YS} may be somewhat higher for titanium alloys, benefits may still be derived from the present fracture mechanics approach.

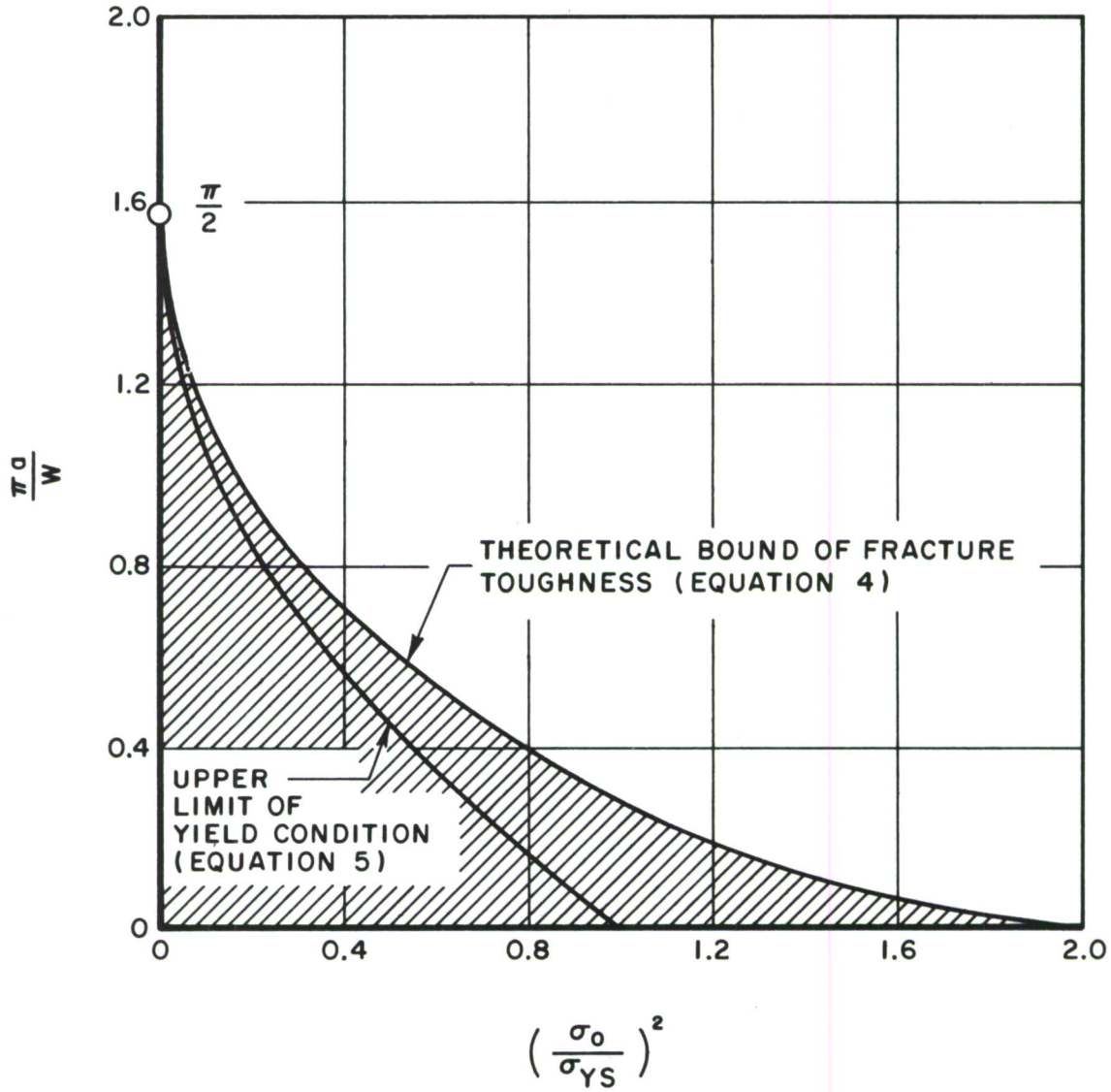


Figure 1. General Limits for Fracture Toughness Analysis (Reference 3)

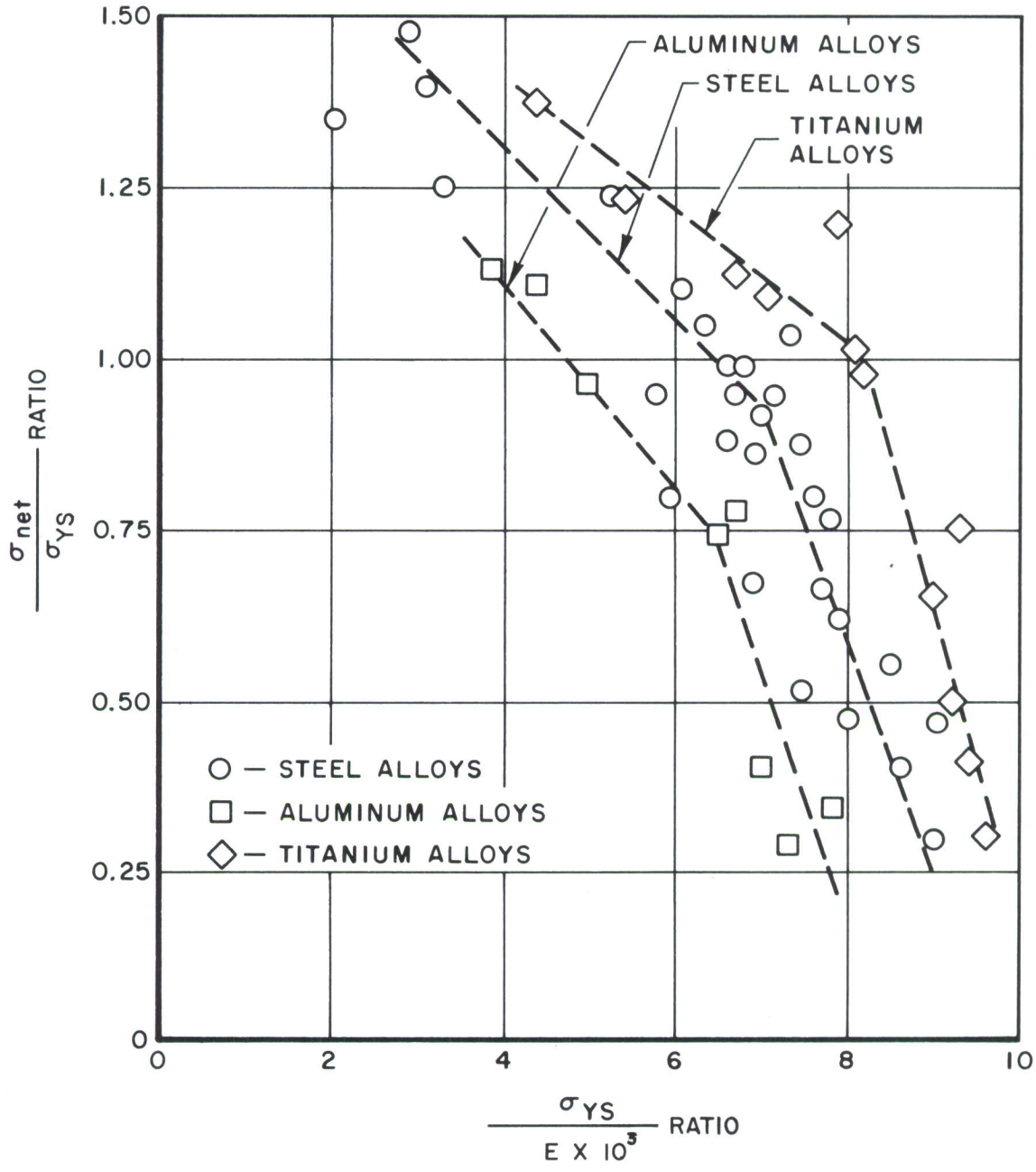


Figure 2. Fracture Transition as Determined by Net Fracture Stress and Yield Stress Data (Reference 3)

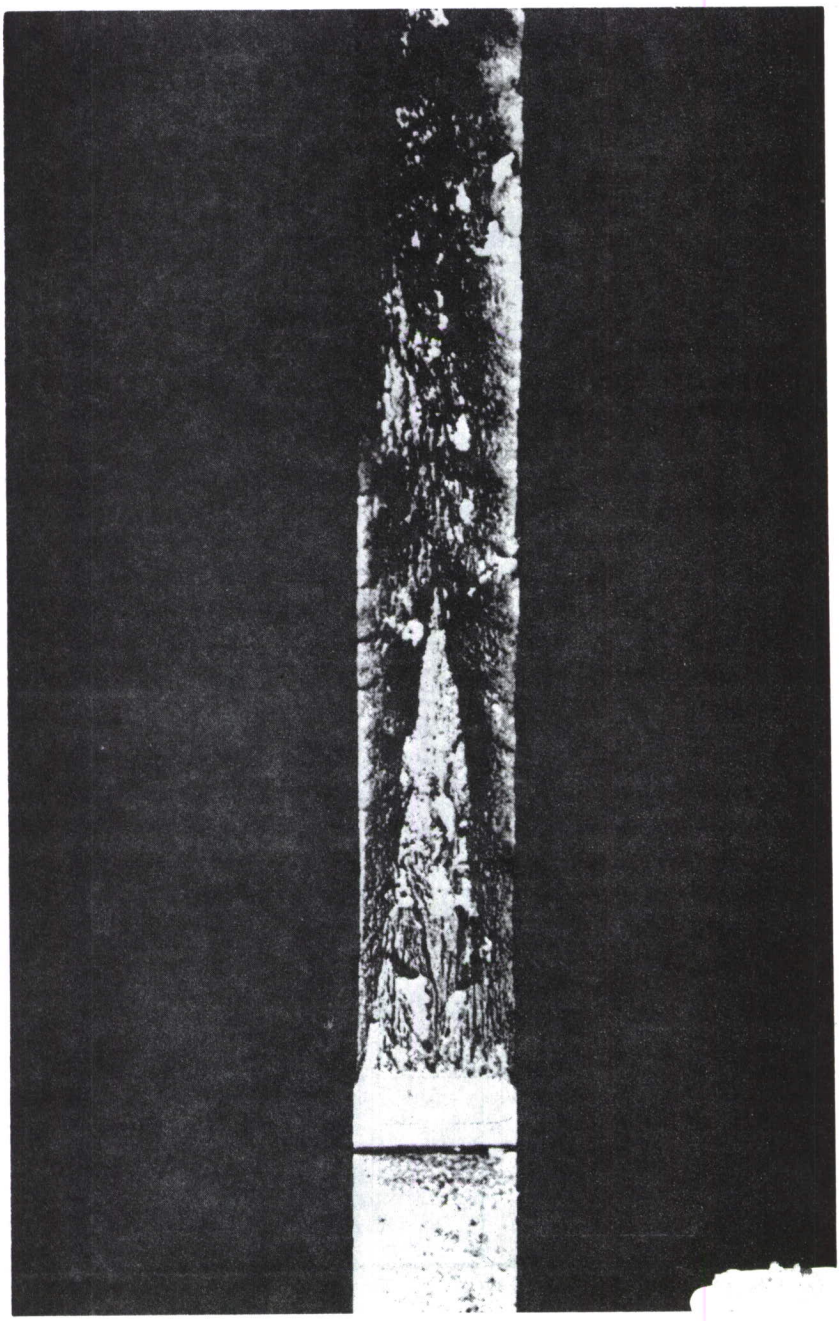


Figure 3. Fracture Surface of 0.10-Inch-Thick Brittle Fracture Specimen (Reference 3)

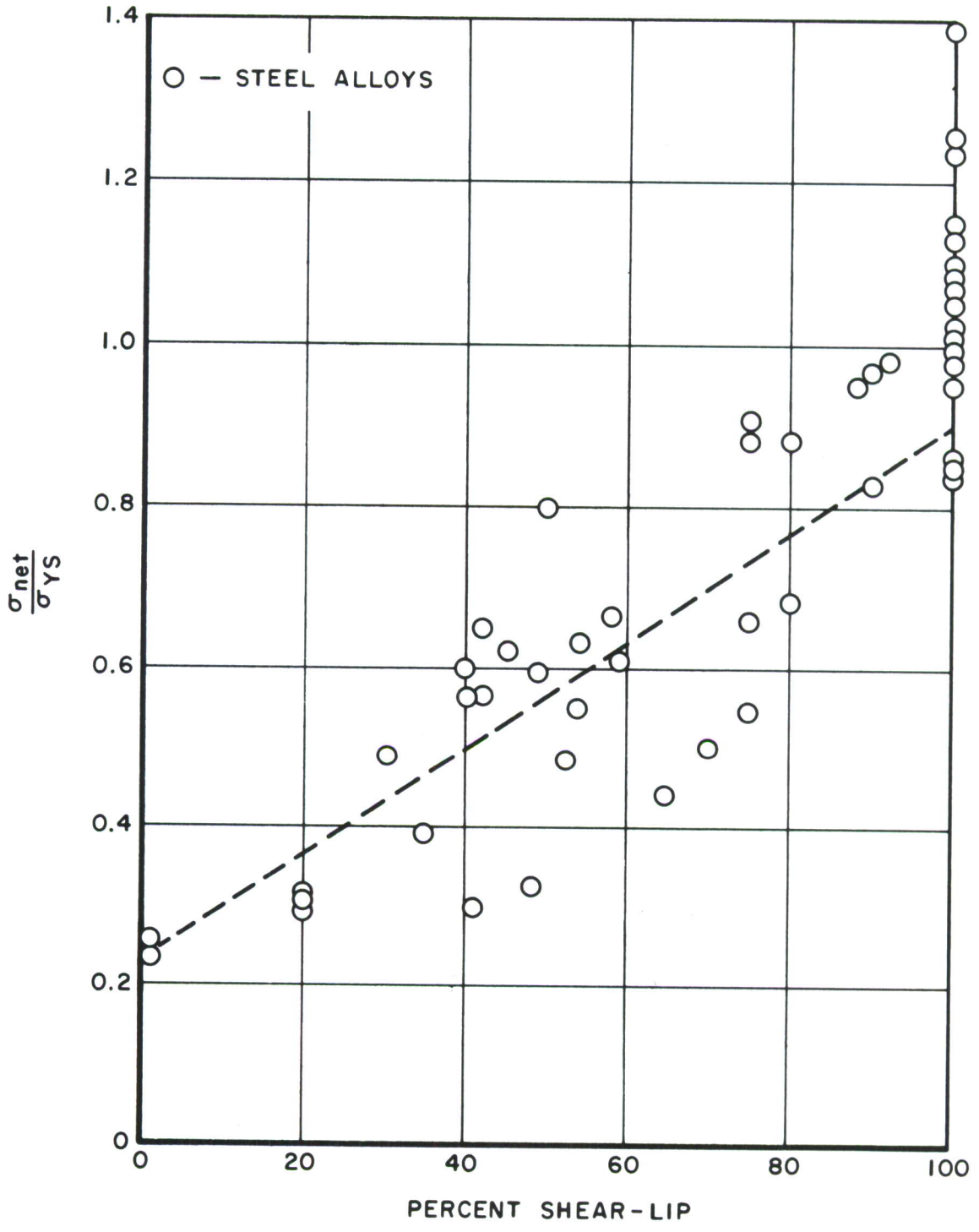


Figure 4. Correlation of σ_{net}/σ_{YS} Ratio to Percent Shear-Lip in Steel Alloys 0.060 to 0.130 Inch Thick (Reference 3)

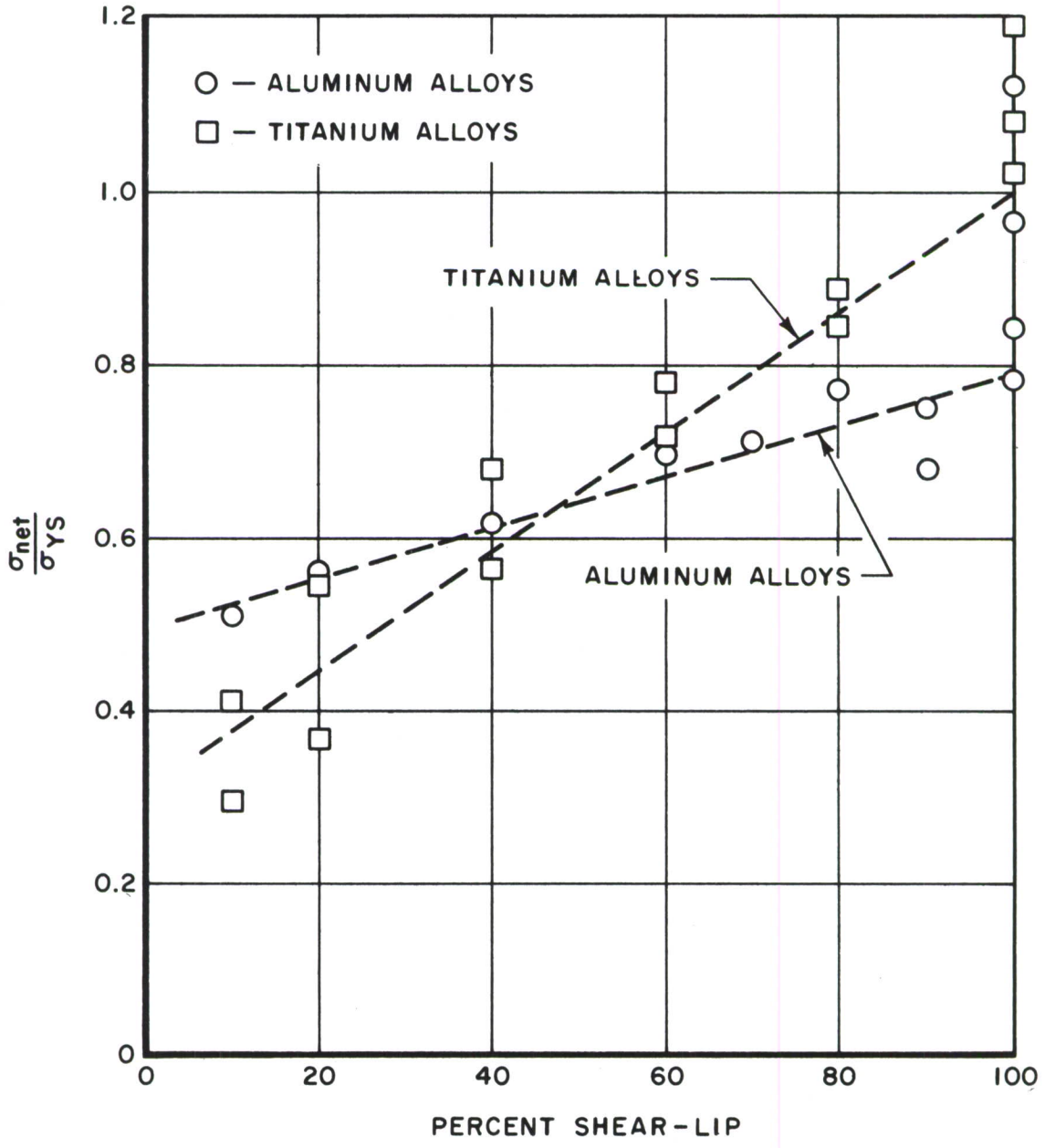


Figure 5. Correlation σ_{net}/σ_{YS} Ratio to Percent Shear-Lip in Aluminum and Titanium Alloys 0.060 to 0.130 Inch Thick (Reference 3)

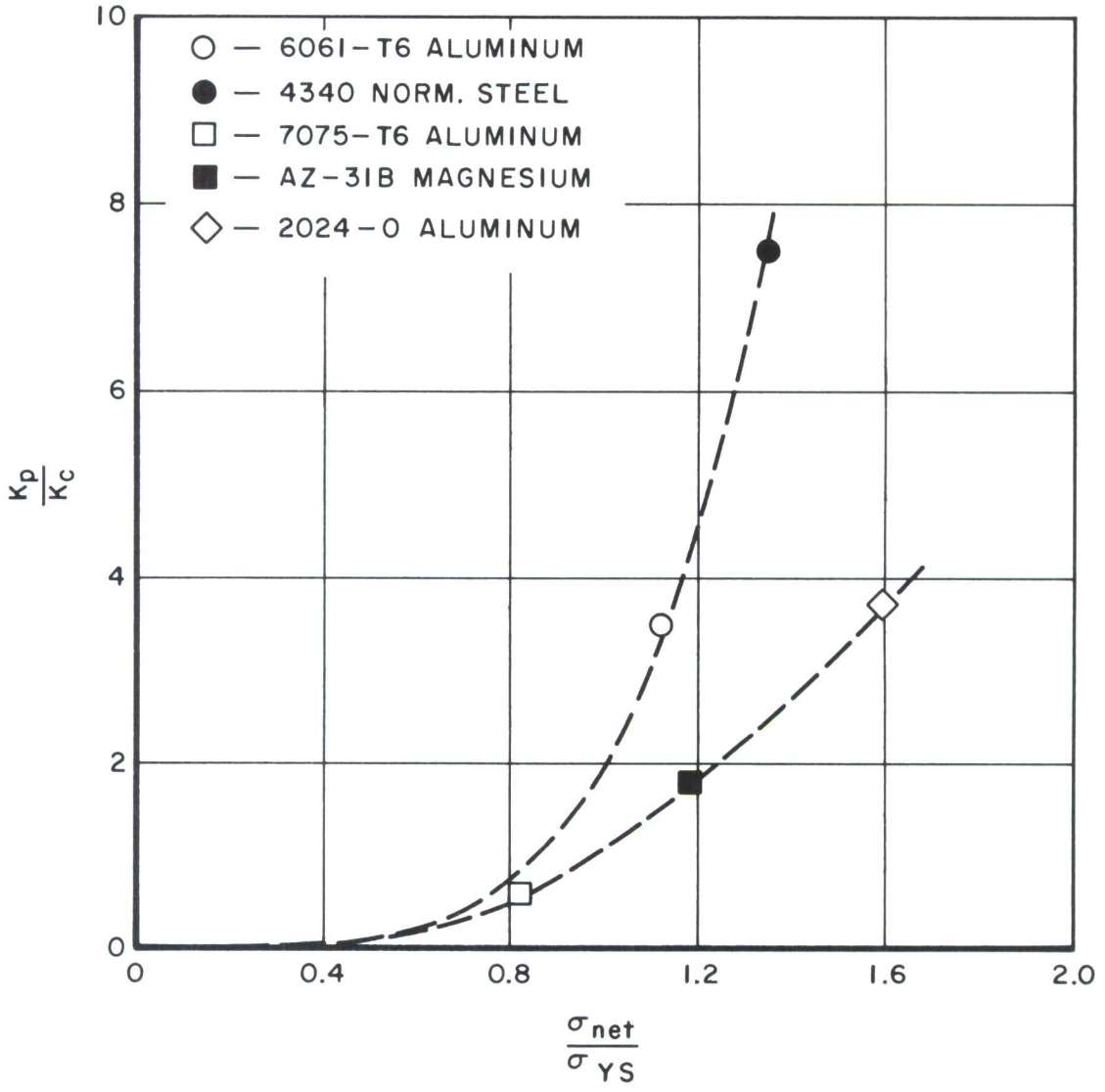


Figure 6. Ratio of Experimental (Plastic) to Theoretical (Elastic + Plastic) Stress Intensity Factors as a Function of σ_{net}/σ_{YS} (Reference 3)

How should we rate more ductile materials as to notch sensitivity? For room temperature testing of thin sections, a specimen with a 1-inch-wide-edge machine notch is probably sufficient for rating the material (Reference 3). If the σ_{net}/σ_{YS} ratio falls below 1, a more sensitive test should be used. Kaufman and Johnson (Reference 15) found, that for rating aluminum alloys, practically any notch configuration could be used if the stress concentration factors are in the range of 3 to 16. The reason for this, of course, is that most of the materials were relatively notch insensitive and the critical root radius for getting a true value of toughness was relatively large (Reference 3). If it is suspected that a material may be notch sensitive or if evaluation is to be made at lower temperatures or on thicker sections, it is desirable to have the sharpest notch possible, a fatigue crack. This is because with lower temperature or increased section sizes a fracture transition from plane stress to plane strain occurs (Reference 3).

PLANE STRAIN

Plane strain deals with crack propagation in thick sections, but one may ask: "How thick is thick?" For some brittle materials, a 0.100-inch-thick specimen is thick enough but for some ductile materials the specimen may well have to be 2.0 inches thick (Reference 3). Boyle et al. (Reference 16), in studying pop-in values for plane strain fracture toughness in sheets of various thicknesses, indicated that the criterion is

$$t \geq 2r_p = \frac{K_c^2}{\pi \sigma_{YS}^2} \tag{8}$$

which means that the thickness should be at least twice as large as the plastic zone size estimated from a K_c test. Measurements of K_c equal to 300 ksi $\sqrt{in.}$ have been made on thin-sheet low-alloy steel that has yield strengths of 200 ksi (Reference 3). According to this parameter a representative material for testing plane strain toughness should be at least 3/4 of an inch thick. For some lower strength materials, the value of K_c is so large as to be indeterminable; thus even larger sections may be required for tests of plane strain fracture toughness.

The need for plane strain fracture toughness is particularly critical now since large motor case boosters require thicknesses larger than 1 inch and just any plane stress criterion is not valid. No standard has been accepted for the K_{Ic} test although there has been considerable interest in four types of tests: the notch round bar tensile test, the partial crack-through-thickness tensile test, the single-edge notch test, and the slow notch bend test. In general, the plane strain fracture toughness may be described by

$$K_{Ic} = \gamma \sigma_{net} \sqrt{D} \tag{9}$$

where σ_{net} is the net section stress at crack initiation, D is the diameter of a notch bar, the depth of a notch bend specimen or the width of a notched plate, and γ is a geometrical parameter that depends upon the notch and specimen configuration, ranging from about 0.35 to 0.70 for 50 percent notch depths (Reference 3).

SECTION III

COMPLIANCE ANALYSIS THEORY FOR WESTERGAARD-IRWIN'S CENTRALLY CRACKED SPECIMENS

WESTERGAARD'S APPROACH (REFERENCE 34)

Westergaard's analysis technique for the general solution of problems of cracks in elastic sheets is based on a semi-inverse stress function method which involves the following mathematical model and general theory of elasticity. The problem considered is an infinite panel loaded in the x-y plane Figure 7A. An Airy stress function, ϕ, must satisfy the equilibrium and compatibility equations in solving for the normal and shear stresses acting on a differential element (dx by dy) of material in the elastic stress field near the crack tip (Reference 38).

For equilibrium and a state of plane stress, $\sigma_z = 0$, the following is applicable:

$$\frac{\delta \sigma_x}{\delta x} + \frac{\delta \tau_{xy}}{\delta y} = 0$$

$$\frac{\delta \sigma_y}{\delta y} + \frac{\delta \tau_{yx}}{\delta x} = 0 \qquad (10)$$

$$\tau_{xy} = \tau_{yx}$$

and the compatibility equation is:

$$\nabla^2 (\sigma_x + \sigma_y) = 0$$

where

$$\nabla^2 = \frac{\delta^2}{\delta x^2} + \frac{\delta^2}{\delta y^2} \qquad (11)$$

In addition, the normal and shear stresses are given in terms of ϕ as:

$$\sigma_x = \frac{\delta^2 \phi}{\delta y^2} \; ; \quad \sigma_y = \frac{\delta^2 \phi}{\delta x^2} \; ; \quad \tau_{xy} = -\frac{\delta^2 \phi}{\delta x \, \delta y} \qquad (12)$$

Combining Equations 10, 11, ad 12 results in the biharmonic equation:

$$\nabla^4 \phi = 0 \; ; \quad \text{where } \nabla^4 = \frac{\delta^4}{\delta x^4} + 2 \frac{\delta^4}{\delta x^2 \, \delta y^2} + \frac{\delta^4}{\delta y^4} \qquad (13)$$

By defining ϕ as:

$$\phi = \text{Re } \bar{\bar{Z}} + y \; \text{Im } \bar{Z} \qquad (14)$$

where $\overline{\overline{Z}}$ is an analytic function of the complex variable ζ,

$$\zeta = x + iy$$

and

$$\overline{Z} = \frac{d\overline{\overline{Z}}}{d\zeta} \; ; \qquad Z = \frac{d\overline{Z}}{d\zeta} \; ; \qquad Z' = \frac{dZ}{d\zeta} \tag{15}$$

results in $\nabla^4 \phi = 0$. Equations 10 then reduce to:

$$\begin{aligned} \sigma_x &= \mathrm{Re}\, Z - y\, \mathrm{Im}\, Z' \\ \sigma_y &= \mathrm{Re}\, Z + y\, \mathrm{Im}\, Z' \\ \tau_{xy} &= -y\, \mathrm{Re}\, Z' \end{aligned} \tag{16}$$

The stress function, $Z(\zeta)$, which solves the infinite panel problem of Figure 7A is

$$Z(\zeta) = \sigma \left[1 - \left(\frac{a}{\zeta} \right) \right]^{-\frac{1}{2}} \tag{17}$$

where σ is a uniformly applied tension stress. Now, along the line of expected crack extension (i.e., along the x axis, where $\theta = 0$, $y = 0$), the normal stress in the y-direction is:

$$\sigma_y = \mathrm{Re}\, Z = \sigma \left[1 - \left(\frac{a}{x} \right)^2 \right]^{-\frac{1}{2}} \tag{18}$$

In addition (Reference 34), σ_y can be expressed as

$$\sigma_y = \frac{K}{\sqrt{2\pi r}} \tag{19}$$

Therefore, combining Equations 18 and 19 results in

$$K = \sigma \left[\frac{2\pi r\, x^2}{x^2 - a^2} \right]^{\frac{1}{2}} \tag{20}$$

where $x = a + r$. Since the stress intensity factor describes the stress field near the crack tip, the following limiting process is taken:

$$K = \lim_{r \to 0} \sigma \left[\frac{2\pi (a + r)^2}{2a + r} \right]^{\frac{1}{2}} = \sigma \sqrt{\pi a} \tag{21}$$

Equation 21 is an infinite panel solution for the crack-tip stress intensity factor K. However, it is of practical interest to determine the stress intensity factor for a centrally cracked panel of finite width. The approach is to consider a collinear array of cracks of length 2a subjected to uniform tension, σ, and spaced at equidistant W as shown in Figure 7B. The appropriate Westergaard stress function that solves the given problem is (References 34 and 38):

$$Z(\zeta) = \frac{\sigma \sin \frac{\pi \zeta}{W}}{\left[\left(\sin \frac{\pi \zeta}{W}\right)^2 - \left(\sin \frac{\pi a}{W}\right)^2\right]^{1/2}} \tag{22}$$

Therefore, along the x-axis:

$$\sigma_y = \mathrm{Re}\, Z = \frac{\sigma \sin \frac{\pi x}{X}}{\left[\left(\sin \frac{\pi x^2}{W}\right) - \left(\sin \frac{\pi a}{W}\right)^2\right]^{1/2}} \tag{23}$$

where x = a + r. The resulting stress intensity factor is:

$$K = \lim_{r \to 0} \sin \frac{\pi (a+r)}{W} \left[\frac{2 \pi r}{\left(\sin \frac{\pi (a+r)}{W}\right)^2 - \left(\sin \frac{\pi a}{W}\right)^2}\right]^{1/2} \tag{24}$$

or

$$K = \sigma \sqrt{\pi a} \left[\frac{W}{\pi a} \tan \frac{\pi a}{W}\right]^{1/2} \tag{25}$$

Therefore, Equation 25 is the stress intensity factor for a finite centrally cracked panel loaded in uniform tension. In comparing Equations 21 and 25, the term $\left[\frac{W}{\pi a} \mathrm{TAN} \frac{\pi a}{W}\right]^{1/2}$ is a stress field correction factor for the finite geometry.

The previous stress analysis of the crack-tip stress field and stress intensity factor for the centrally cracked fracture specimen configuration is based on mathematical elastic theory techniques. Therefore, certain corrections and limitations will be placed on the solution for the stress intensity factor due to localized plastic deformation at the crack tip.

Of primary interest is the size of the plastic enclave or zone at the tip of the crack. This is readily determined by applying a yield criterion and incorporating the stress field equations given previously (Reference 34). The yield criterion which gives results in good agreement with test results is the Henky-von Mises distortional energy criterion (Reference 35). For the state of plane stress or biaxial stress condition, the yielding theory can be expressed as:

$$\sigma_x^2 - \sigma_x \sigma_y + \sigma_y^2 + 3\tau_{xy}^2 = \sigma_{YS}^2 \tag{26}$$

where σ_{YS} is the yield stress as determined from an axial test. Substitution of Equations 5 of Reference 34 into the above Equation 26 results in the following expression, which defines the extent of the plastic zone in terms of polar coordinates r and θ.

$$r = \frac{K^2}{2\pi\sigma_{YS}^2} \cos^2 \frac{\theta}{2} \left[1 + 3 \sin^2 \frac{\theta}{2}\right] \tag{27}$$

Along the line of crack extension, i.e., $\theta = 0$ degrees, the width of the plastic zone,

$$W = r = \frac{K^2}{2\pi\sigma_{YS}^2} \tag{28}$$

The width of the plastic zone is considered as an added effective crack length. Therefore, Equation 25 , when corrected for this additional crack length, becomes:

$$K = \sigma \left[W \tan\left(\frac{\pi a}{W} + \frac{K^2}{2W\sigma_{YS}^2}\right)\right]^{1/2} \tag{29}$$

Based on observations of experimental data, the ASTM Committee on Fracture Testing of High-Strength Materials (Reference 36) recommends that centrally cracked panels be so designed that $\sigma_n = 0.8\,\sigma_{YS}$, where σ_n is the net section failure stress.

THE WESTERGAARD-IRWIN COMPLIANCE EQUATION (REFERENCE 37)

Westergaard (Reference 38) has provided a convenient two-dimensional stress analysis in rectangular coordinates of a very large flat plate with tension applied in the y direction and a system of cracks along the x axis each of length 2a and the center at x = o, ±L, ±2L . . .as shown previously in Figure 7B.

The pertinent values are given in terms of an analytic function, of the complex variable z = x + iy, in Equation 22 and as follows:

$$Z = \frac{\sigma}{\sqrt{1 - \left(\dfrac{\sin\left(\frac{\pi a}{L}\right)}{\sin\left(\frac{\pi z}{L}\right)}\right)^2}} \tag{30}$$

In Westergaard's notation:

$$Z = \frac{d\overline{Z}}{dZ}$$

$$Z' = \frac{dZ}{dz}$$

and

$$Z = Z(z) = \text{Re } Z + i \text{ Im } Z$$

According to this method the stresses are assumed to be functions of x and y only and are expressed as:

$$\sigma_y = \text{Re } Z + y \text{ Im } Z'$$

$$\sigma_x = \text{Re } Z - y \text{ Im } Z'$$

$$\tau_{xy} = -y \text{ Re } Z'$$

and the displacement, v, in the y direction for a plane strain situation

$$Ev = 2(1 - \nu^2) \text{ Im } \bar{Z} - (1 + \nu) y \text{ Re } Z \qquad (31)$$

where ν is Poisson's ratio and E is the modulus of elasticity.

Irwin has shown (Reference 39) that the above stress analysis is a good approximation to the stress situation in a centrally cracked sheet specimen (with vertical and horizontal axes of symmetry of the specimen as y and x axes). The specimen, with width W = L is considered to be one unit of the crack system (i.e., the plate with the system of cracks is regarded as being made up of a large number of centrally cracked specimens placed edge to edge). Thus the specimen edges are at $x = \pm L/2$ and the crack extends from x = -a to x = +a; see Figure 7A.

Boundary conditions require the stresses σ_y and τ_{xy} to be zero along the borders of the crack and the stresses σ_x and τ_{xy} to be zero along the side boundaries. All of these conditions are fulfilled except the condition when $\sigma_x = 0$ along the side boundary. Irwin has remedied the situation by rewriting σ_x as

$$\sigma_x = \text{Re } Z - y \text{ Im } Z' - \sigma_{ox}^*$$

where σ_{ox} is a constant stress adjusted so that

$$\int_0^\infty \sigma_x \, dy = 0 \qquad \text{at } x = \pm \frac{L}{2}$$

* Westergaard stated that an arbitrary constant stress could be applied in the x direction without disturbing the validity of the solution.

The introduction of the constant σ_{ox} does not make σ_x zero everywhere along the side boundaries, but it does reduce σ_x to a small value. It is assumed that this deviation from an exact solution is smaller than the relatively small errors introduced in practical application by the departure from linear elasticity theory at finite strains.

Irwin modified the equation giving displacement in the y direction to make it applicable to a generalized plane stress situation. The Westergaard-Irwin equation is

$$Ev = 2 \operatorname{Im} \bar{Z} - (1 + \nu) y \operatorname{Re} Z \tag{32}$$

The Westergaard-Irwin equation shows an expression for compliance at the specimen edges. The conditions at the edge of the specimen are $x = \pm L/2$ so that $z = \pm L/2 + iy$ where y will be 1/2 of the specimen gage length.

The integration

$$\bar{Z} = \int Z \, dz$$

gives

$$\bar{Z} = -\frac{L\sigma}{\pi} \sin^{-1} \left[\frac{\cos \frac{\pi z}{L}}{\cos \frac{\pi a}{L}} \right] + C$$

where C is a complex constant of integration to be evaluated later using the known conditions at a = o.

Making use of the identities:

$$\cos \left[\frac{\pi}{L} \left(\frac{L}{2} + iy \right) \right] = -i \sinh \frac{\pi y}{L}$$

$$\sin \left[\frac{\pi}{L} \left(\frac{L}{2} + iy \right) \right] = \cosh \frac{\pi y}{L}$$

and

$$-\sin^{-1} (-im) = i \sinh^{-1} (m)$$

then

$$\bar{Z} = \frac{iL\sigma}{\pi} \sinh^{-1} \left[\frac{\sinh \frac{\pi y}{L}}{\cos \frac{\pi a}{L}} \right] + \operatorname{Re} C + i \operatorname{Im} C$$

so that

$$\text{Im } \bar{Z} = \frac{iL\sigma}{\pi} \sinh^{-1} \left[\frac{\sinh \frac{\pi y}{L}}{\cos \frac{\pi a}{L}} \right] + \text{Im } C$$

also $x = \pm L/2$

$$Z = \frac{\sigma}{\sqrt{1 - \left(\frac{\sin \left(\frac{\pi a}{L} \right)}{\cosh \left(\frac{\pi a}{L} \right)} \right)^2}}$$

is real so that

$$\text{Re } Z = Z \qquad \text{at } x = \pm \frac{L}{2}$$

The expression for displacement v is found by substitution into Equation 32. Following Boyle (Reference 40) the compliance can be expressed in the dimensionless form $Ev/\sigma W$ by multiplying the expression by the modulus of elasticity and dividing by the specimen width w.

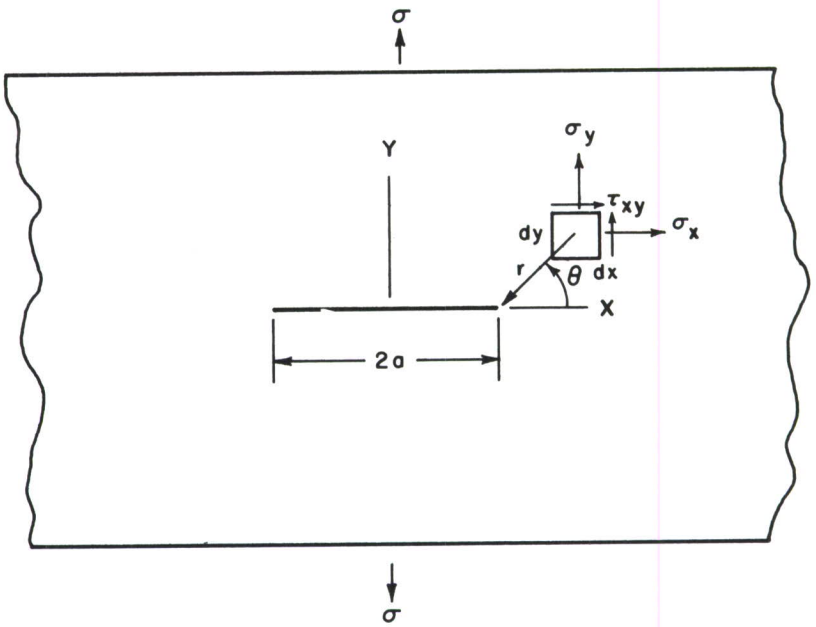
Observing that L = W,

$$\frac{Ev}{\sigma W} = \frac{2}{\pi} \sinh^{-1} \left(\frac{\sinh \frac{\pi y}{W}}{\cos \frac{\pi a}{W}} \right) + \frac{2 \text{ Im } C}{\sigma W} - \frac{y}{W} \frac{(1+\nu)}{\sqrt{1 - \frac{\sin^2 \frac{\pi a}{W}}{\cosh^2 \frac{\pi y}{W}}}} \qquad (33)$$

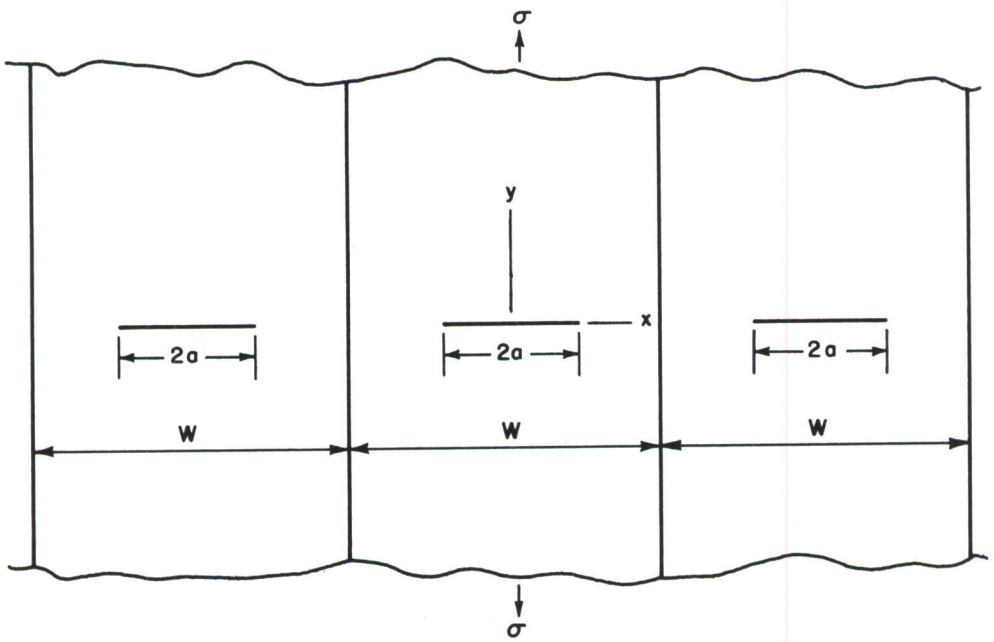
Im C is evaluated by noting that at a = o the specimen corresponds to an unnotched specimen and $Ev/\sigma W$ is equal to y/W:

$$\frac{Ev}{\sigma W} = \frac{2}{\pi} \sinh^{-1} \left(\frac{\sinh \frac{\pi y}{W}}{\cos \frac{\pi a}{W}} \right) - \frac{y}{W} \frac{(1+\nu)}{\sqrt{1 - \frac{\sin^2 \frac{\pi a}{W}}{\cosh^2 \frac{\pi y}{W}}}} + \frac{\nu y}{W} \qquad (34)$$

Where $\frac{Ev}{\sigma W}$ is the mechanical compliance of a centrally cracked finite width specimen.



(A) INFINITE PANEL SUBJECTED TO UNIFORM TENSION



(B) COLLINEAR ARRAY OF CRACKS SUBJECTED TO UNIFORM TENSION

Figure 7. Centrally Cracked Panel Configuration With Infinite and Finite Widths.

SECTION IV

BOYLE'S COMPLIANCE EXPERIMENTAL ANALYSIS OF A CENTRALLY CRACKED SPECIMEN AT ROOM TEMPERATURE

Boyle (Reference 40) has described a method of measuring the mechanical compliance, which is the extension-load ratio of a centrally notched or cracked sheet specimen, and has demonstrated how this measurement of compliance can be used to give a reliable estimate of notch depth or of notch depth plus cracks extending from the notch roots. The method is based on the fact that the compliance of a centrally cracked sheet is a function of the length of the crack (more accurately a function of the projection of the length of the crack on the transverse axis). As a crack extends, the compliance increases (stress now being taken as the gross stress calculated from the dimensions of the uncracked specimen) finally increasing without bounds as the crack reaches the edges of the specimen. As tension is applied to a centrally cracked sheet specimen, the extension of the specimen increases approximately linearly with applied gross stress until a stress level is reached at which crack extension occurs. As the crack extends, the slope of the load-extension curve decreases (load as ordinate) because of the increased compliance of the specimen. When the stress reaches an appropriate level, the specimen fails (the crack propagates rapidly across the remaining specimen width). The validity of the calculation of critical crack length depends on an assumption that the compliance value calculated from the slope of a line drawn from the origin of the load-extension curve to the point of discontinuity as shown in Figure 8 is the same as the compliance value of a specimen that contains an original crack the same length as the critical crack. Boyle proved this assumption valid (Figure 9).

In using the method described by Boyle (Reference 41), data from the compliance curve are used to calculate a numerical value for the dimensionless compliance factor:

$$\frac{Ev}{\sigma W}$$

E = the elastic modulus of the material.

v = the total displacement between the attachment points of the compliance gage (which are 2 inches apart) divided by 2.

σ = the gross stress.

W = the width of the specimen.

The numerical value for the compliance factor is selected on the ordinate of the calibration curve shown in Figure 9. This calibration curve was constructed by making load-deflection curves on a series of 3 by 12 inch slotted specimens of 7075-T6 aluminum alloy which were loaded only in the elastic range. The dimensional units used for the calibration curve permit the same curve to be used for other materials and any centrally cracked specimens in which the deformation is measured over a length equal to 2W/3 where W is equal to the specimen width. The corresponding value for $\frac{\pi a}{W}$ can be obtained directly from the calibration curve, and this can be used in the equation for plane-stress tests in Figure 10 to determine G_c and/or K_c.

PLANE STRESS TESTS

When sheet material is involved, fracturing at flaws is usually by mixed mode or by plane-stress mechanisms. In other words, there is considerable shear-lip development associated

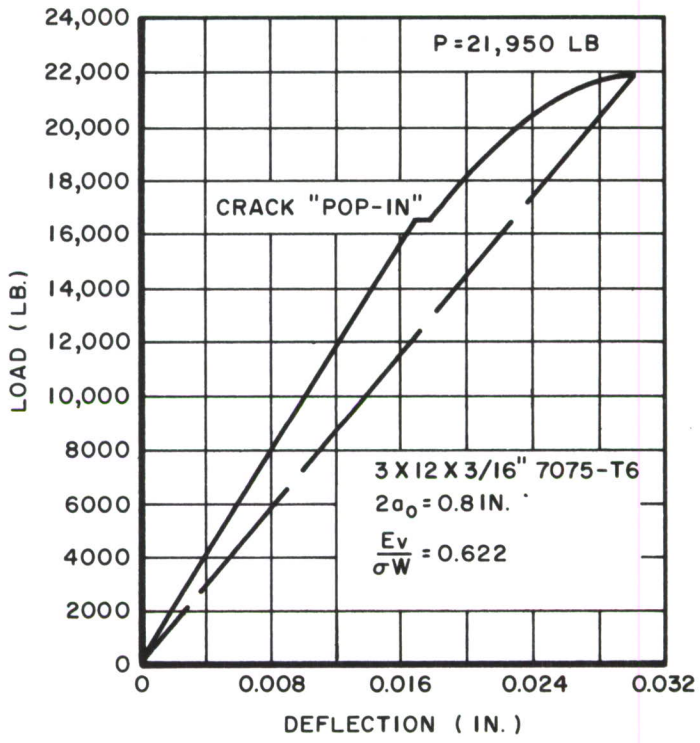


Figure 8. Typical Load-Deflection Curve for Centrally Cracked Sheet Specimens Showing Pop-In (Reference 41)

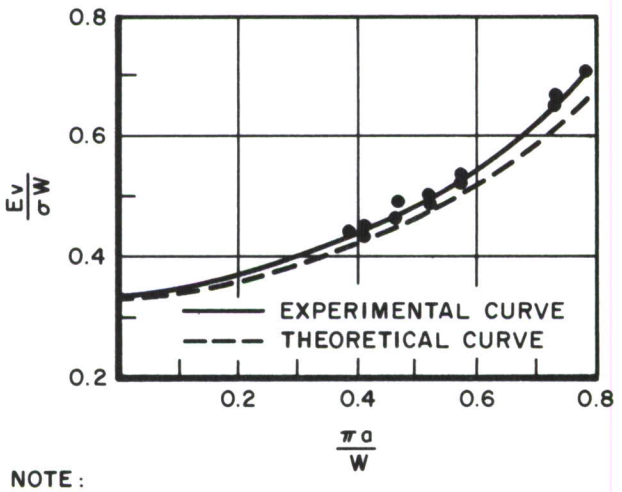
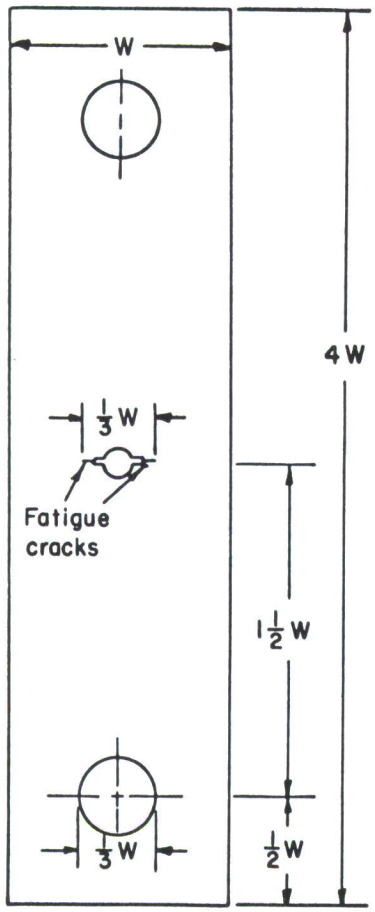
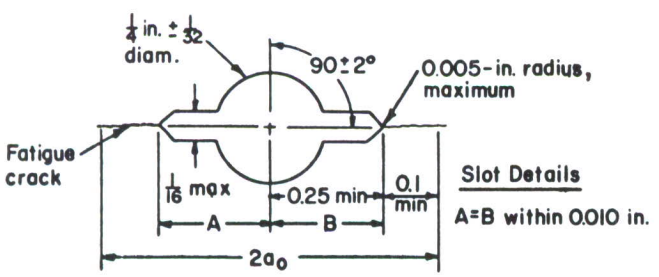


Figure 9. Calibration Curve Derived From Compliance Measurements on a Series of Specimens Having Various Slot Length (Reference 41)





For plane-strain tests:

Initial crack length = $\frac{1}{3}W = 2a_o$

$\frac{\text{Width}}{\text{Thickness}} \geqslant 8$

$EG_{Ic} = K_{Ic}^2 (1 - \nu^2) = \sigma^2 W \tan \frac{\pi a}{W}$

ν = Poisson's ratio

σ = Gross stress at pop-in = $\frac{\text{Load in pounds}}{W \times \text{Thickness}}$

E = Elastic modulus

$a = \frac{1}{2}$ crack length at pop-in (usually $a_o + \frac{EG_{Ic}}{6\pi\sigma_{YS}^2}$)

a_o may be measured on the fracture.

σ_{YS} = Yield strength of the material at 0.2 percent offset

$\frac{EG_{Ic}}{6\pi\sigma_{YS}^2}$ is often neglected if it is very small compared to a_o.

For plane-stress tests:

Initial crack length = $\frac{1}{3}W = 2a_o$

For $\frac{\text{Width}}{\text{Thickness}}$ greater than 16 and less than 45.

$EG_c = K_c^2 = \sigma^2 W \tan \frac{\pi a}{W}$

σ = Gross stress at maximum load = $\frac{\text{Maximum load in pounds}}{W \times \text{Thickness}}$

$a = \frac{1}{2}$ total crack length at maximum load + $\frac{K_c^2}{2\pi\sigma_{YS}^2}$

Note: In one common specimen design for sheet and plate to 3/8-inch thickness, the width is 3 inches and the length is 12 inches.

Figure 10. Symmetrical Centrally Cracked Tensile Specimen For Sheet and Plate (Reference 43)

with the propagation of the fractures. In testing of precracked sheet specimens, the critical plane-stress condition occurs at the "onset of rapid crack propagation" which usually results after some "slow" crack development. For the stress analysis to be applicable, it is necessary to know the crack length at the start of rapid crack propagation at maximum load. The compliance gage discussed above was developed for this purpose. A typical compliance-gage record for the mechanical type of gage is shown in Figure 8. The slope of the straight line that is the initial part of the compliance curve is dependent on the initial crack length as well as on the dimensions and elastic modulus of the specimen. Ideally, the slope of the line from the point of initiation of rapid fracturing to the origin would be dependent on the length of the crack at the point of instability as well as the dimensions and elastic modulus of the specmen. If the specimen is unloaded before fracturing, the trace of the unloading line will not go through the origin because of the slight amount of plastic deformation at the leading edge of the crack. However, if the slope of this line is "adjusted" to pass through the origin, it is assumed that this compensates for the effect of the plastic zone on the apparent crack length.

PLANE-STRAIN TESTS

During development of the compliance gage, Boyle (Reference 41) noted that under certain conditions there was a sharp discontinuity or step in the compliance curve at the upper end of the initial straight-line portion. This step in the curve (shown in Figure 8) represented rapid crack propagation with no increase in load until after the rapid crack propagation had stopped. Further examination indicated that it was representative of plane-strain fracturing (often referred to as crack opening mode or opening mode of crack extension) since it was a square-type fracture not associated with shear-lip formation. The load at the step in the curve is called the pop-in load, and the phenomenon is called meta-instablility since it is not necessarily continuous. Equation for calculating the plane-strain parameters for the center-cracked and edge-cracked specimens at the pop-in loads is shown in Figure 10.

According to definition, the plane-strain fracture toughness is associated with unstable fracturing which produces a square fracture and a step or pop-in in the compliance curve. For relatively thick precracked specimens where there is considerable restraint at the crack front, specimens of high-strength alloys may fail completely under plane-strain conditions once crack propagation is started by the pop-in mechanism. This is usually true for the surface-cracked tensile specimens and the round circumferentially notched-and-precracked specimens. For this reason, compliance gages normally have not been used on the surface-cracked or round-precracked specimens during testing. However, there are certain limitations in making these tests and in interpreting the data which is beyond the scope of this discussion.

A Boyle room temperature compliance gage, which was fabricated at the AF Materials Laboratory and used by the author on a previous program in determination of the fracture toughness of several high strength steels, is depicted in Figures 11 and 12. The compliance gage was supplemented with a load-acoustical pickup system to increase sensitivity to plane strain load pop-in and make it readily discernible for gross stress calculations for plane strain fracture toughness material evaluation.

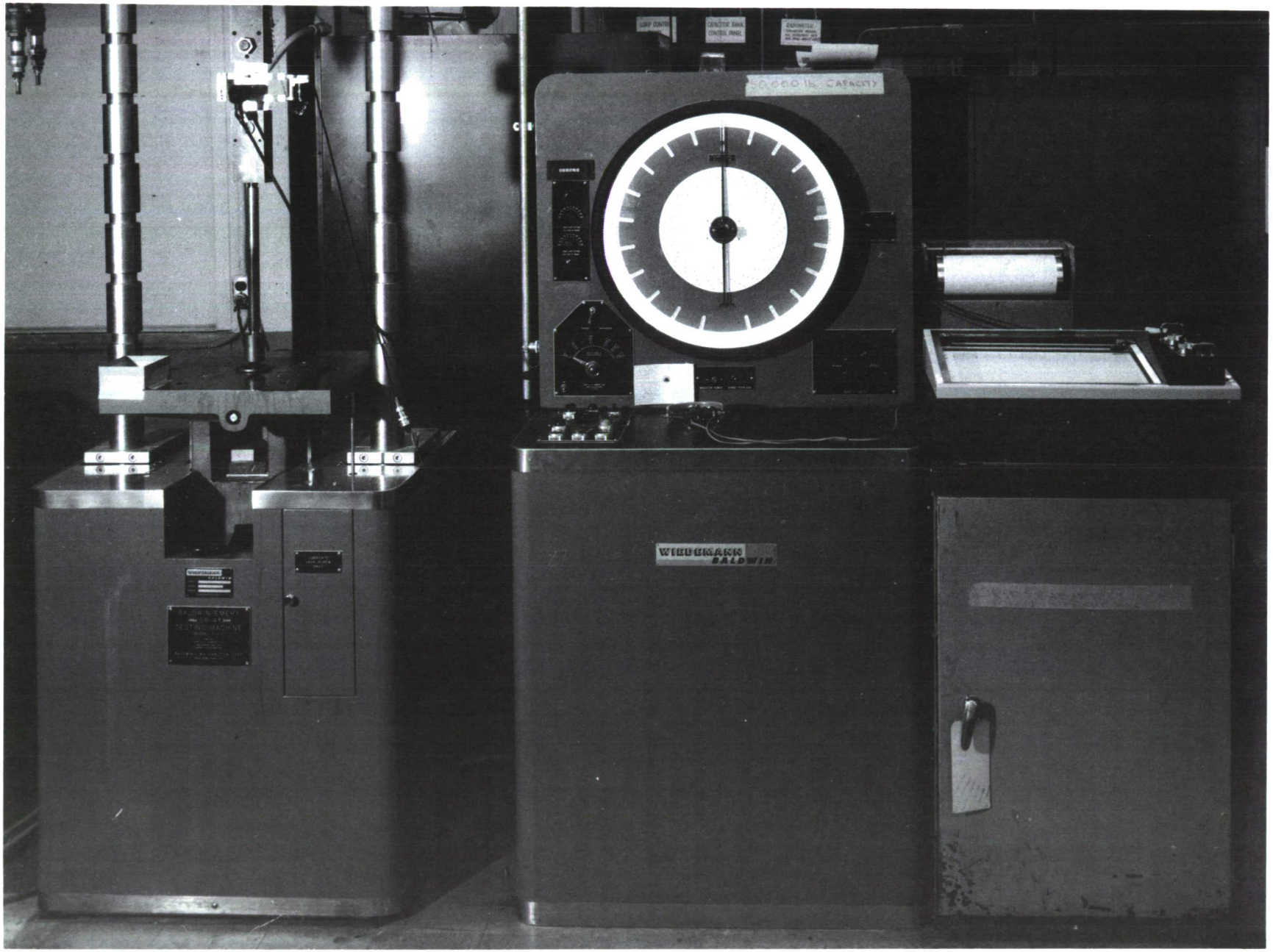


Figure 11. Boyle Room Temperature Compliance Gage Load-Extension System Combined With a Load-Acoustical Measurement System

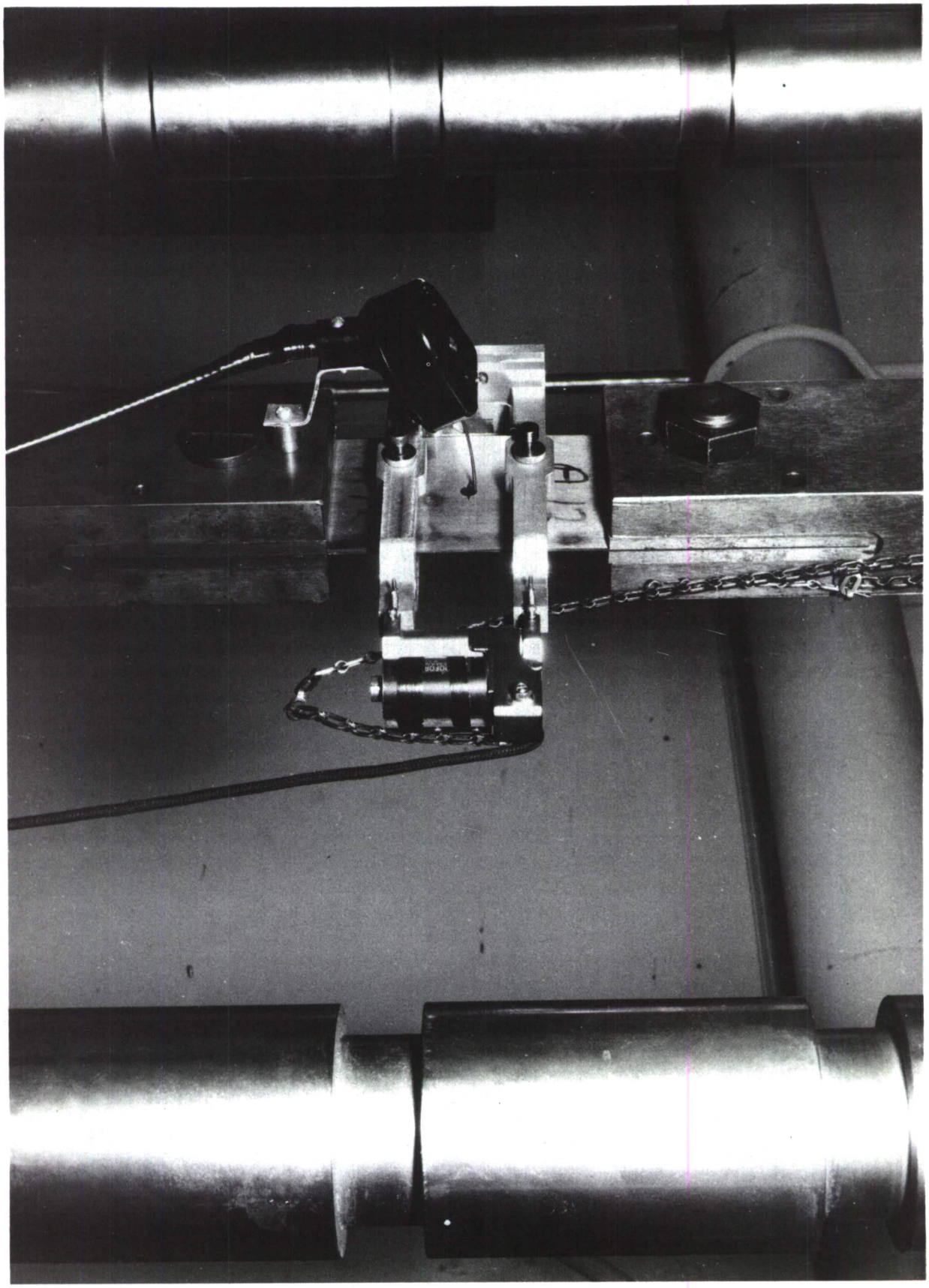


Figure 12. Detail View of Boyle Compliance Gage and Acoustical Pickup Crystal

SECTION V

DEVELOPMENT OF A CRYOGENIC, ELEVATED TEMPERATURE COMPLIANCE GAGE

GENERAL BACKGROUND INFORMATION

More and more heat treatable ferrous and nonferrous metallic materials are being used at higher yield strength levels in cryogenic and elevated temperature environments. Since one can never quite be sure that some metallurgical embrittlement has not occurred, it is safest to fatigue crack all fracture toughness specimens and test for crack initiation and propagation resistance under plane strain and plane stress, respectively, under previously mentioned environments. When evaluating thick structural materials under K_{Ic} plane strain fracture toughness, it is desirable to have a displacement gage of some kind to detect the initial stage of crack propagation. The reason for this is that even in thick sections, the critical crack may be arrested in very tough materials. Thus, to accurately measure K_{Ic}, the stress at which the first sign of cracking is detected must be recorded. This has been accomplished by using gages that sense displacement, voltage or resistance and effectively measure the crack initiation point when recorded on an x-y plotter with load.

The ASTM method (Reference 2) for fracture toughness testing under plane stress conditions has been fairly well established. This method utilizes either edge or center slots in relatively thin sheets pulled in tension to failure. From the standpoint of obtaining simultaneous crack development in both halves of a specimen during testing, the centrally cracked specimen is preferred over the edge-cracked specimen. Instability conditions were estimated using an ink method to estimate slow crack growth or a percent shear-lip method. Since the original standard was devised, several improvements have been made for the following reasons:

(1) The ink method is undesirable from two standpoints. First, in some materials the ink environment increases crack susceptibility and the measured value of toughness may be in error. Secondly, in some instances the ink has been observed to run further after the transition from slow to rapid cracking.

(2) The present shear-lip estimate used in determining K_c is not adequate since the relationship of percent shear to relative plastic zone size is not consistent from material to material or from thickness to thickness as shown by Gerberich (Reference 4).

(3) The extension of the elastic analysis to account for the apparent increase in crack length due to plasticity at the crack tip is not an exact method (Reference 3).

(4) For some materials, the recommended notch root radius of 0.001 inch is not small enough. It has been suggested by Irwin that the notch root radius should be less than about one-tenth the relative plastic zone size or,

$$\rho_c = \frac{K^2}{20 \pi \sigma_{YS}^2} \tag{35}$$

to obtain the true value of fracture toughness.

To remedy the first three objections, a room temperature testing compliance gage technique has been proposed by Boyle which essentially measures the displacement of the crack through a strain gage monitoring device as shown in Figures 11 and 12. This inherently measures slow crack growth so that no estimates of slow crack growth are needed. It also avoids the necessity of estimating the plastic zone size at the crack tip. To resolve the notch sharpness problem, previously mentioned fatigue cracking prior to testing has been proposed (Reference 43). However, this only solved the problem of measuring the mechanical brittle fracture toughness or resistance to fracture of high strength heat treatable metallic materials under room temperature conditions. The actual environments in service will range from cryogenic to elevated temperatures for future airborne systems. In addition, chemical-mechanical brittle fracture rather than pure mechanical brittle fracture under previously mentioned temperature conditions will have to be considered as a materials evaluation and selection criteria for designing reliability into structures. This is based upon projected higher yield strength levels in alloy development. However, the gage developed by the author was designed to solve the temperature environmental testing problem associated with brittle fracture resistance measurements.

Irwin has indicated that compliance, measured away from the specimen's central axis, is not as large as compliance measured on the axis (Reference 37). Accordingly, it was decided to develop a compliance gage capable of and sensitive to measuring compliance of the specimen on the axis for determinations of crack initiation and slow crack extension. First, an analysis was carried out, based on Irwin's modification of Westergaard's equation for compliance as measured at the edges of the specimen. Figure 9 shows the theoretical plot of compliance as a function of crack length from the derived equation as shown below:

$$\frac{Ev}{\sigma W} = \frac{2}{\pi} \sinh^{-1}\left[\frac{\sinh \frac{\pi y}{W}}{\cos \frac{\pi a}{W}}\right] - \frac{y}{W}\frac{(1+\nu)}{\sqrt{1-\frac{\sin^2 \frac{\pi a}{W}}{\cosh^2 \frac{\pi y}{W}}}} + \frac{\nu y}{W} \qquad (36)$$

The units are those used by Irwin and Boyle (References 39 and 40): a is one-half of the crack length, W is the specimen width, v is one-half of the specimen extension, σ is the gross stress calculated from the dimensions of the uncracked specimen, and E is Young's modulus. Section III shows the derivation of the equation that adapts the Westergaard-Irwin equation for compliance at the edges of the specimen. Boyle (Reference 41) derived the following conclusions concerning the previous techniques used to determine slow-crack growth prior to or at the point of fast fracture instability on a centrally notched fracture specimen:

(1) Surface measurements are unreliable due to tunneling which often obscures the true tip of the crack.

(2) The relatively simple ink-staining procedure previously recommended by the ASTM Committee also had disadvantages.

(3) Considerable judgment as to the quantity of ink applied in the root of the specimen notch is required.

(4) Too much ink results in excessive splatter of the ink over the fracture surface, while too little ink in the root of the notch causes exhaustion of marking fluid before fast fracture instability and a corresponding underestimate of critical crack length.

(5) Ink fluids have been deleterious to the slow growth toughness of certain steels.

(6) Visual and ink-staining measurements are insensitive to the perturbation to the stress field resulting from plastic flow relaxation at the crack tip.

Boyle's (Reference 41) alternate method shown in Figure 12 is based upon the following propositions:

(1) In a valid fracture-toughness test the crack-tip plastic zone is small in relation to the crack dimensions and the elastic stress field.

(2) Under such conditions the effective stiffness or the compliance of the specimen containing the crack will be a function of the extent by which the specimen has been divided by a crack.

(3) With crack growth, less of the section remains to supoort the load and the strains become correspondingly higher, with the result that the extension-to-load ratio (compliance) increases.

(4) Ideally, a load-extension curve between points on either side of a centrally notched plate should show an initially constant slope characteristic of the notch origin of crack pop-in (Figure 8).

(5) Then, as a crack propagates from the crack pop-in point, a decrease in slope (onset of slow crack growth) similar to the onset of plastic flow in an unnotched specimen would appear.

(6) This curve (Figure 8) would differ from a normal stress-strain curve, because upon unloading it would return to the origin along a straigh line.

(7) The slope of the straight line would be characteristic of the total crack length attained.

(8) Accordingly, a line drawn from the origin to any point on the curve would have a slope characteristic of the crack length attained at that point.

(9) Thus, measurement of extension of the notched specimen during loading up to the point of fast fracture instability (point of discontinuity where P = 21,950 lb in Figure 8) should provide a measure of the crack length at that point.

This report describes a compliance gage that is capable of fulfilling the preceding propositions hypothesized by Boyle at cryogenic and elevated temperatures.

CRYOGENIC, ELEVATED TEMPERATURE COMPLIANCE GAGE

Initially, a compliance gage similar to a creep measurement extensometer was fabricated of 304 stainless steel rods, tubes, and bar stock. This steel was selected because: (1) it has high modulus down to -400°F and up to 800°F, (2) its carbide precipitation susceptibility usually does not occur below 800°F to any serious degree, (3) it can be welded by all common methods, and (4) it has good corrosion resistance to various atmospheres and acids.

The split bushings, two support clamps, and the clamp-on head assembly in Figure 13 were not developed as components of the original compliance gage. As a consequence, the electrical extensometer shown in Figure 17 was attached directly to the rod through a slot in the tube and on the tube. This was primarily to measure the relative motion of the rod and tube and in turn

the compliance of a specimen attached between the rod and tube head. The center axis of the preceding former and latter were aligned with the center longitudinal axis of the specimen. The rods and tubes of the gage were made long to move the electrical extensometer (Figure 17) out of the test temperature environment (cryogenic or elevated temperature) so that accurate deflections or extensions could be measured.

The major problems to be solved on the original compliance gage appeared to be a lack of sensitivity to small deformation, friction, and deformation of compliance gage elements on fracture. To solve these problems, the following four steps were performed:

(1) Obtain reference performance characteristics of the present compliance gage in its current condition at room temperature.

(2) Modify the present gage by removing probable sources of measurement error.

(3) Obtain performance data on the modified gage.

(4) Define the magnitude of remaining problems and the next stage of development.

The initial performance characteristics obtained are shown in Figure 14. The old compliance gage was mounted on a Rene'41 tensile specimen at a 2-inch gage length setting with a Riehle serial R 74749 extensometer mounted on the side rod and tube. The curves are typical of a number of attempts to obtain an interpretable record. In this gage, the interrelated effects of friction, gage deformation, and gage deflections were too complex for interpretation or analysis.

To accomplish the program objective, the original gage was modified by:

(1) eliminating friction points between tube and rod structures and the extensometer mounts;

(2) adding a rigid-box forming connection between rod ends and tube ends. This includes flexure plates for precise location of rods with respect to the tubes at the extensometer end and removable centering guides at the specimen end; and

(3) providing spring-loaded fastenings for the rod to guide head to permit axial extension on fracture without damage to the gage.

A picture of the modified compliance gage is shown in Figures 13 and 17. Data obtained with the Baldwin Model PS-5M extensometer at an estimated 3000X strain magnification and with a Riehle extensometer at 1000X strain magnification are shown in Figures 18 and 19, respectively. The curves with the extensometers mounted on the gage rod and tube show a precision comparison between sides with a reduction of friction and deflection effects. An averaging mount between and offset from the legs exhibited deflection effects resulting from extensometer friction and operating forces. Averaging could be obtained with a zero force extensometer (if one existed). Because of this, the averaging concept was abandoned.

Further attempts at the design and construction of a compliance gage meeting higher temperature objectives depends on:

(1) availability of formable materials with a high modulus over the desired operating temperature range.

(2) a more specific definition of overall gage precision and accuracy with respect to specimen configuration and properties.

DISCUSSION

The change of the compliance gage from a U to a rigid-box structure was accomplished by the addition of the clamp-on head assembly shown in Figure 15 and 16. The head assembly is attached to the ends of the tubes with split clamps.

The rod head is attached to the tube head with two 3/8 by .010 inch spring steel flexure plates which provide rigid centering of rods and tubes with minimal axial loading. These rods are firmly located in the Vee grooves in the rod head by plastic-tipped spring plungers (Vlier Engineering Company No. NS-52) which permit the rods to slip without damage to themselves and the rod head. The specimen end tube head is counterbored at the rod holes for split centering bushings. They are used during attachment of the gage to the specimen and are removed before the specimen is tested. The load-compliance test system and x-y recorder are shown in Figure 20.

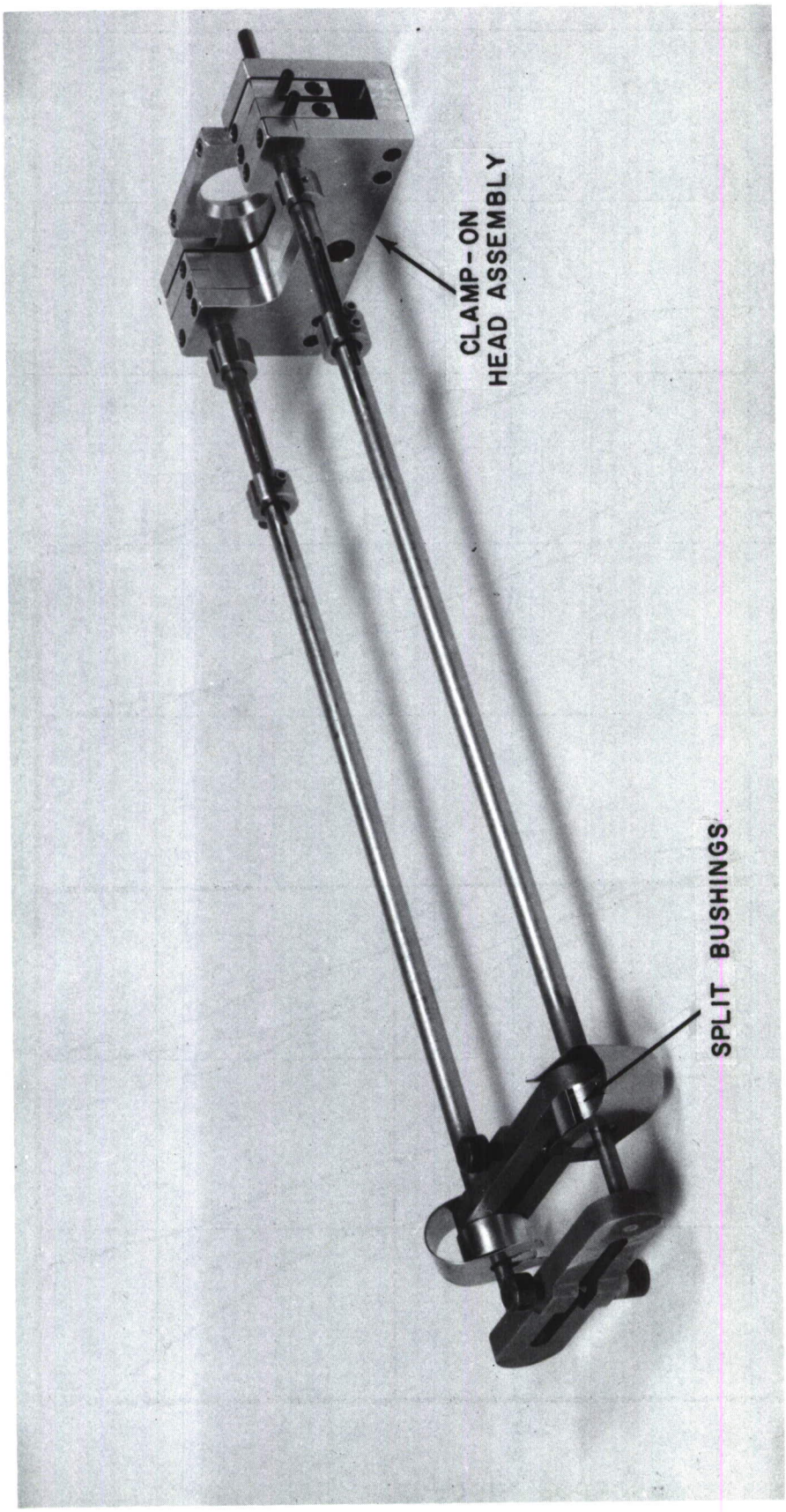


Figure 13. Modified Compliance Gage

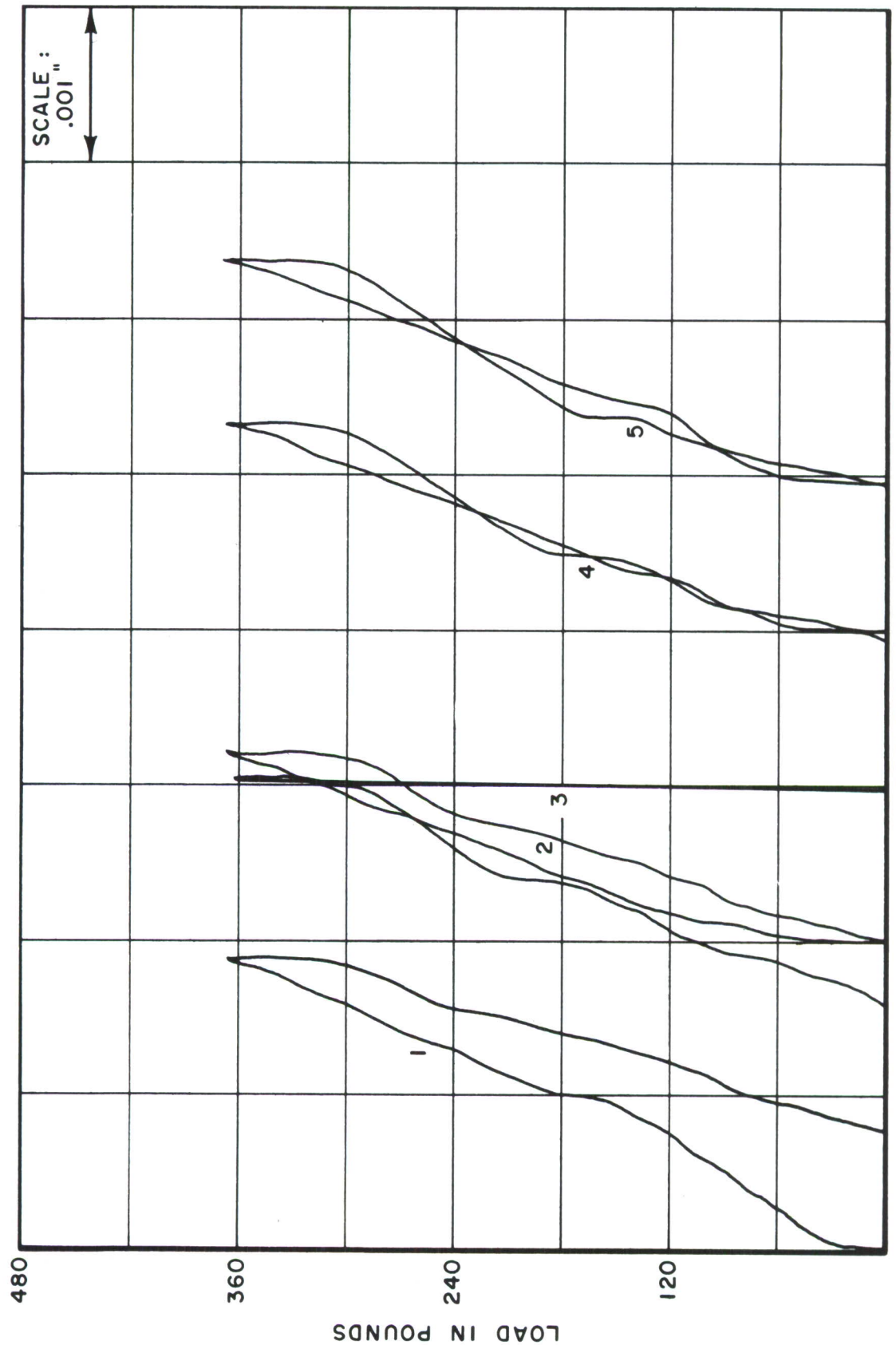


Figure 14. Initial Compliance Gage Performance

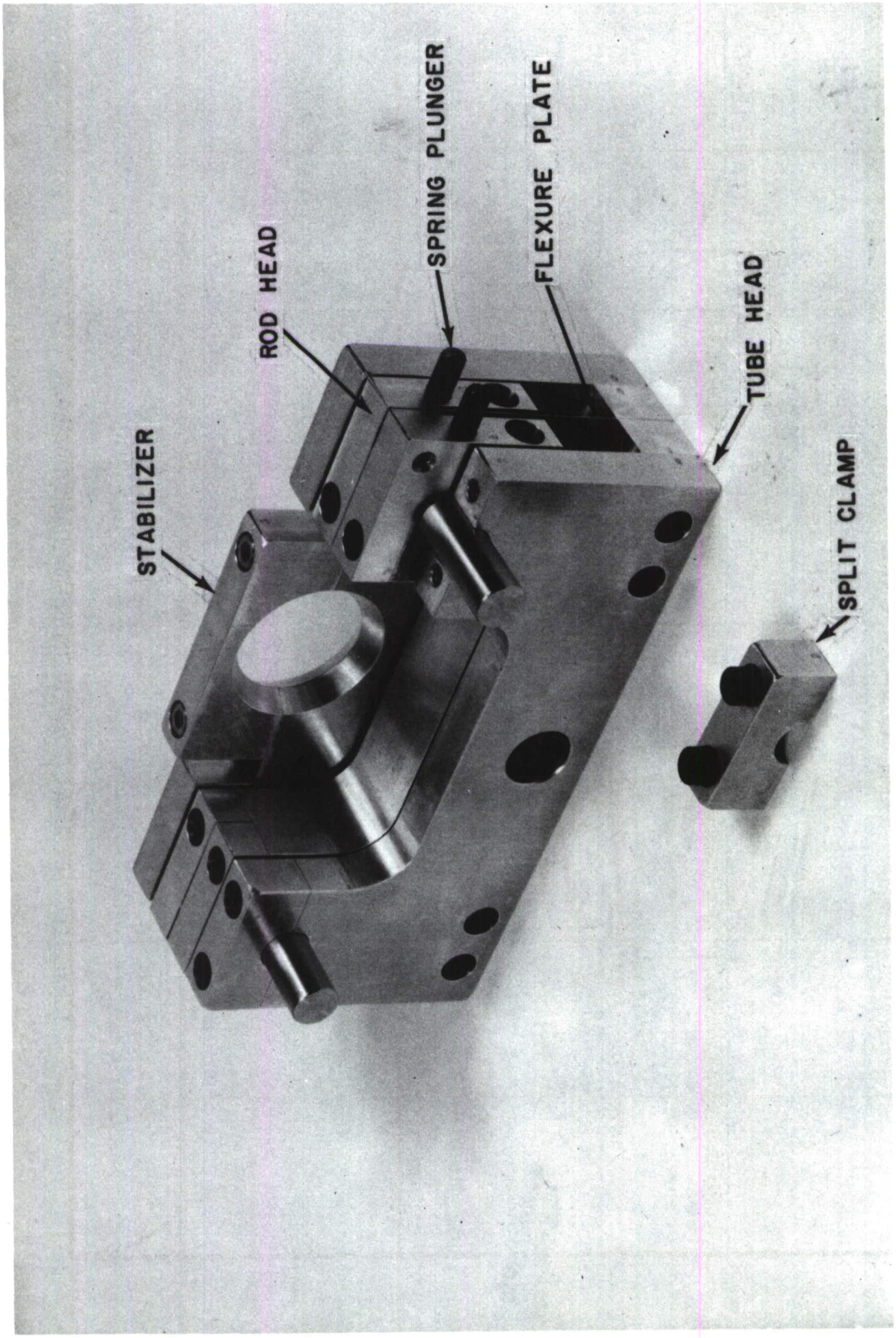


Figure 15. Clamp-On Head Assembly

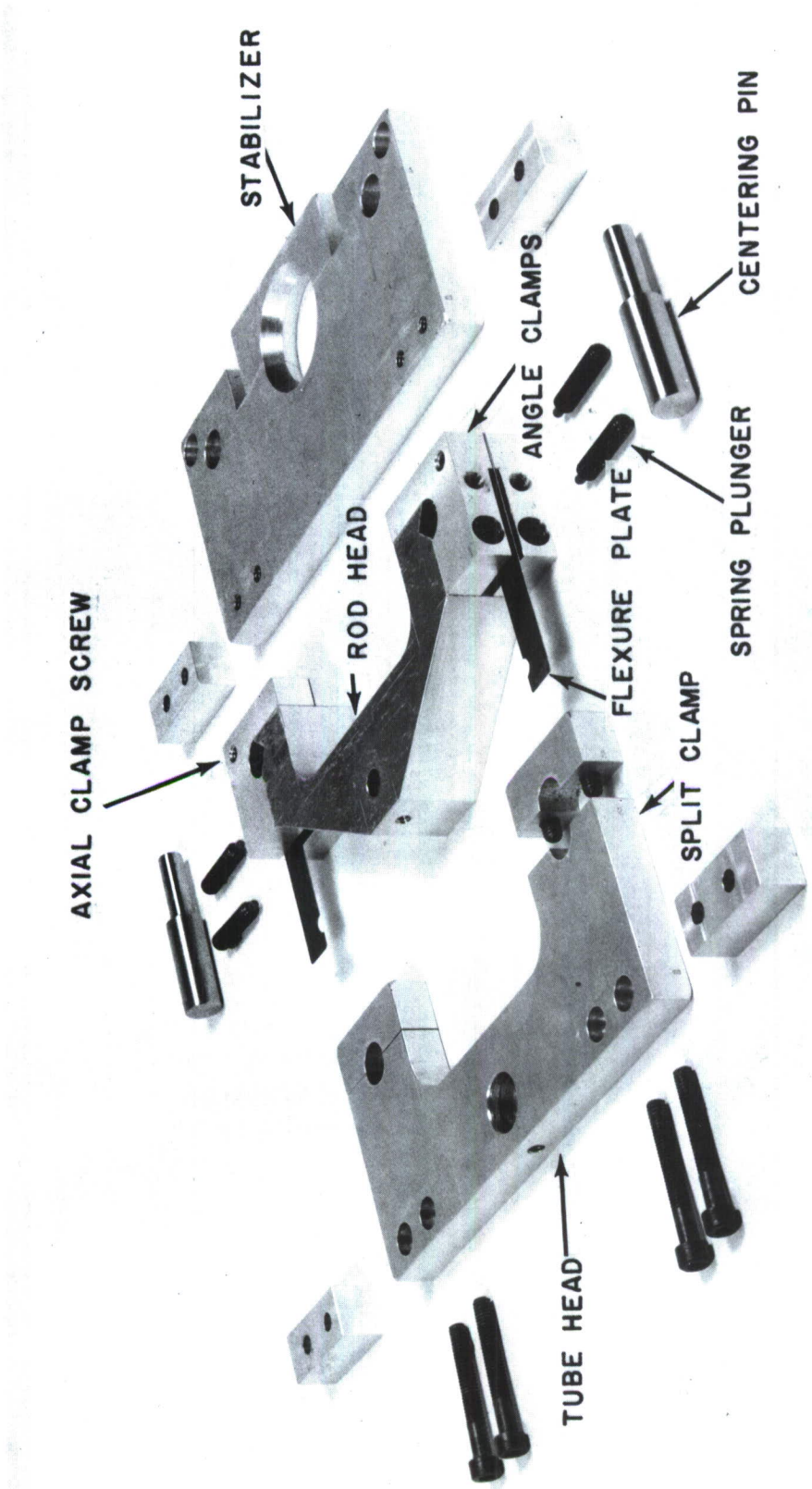


Figure 16. Exploded View of Clamp-On Head Assembly

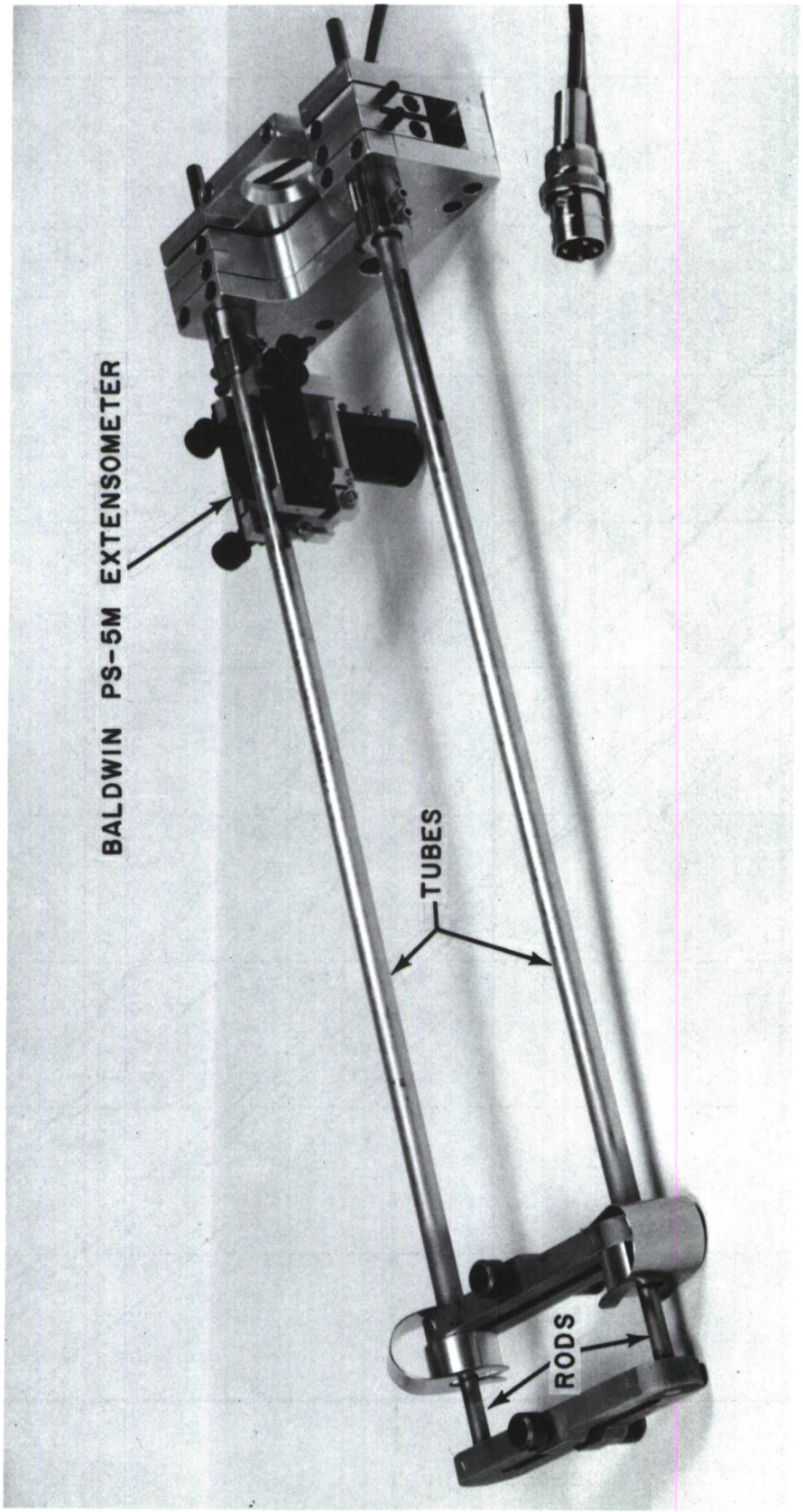


Figure 17. Baldwin Model PS-5M Releasable Extensometer Mounted on the Compliance Gage

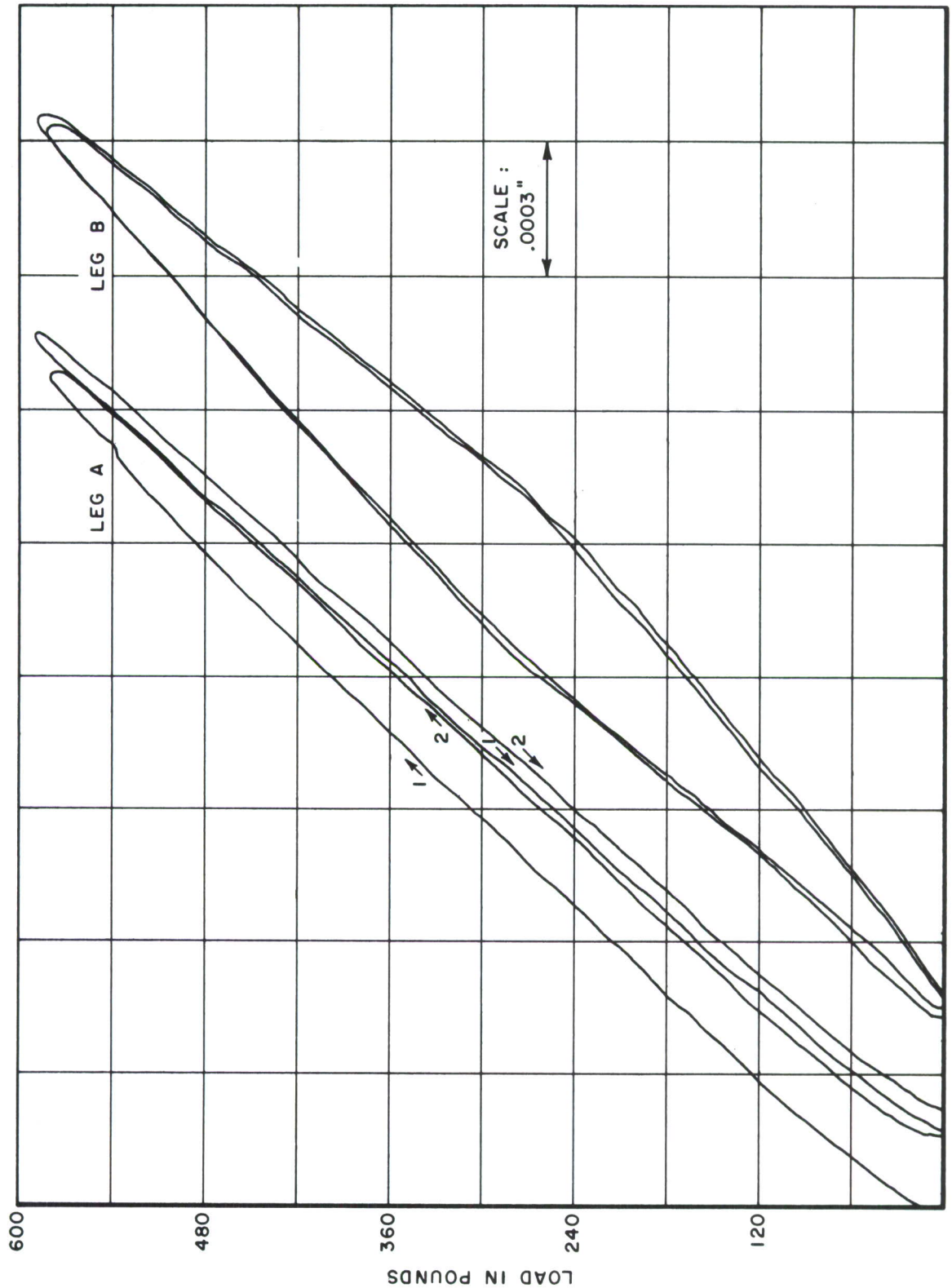


Figure 18. Modified Compliance Gage Performance With a Baldwin Extensometer

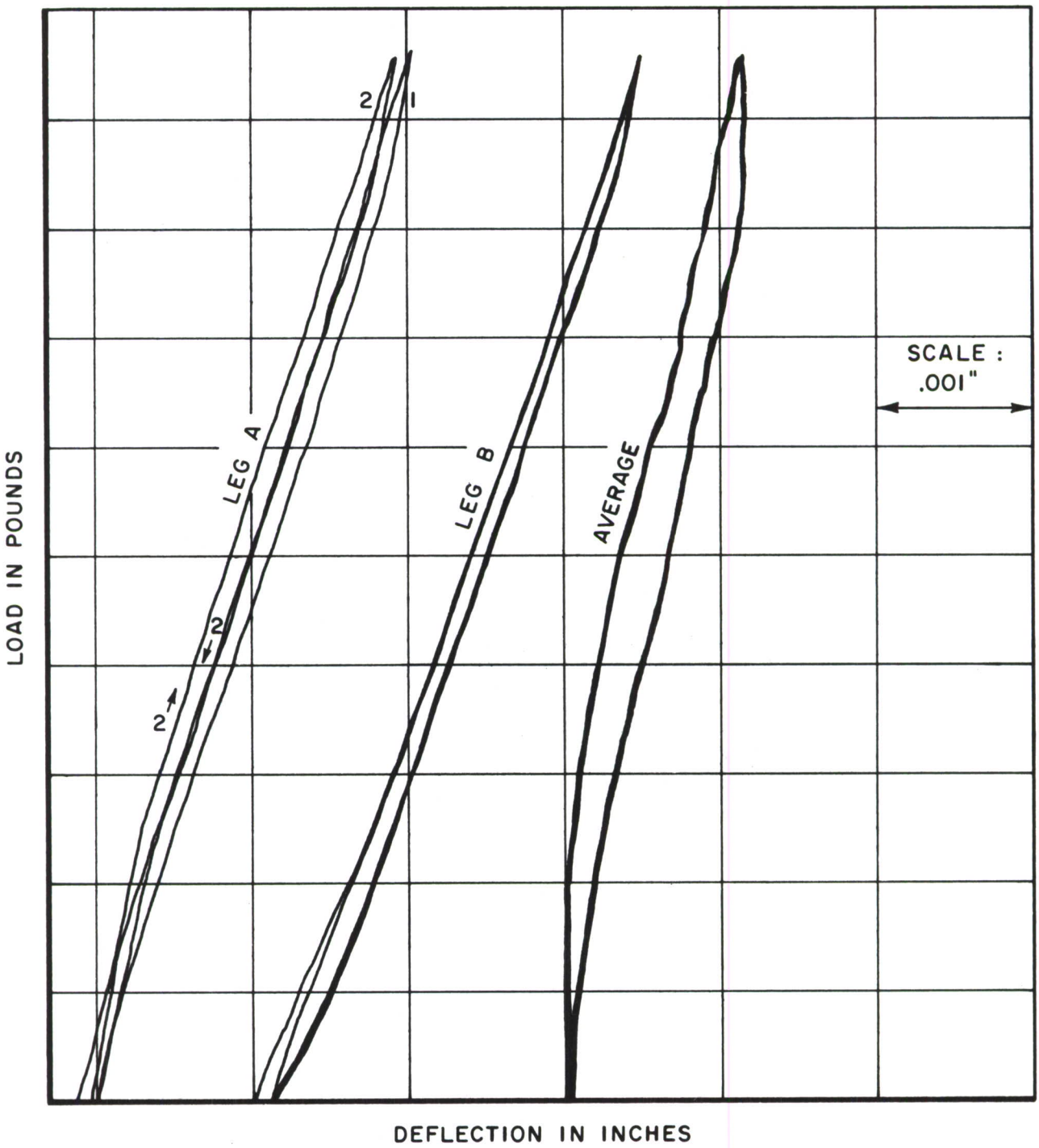


Figure 19. Modified Compliance Gage Performance With a Riehle Extersometer

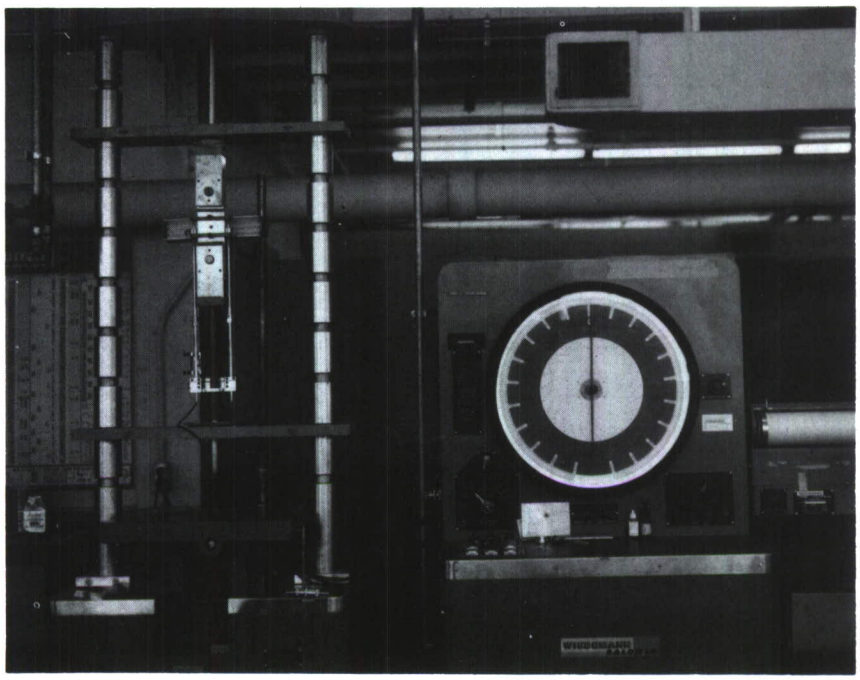
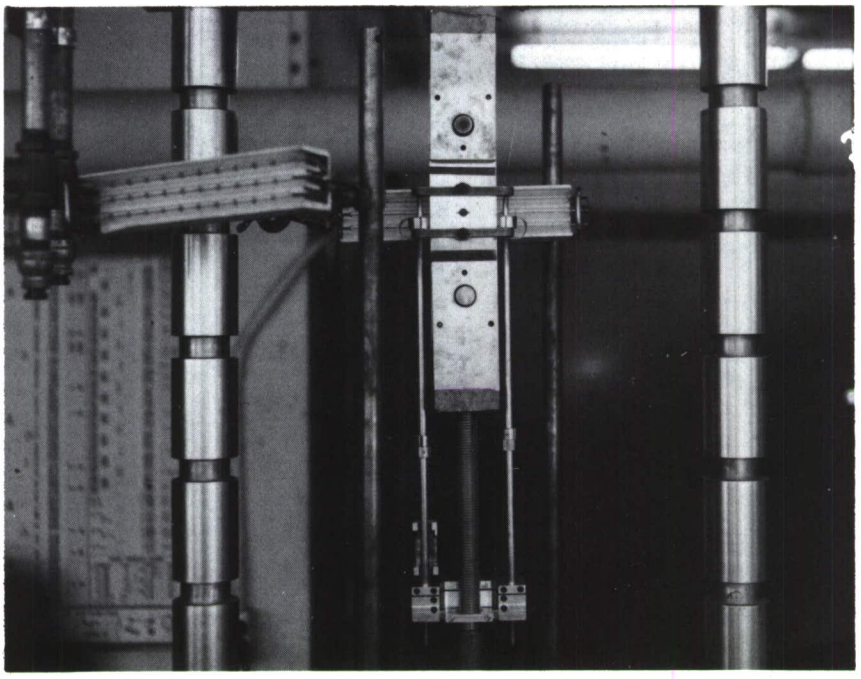
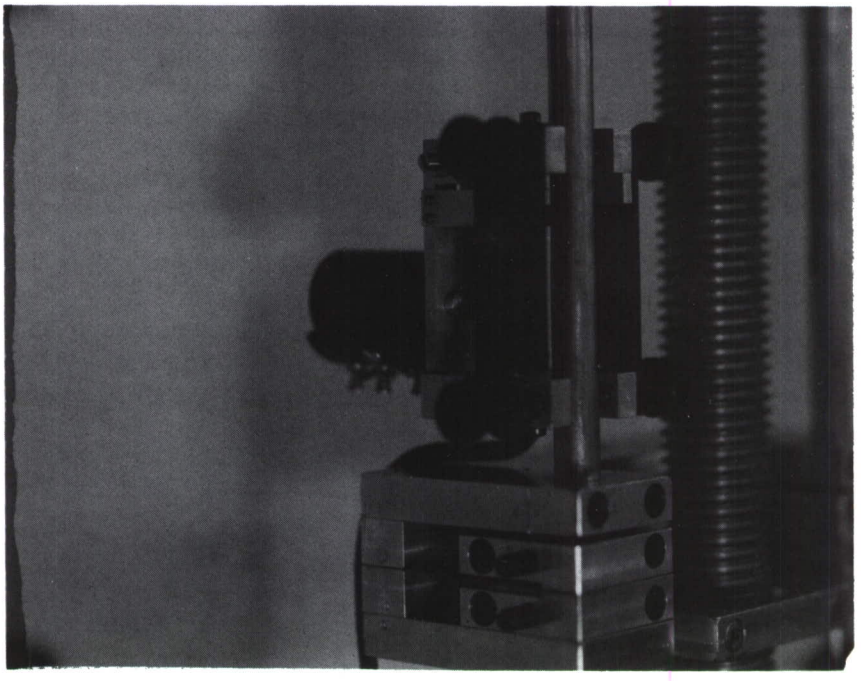


Figure 20. Load Compliance System and X-Y Recorder for Cryogenic, Elevated Temperature Compliance Gage



A. Compliance Gage Attached to Specimen



B. Deflection Measurement Extensometer

Figure 21. Detail View of Cryogenic, Elevated Temperature Compliance Gage

SECTION VI

CRYOGENIC, ELEVATED TEMPERATURE COMPLIANCE GAGE CALIBRATION EXPERIMENTAL RESULTS AND DISCUSSION

Table I gives the composition, heat treatment, and average room temperature unnotched tensile information for the material tested.

TABLE I

MATERIAL INFORMATION

Material	Supplier	Si	Cu	Mn	Mg	Fe	Al
2024-T3	Alcoa	0.14	4.23	0.7	1.46	0.24	Bal

Heat Treatment: T3-Solution heat treatment followed by 1% strain hardening.

Avg. Tensile Data (Flat Sheet):

Source	Material	σ_{tu}	0.2% σ_{YS}	%e	Modulus E (10^6)
*Author's	2024-T3	71,725	49,600	16.3	10.2
Alcoa Aluminum Handbook (Typical Values)	"	70,000	50,000	17.0	10.6

*The author's tensile data was obtained with the developed compliance gage attached to the tensile specimen on the center axis over a 2-inch length. This was performed to check the ability of the gage to measure compliance accurately. The measured 0.2% yield stress and modulus with the compliance gage agreed with the handbook values as shown above. This agreement validated the integrity of the gage according to the tensile test data obtained experimentally.

SPECIMENS

Tensile and centrally notched fracture toughness specimens were machined from one-eighth of an inch 2024 aluminum plate in the T-3 condition to the configurations shown in Figures 22 and 23. The centrally notched fracture-toughness calibration specimens were initially machined without the .010 inch root radius notch so that a load deflection curve could be obtained when 2a = 0. 2a is the total crack length of the notch of the specimen in Figure 23. After the load-deflection curve was obtained for 2a = 0, the notch shown in Figure 23 was machined into the specimen.

TEST SCHEDULE

Table II presents a general outline of the test program. Table III shows a detailed test schedule. The tensile test specimens were required to determine modulus and the yield stress. The yield stress was used as a reference point to select linear elastic compliance loads for the load-deflection curves. The modulus was used in the compliance parameter calculations. The centrally notched fracture-toughness specimens were utilized to check the elastic compliance as a function of crack length and to determine the fracture toughness of 2024-T3 at -320°, 75°, and 350°F using fracture mechanics concepts.

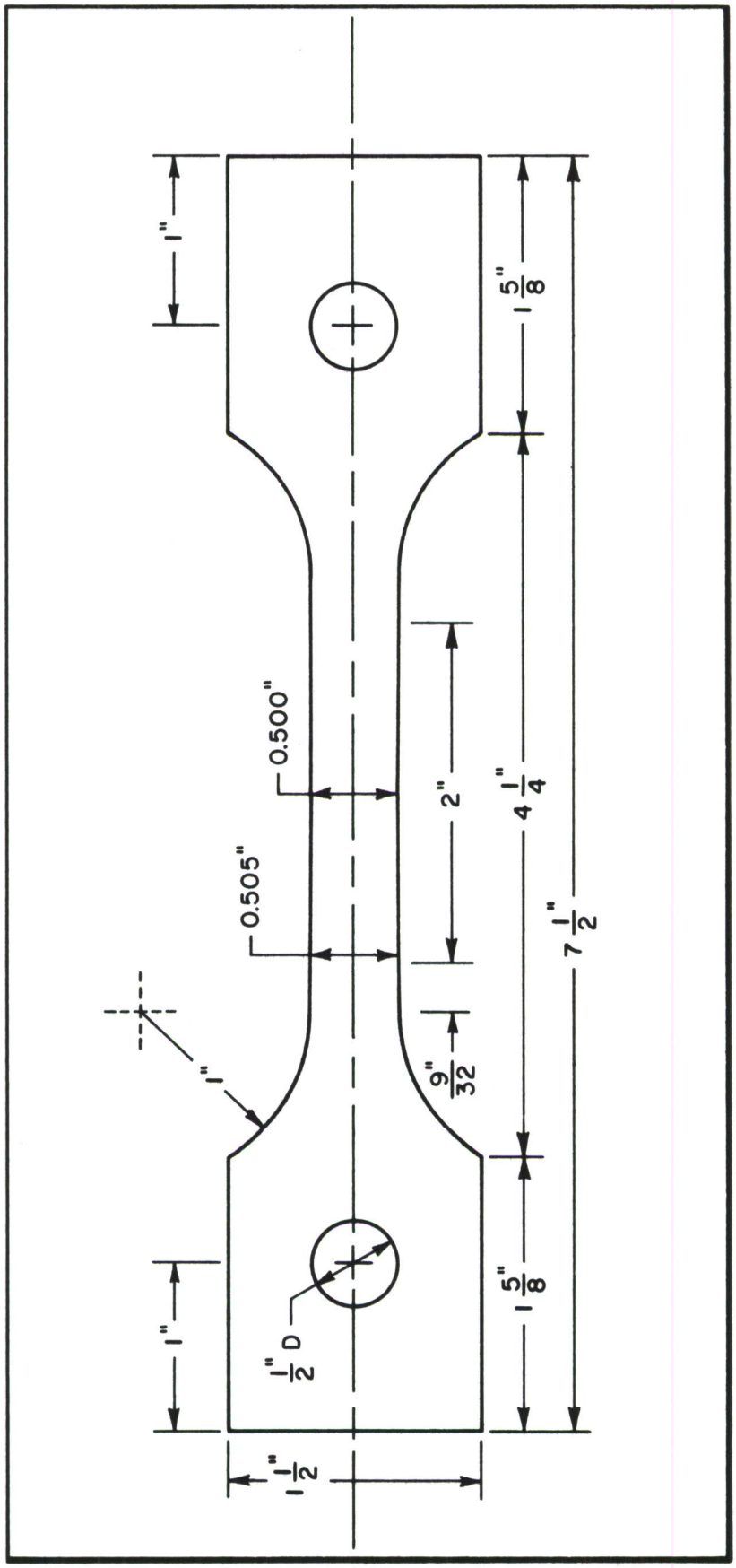


Figure 22. Flat Hot-Test Specimen

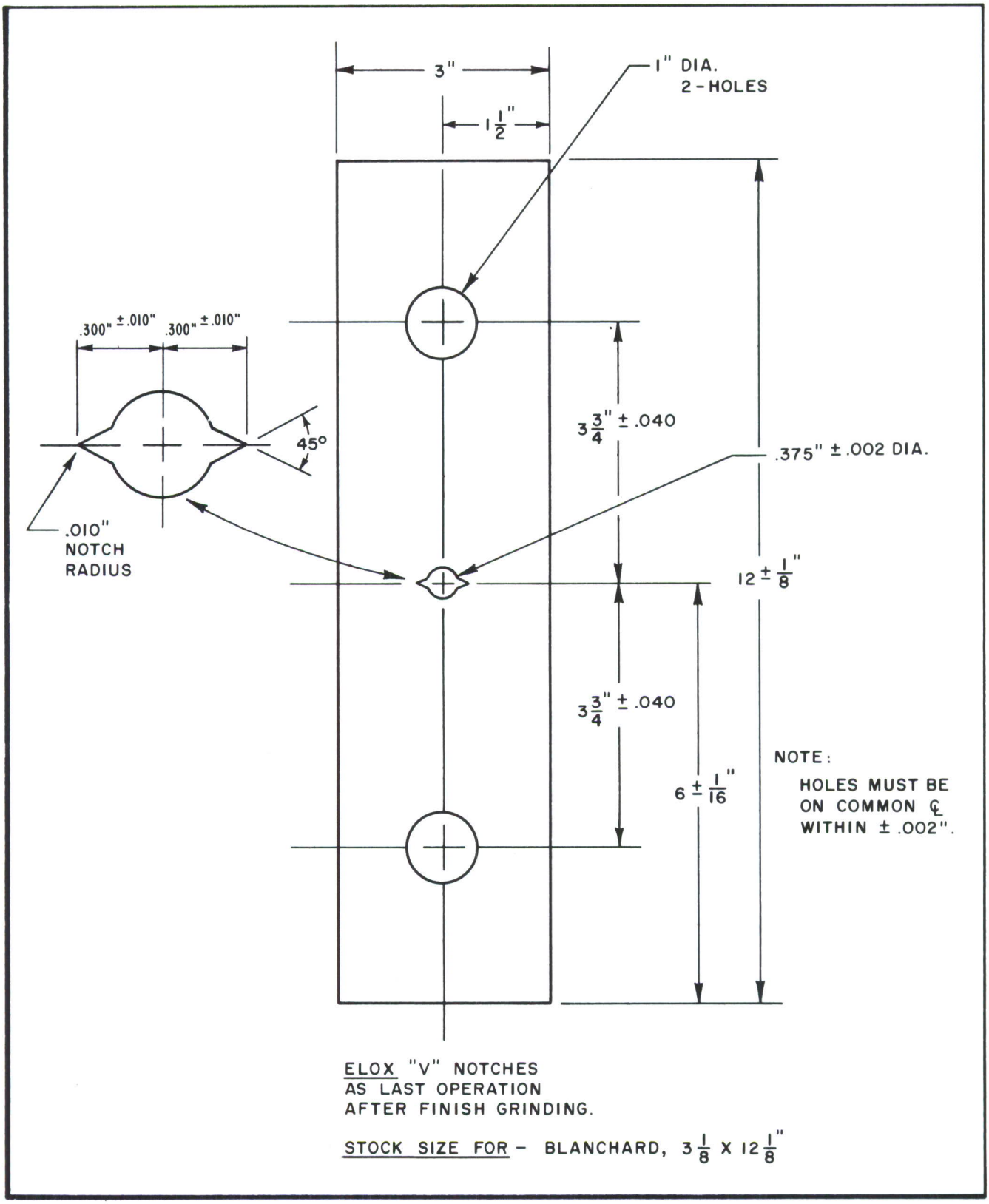


Figure 23. Fatigue-Cracked Centrally Notched 3-Inch-Wide Tensile Specimen

TABLE II

2024-T3 CALIBRATION TEST SPECIMEN SCHEDULE

Type of Specimen	Test Temperatures (°F)				Specimen/Conditions
Tensile (un)	-320	75	200	350	
L	2	2	2	2	8
T	2	2	2	2	8
Total					16
Centrally Notched *Fracture (un)					
L		1		1	2
T		1		1	2
Total					4
Centrally Notched Fracture (n)					
L	1	1		1	3
T	1	1		1	3
Total					6

*These specimens were machined initially without center notches. After obtaining load-deflection curves, they were notched.

TABLE III

DETAIL CALIBRATION TEST SPECIMEN SCHEDULE

Type of Specimen	Test Temperature (°F)			
Tensile (un)	-320	75	200	350
L	*L-1	L-7	L-3	L-5
	L-2	L-8	L-4	L-6
T	T-1	T-7	T-3	T-5
	T-2	T-8	T-4	T-6
Fracture (un)				
L		LC-1-75		LC-3-350
T		TC-1-75		TC-3-350
Fracture (n)				
L	LC-0-320	LC-1-75		LC-3-350
T	TC-0-320	TC-1-75		TC-3-350

*Specimen number

TEST PROCEDURES

Tensile test data were generated in accordance with test schedule in Tables II and III. The results mentioned above are tabulated in Tables V, VI, VII, and VIII. The original curves are shown in Figures 47 through 58. The latter are in the Appendix and were obtained in accordance with ASTM standards.

A fractograph is shown of the fracture surfaces of the tensile specimens tested at -320°, 75°, 200°, and 350°F, respectively, in Figure 24. Material was very ductile at 75°, 200°, and 350°F. Cleavage type of fracture was observed at -320°F. At 75°, 200°, and 350°F shear mode of fracture predominated.

The centrally notched specimens' load-compliance (deflection) curves were obtained on specimens LC-1-75, TC-1-75, LC-3-350, and TC-3-350 at 2a = 0 at a stress of 24,000 psi. These specimens were returned to the machine shop to be notched in accordance with test schedule. The preceding specimens plus others outlined in Tables II and III were planned to be individually machine notched to 2a = 0.6, 0.8, 1.0, 1.2, and 1.4 inches. However, the machine shop could not meet the test schedule in a minimum of time with respect to machining the notches with a jeweler's saw. As a consequence, the test schedule was changed as outlined in Table IV for the centrally notched specimens. These specimens, shown in Figure 25, were deflected at a reduced constant load as a function of increased crack length. The testing temperature environments used were -320°, 75°, and 350°F.

The 350°F tensile and centrally notched fracture specimens were heated to test temperature with quartz lamps shown on the back side of the centrally notched specimen in Figure 20 and on the front and back sides of the specimen in Figure 21A. Three quartz lamps per half section of furnance were used on the front and opposite sides of the specimen as shown in Figure 21A. The quartz lamps were mounted in an Al_2O_3 heat shield for reflectivity of heat to test section surface area of the specimen. Three Chromel-Alumel thermocouples were mounted on the x-y axis of the specimens, respectively. The 350°F temperature was uniform over a 2-inch gage length and across the width of the specimen.

The -320°F tensile and centrally notched specimens were cooled to cryogenic test temperature with liquid nitrogen with the apparatus shown in Figure 26A. The liquid nitrogen was forced from the Dewar with high pressure gaseous nitrogen through a rubber tube (see Figure 26A) and in turn sprayed a fine mist on the specimen and grips through a copper tube as shown in Figures 26B and C. Iron constantan thermocouples were placed on the x-y axis test section of each specimen along the outer edges and the gage length, respectively. These thermocouples were calibrated in liquid nitrogen before they were used in the tests to establish when the test specimens had reached equilbrium cryogenic temperature in the test section. The polystyrene, expanded styrofoam, cold box (which has a very low thermal conductivity, ($k \approx .021$), was closed and sealed with masking tape (as shown in Figure 26D) before obtaining -320°F temperature. The entire specimen, inclusive of the gripping ends, were cooled to -320°F to avoid breaking the specimens in the pinholes. The time for temperature stabilization was 15 to 20 minutes with a constant spray mist of liquid N_2 impinging directly on both sides of the specimen.

RESULTS

All raw detailed tensile test curves are listed in the Appendix. In addition, the original anelastic load-deflection curves obtained with the compliance gage under the various test temperatures and machined notch conditions are also listed in the Appendix. The load-deflection curves derived from compliance measurements on a series of specimens of various initial slot or crack lengths at -320°, 75°, and 350°F to determine σ and V (V = 1/2 total

TABLE IV

REVISED DETAIL CALIBRATION TEST SPECIMEN SCHEDULE

Specimen No.	Test Temperature (°F)	Compliance Crack Length (In.) 2a
LC-1-75	75	0.0
LC-2-75	"	0.6
LC-3-75	75	0.8
LC-4-75	"	1.0
LC-5-75	75	1.4
TC-1-75	75	0.0
TC-2-75	"	0.6
TC-3-75	75	0.8
TC-4-75	"	1.0
TC-5-75	75	1.4
LC-1-350	350	0.0
LC-2-350	"	0.6
LC-3-350	350	0.8
LC-4-350	"	1.0
LC-5-350	350	1.4
TC-1-350	350	0.0
TC-2-350	"	0.6
TC-3-350	350	0.8
TC-4-350	"	1.0
TC-5-350	350	1.4
LC-2-320	-320	0.6
LC-3-320	"	0.8
LC-4-320	-320	1.0
LC-5-320	"	1.4

Note: L = Longitudinal
T = Transverse
C = Calibration

TABLE V

TENSILE TEST DATA OF 2024-T3 ALUMINUM ALLOY AT ROOM TEMPERATURE (75°F)

Sample No.	T-7	T-8	L-7	L-8
Type of Specimen	Flat	Flat	Flat	Flat
Gage Length-In.	2	2	2	2
Width or Diam. Orig. In.	.5011	.5012	.5017	.5007
Thickness-In.	.125	.1257	.1256	.1250
Area-Original Sq. In.	.0626	.0629	.0628	.0625
YS, Lb. Offset 2%	2790	2890	3380	3370
YS, PSI	44,500	46,000	54,000	53,900
Maximum Load-Lb	4380	4440	4610	4560
Ult. Strength, PSI	70,000	70,500	73,400	73,000
Mod. of Elast., PSI	10.35×10^6	10.05×10^6	10.61×10^6	9.81×10^6
Elongation in 2 In.	.330	.360	.340	.270
Elongation in 2 In., %	16.5%	18%	17%	13.5%

TABLE VI

TENSILE TEST DATA OF 2024-T3 AL ALLOY AT 200 F

Sample No.	T-3	T-4	L-3	L-4
Type of Specimen	Flat	Flat	Flat	Flat
Gage Length, In.	2	2	2	2
Width or Diam., Orig., In.	.5006	.4998	.5011	.5003
Thickness, In.	.125	.125	.1250	.1257
Area, Original, Sq. In.	.0625	.0624	.0626	.0628
YS, Lb, Offset 2%	2830	2830	3340	3320
YS, PSI	45,300	45,300	53,400	52,000
Maximum Load, Lb.	4240	4240	4460	4450
Ult. Strength, PSI	67,700	67,800	71,200	70,900
Mod. of Elast., PSI	9.75×10^6	9.65×10^7	10.2×10^6	9.72×10^6
Elongation in 2 in.	.370	.35	.40	.380
Elongation in 2 in., %	18.5%	17.5%	20%	19%

TABLE VII

TENSILE TEST DATA OF 2024-T3 AL ALLOY AT 350 F

Sample No.	T-5	T-6	L-5	L-6
Type of Specimen	Flat	Flat	Flat	Flat
Gage Length, In.	2	2	2	2
Width or Diam., Orig., In.	.5014	.5008	.5012	.5009
Thickness, In.	.1250	.1251	.1255	.1255
Area, Original, Sq. In.	.0626	.0626	.0628	.0628
YS, Lb., Offset 2%	2750	2750	3200	3270
YS, PSI	43,900	43,900	51,000	52,000
Maximum Load, Lb.	3930	3890	4100	4320
Ult. Strength, PSI	62,700	62,000	65,000	68,800
Mod. of Elast, PSI	9.17×10^6	9.45×10^6	8.38×10^6	9.08×10^6
Elongation in 2 in.	.46	.40	.40	.35
Elongation in 2 in, %	23%	20%	20%	17.5%

TABLE VIII

AVERAGE TENSILE DATA OF 2024-T3 AL ALLOY AT -320°, 75°, and 350°F

Source	Temp. °F	σ_{tu}	σ_{YS}	% Elong.	E
*AFML	-320	82,750	54,900	22%	11×10^6
Alcoa	-320	85,000	62,000	18%	11.87×10^6
AFML	75	71,725	49,600	16.3%	10.21×10^6
Alcoa	75	70,000	50,000	17%	10.6×10^6
AFML	200	69,400	49,000	18.8%	9.83×10^6
Alcoa	200	66,500	48,100	16%	10.39×10^6
AFML	350	64,625	47,700	20%	9.47×10^6
Alcoa	350	43,500	37,000	17%	9.86×10^6

*The cryogenic tensile test values were obtained from AFML Cryogenic Materials Data Handbook. All other AFML tensile data were generated in AFML in-house laboratory by the author.

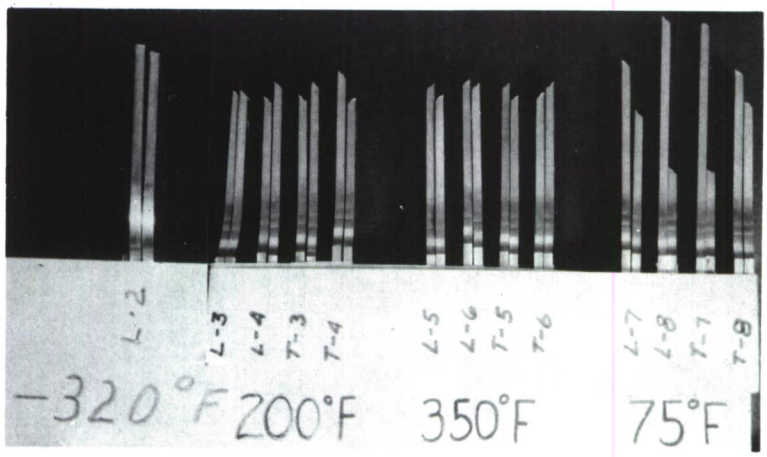


Figure 24. Fractograph of Fractured Surfaces of 2024-T3 Tensile Test Specimens

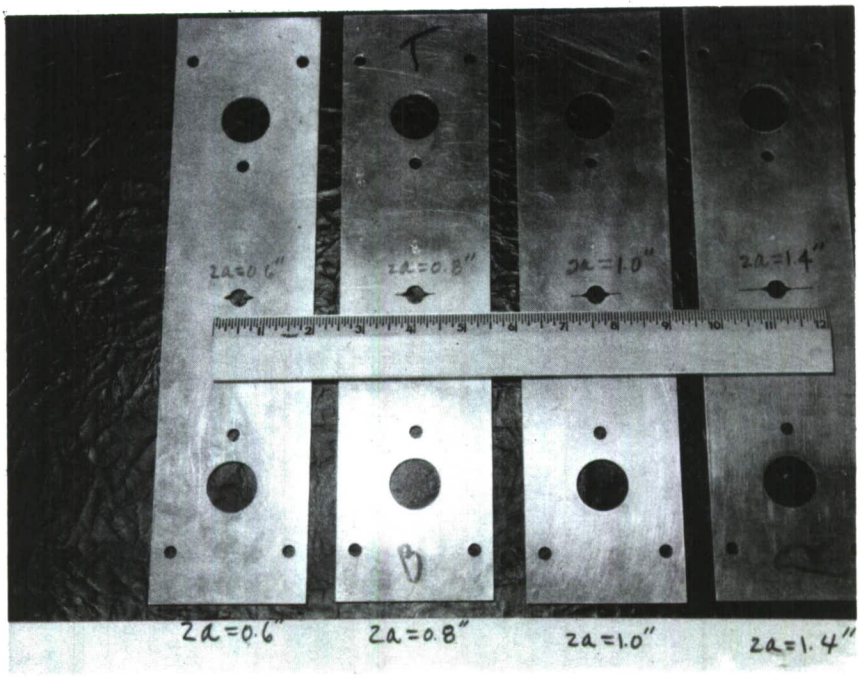
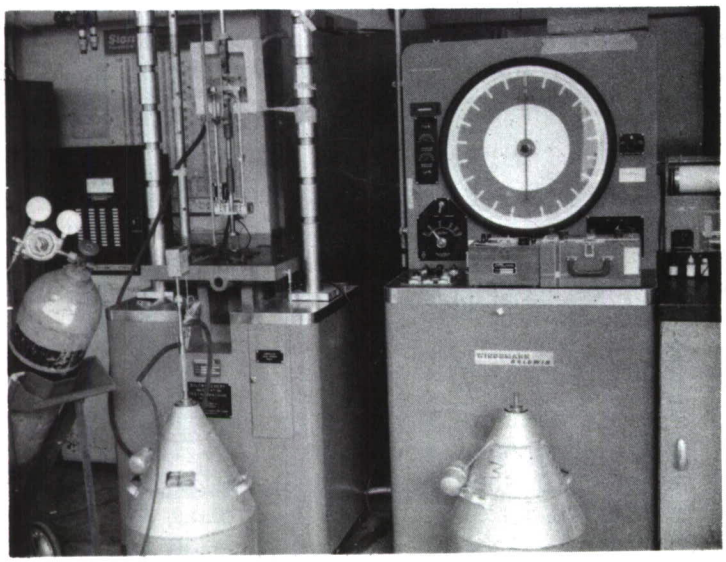
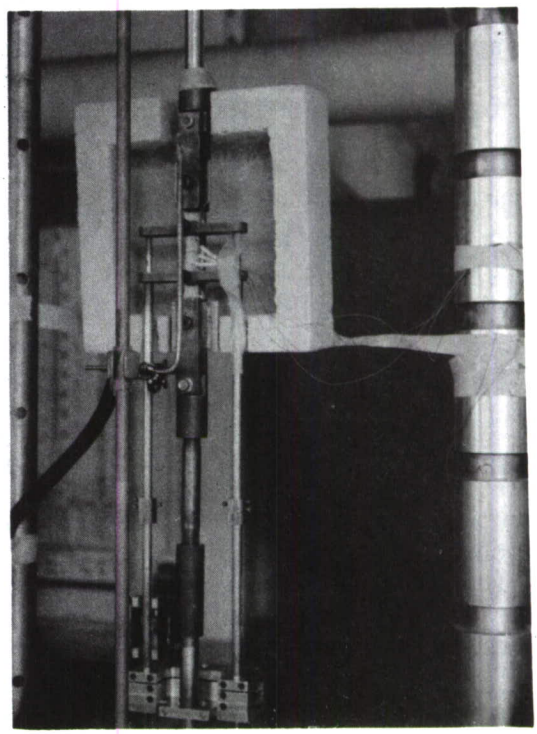


Figure 25. Three-Inch Wide Centrally Notched Specimens With Fracture Toughness Varying in 2a Crack Length From 0.6 to 1.4 Inches



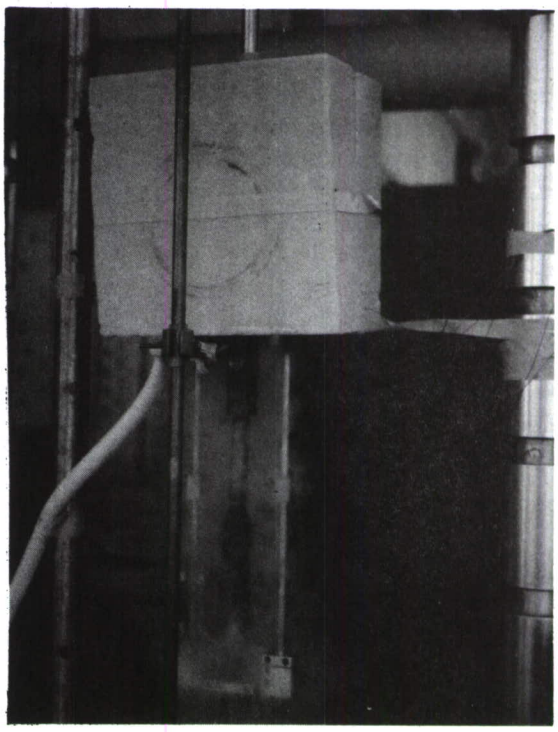
(A)



(B)



(C)



(D)

Figure 26. Cryogenic Tensile Testing Compliance Calibration and Fracture Toughness Apparatus

deflection at σ) are shown in Figures 27 through 40. The experimentally obtained and calculated compliance data for 75° and 350°F (uncorrected for E) are shown in Table IX and plotted in Figure 41 in comparison with the theoretical curve predicted by Westergaard-Irwin equation uncorrected for modulus at 350°F. The theoretical curve is based upon E (modulus of elasticity) and μ (poisson ratio at 75°F).

The calculated compliance data (for 2a crack lengths of 0 to 1.4 at -320°, 75°, and 350°F) from load-deflection experimentally obtained results are tabulated in Table X. The resulting experimentally obtained points are plotted in Figures 42 through 44 to show comparison with theoretical compliance data as a function of crack length for 2024-T3 aluminum alloy.

DISCUSSION

The room and elevated temperature tensile modulus and 0.2 percent yield strength curves were obtained with the developed compliance gage. The above mechanical properties obtained with the compliance gage were in agreement with published data in the open literature. The compliance gage dynamic repeatability was established also by fatigue low-cycling a centrally notched fracture specimen of 2024-T36 with a .010-inch notched radius for a period of 16 hours at 100 cpm. The results showed superposition of hysteresis loops at 20 percent of the yield stress of the specimen and no zero shift at the origin of the loop. From these results, there were present:

1. sensitivity to small deformation
2. negligible friction and deformation of compliance gage

The load-deflection curve for centrally notched fracture specimen (stressed to a pop-in load where a crack initiates under plane strain from a 0.00025-inch radius fatigue crack and grows slowly to a length below the instability crack length under plane stress) is unlike an ordinary elastic-plastic stress-strain curve, since with unloading, the curve tends to return to zero or the origin. The above-mentioned observation was derived from the results of a 2024-T36 aluminum specimen stressed to extend the fatigue crack under slow growth to one-third of the specimen's width. The unloaded curve obtained with the compliance gage on this specimen returned to the zero point. The area within the curve appeared to approximate the elastic energy used to extend the crack.

The experimentally determined load-deflection results obtained on 2024-T3 aluminum alloy tested in accordance with Table IV and automatically curve plotted with the compliance gage as shown in Figures 59 through 64 and reduced as shown in Figures 27 through 40 were used to calculate $\frac{Ev}{\sigma W}$ versus $\frac{\pi a}{W}$ values as shown in Tables IX and X. The plot of the results in Figures 41 through 44 show good agreement of the author's results with Boyle's experimental results and the calculated results from Westergaard-Irwin theoretical equation. The centrally notched test specimens with various 2a crack lengths used in the program are shown in Figure 25.

No problems were encountered while calibrating the compliance gage at room and elevated temperature. However, at cryogenic temperature (-320°F) it was found that the entire test specimen and grips had to be cooled to avoid specimen failure at the grip ends of the specimen rather than in the test section. When only the test section was cooled down to -320°F, the tensile and centrally notched specimens would fracture in the pinholes of the gripping ends of the specimens. This was attributed to the increased fracture strength in the cryogenic cooled section of the test specimen as opposed to the uncooled ends. The increase in strength under the above condition was enough to offset the loss in ductility to shift failure to the pinholes, because the fracture strength at the pinholes was lower than the test section fracture strength. As a result, failure occurred in the pinholes.

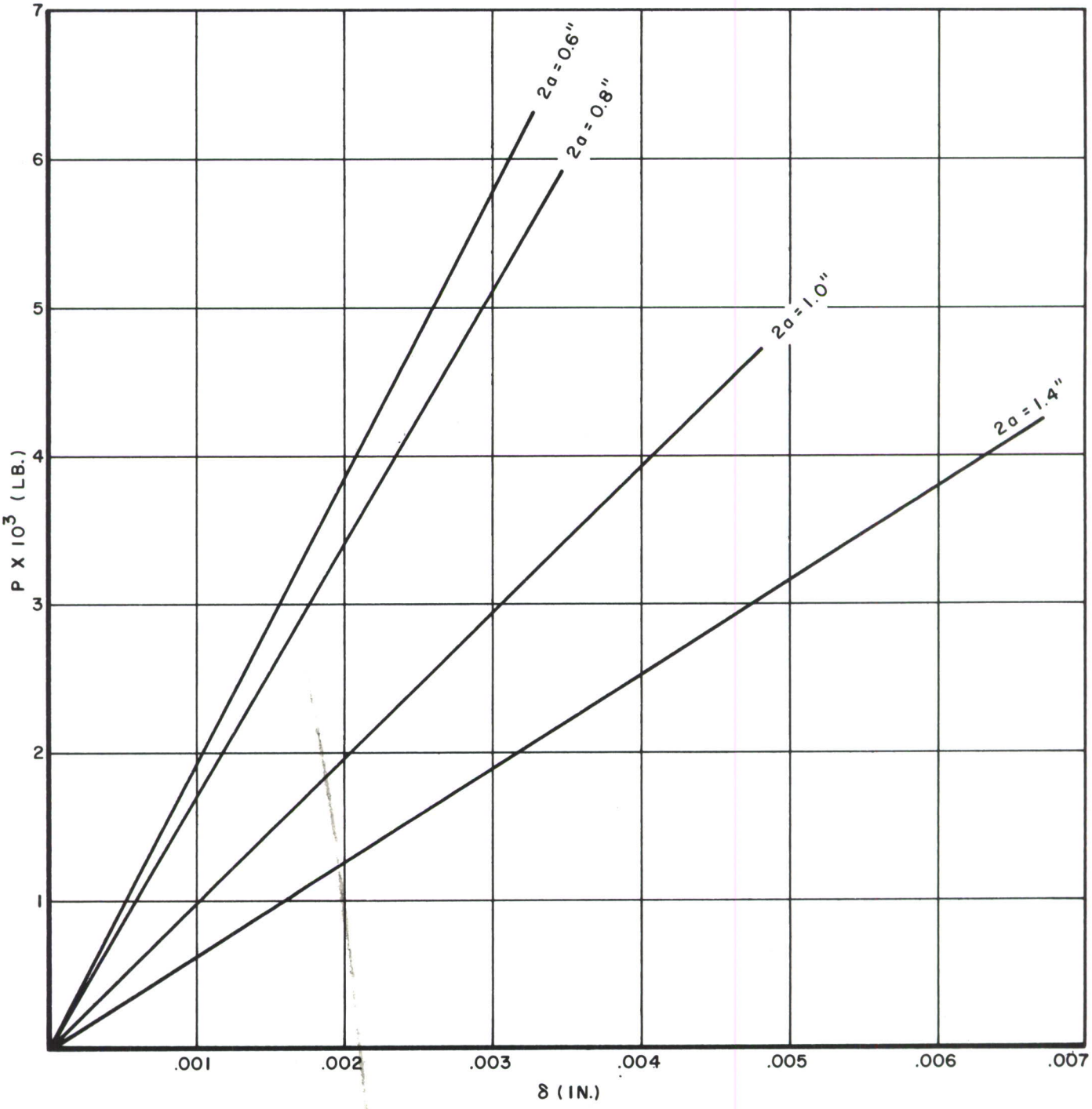


Figure 27. Derived Load-Deflection Curves for Centrally Notched Specimens, -320°F, Longitudinal

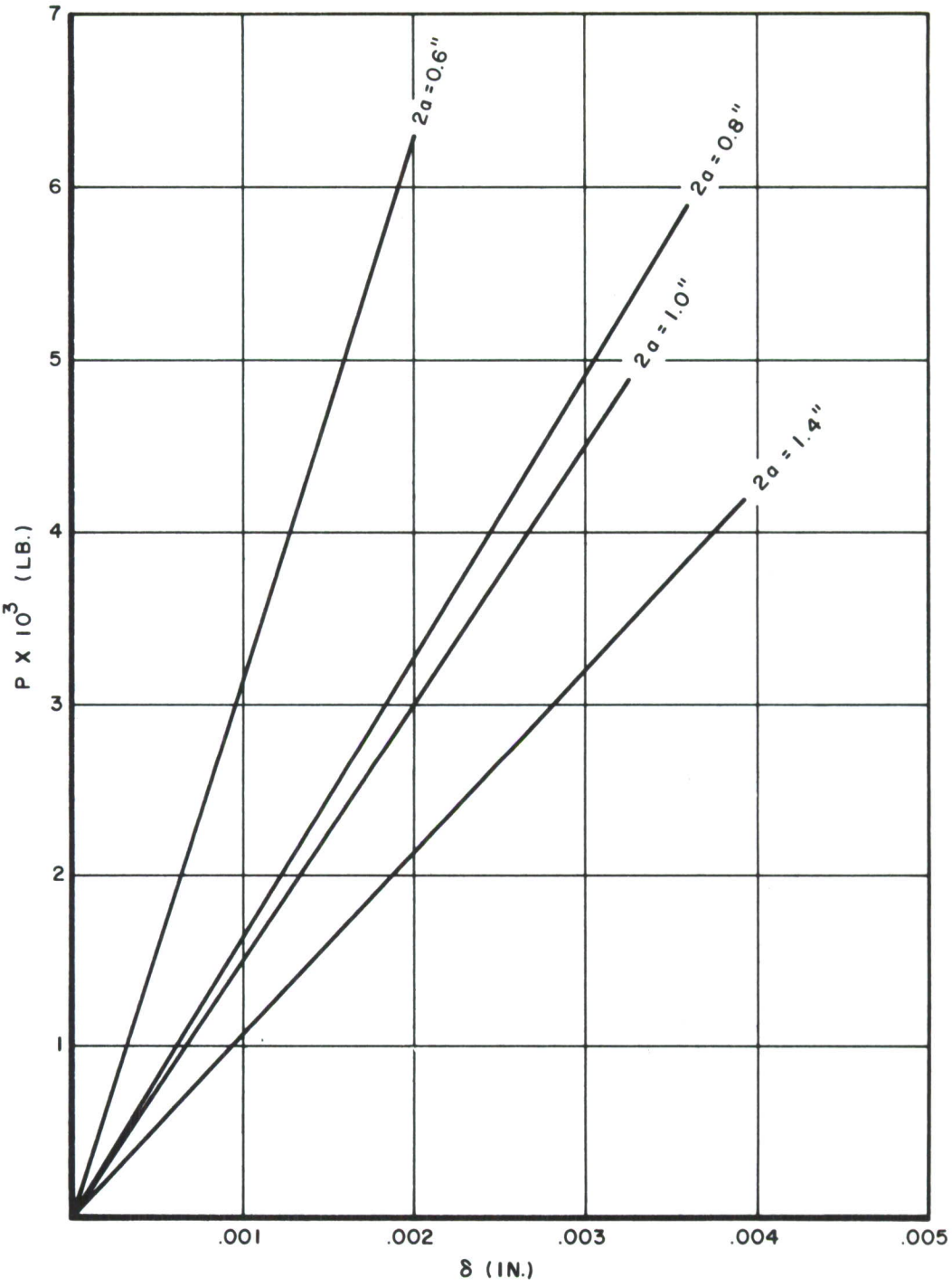


Figure 28. Derived Load-Deflection Curves for Centrally Notched Specimens, -320°F, Transverse

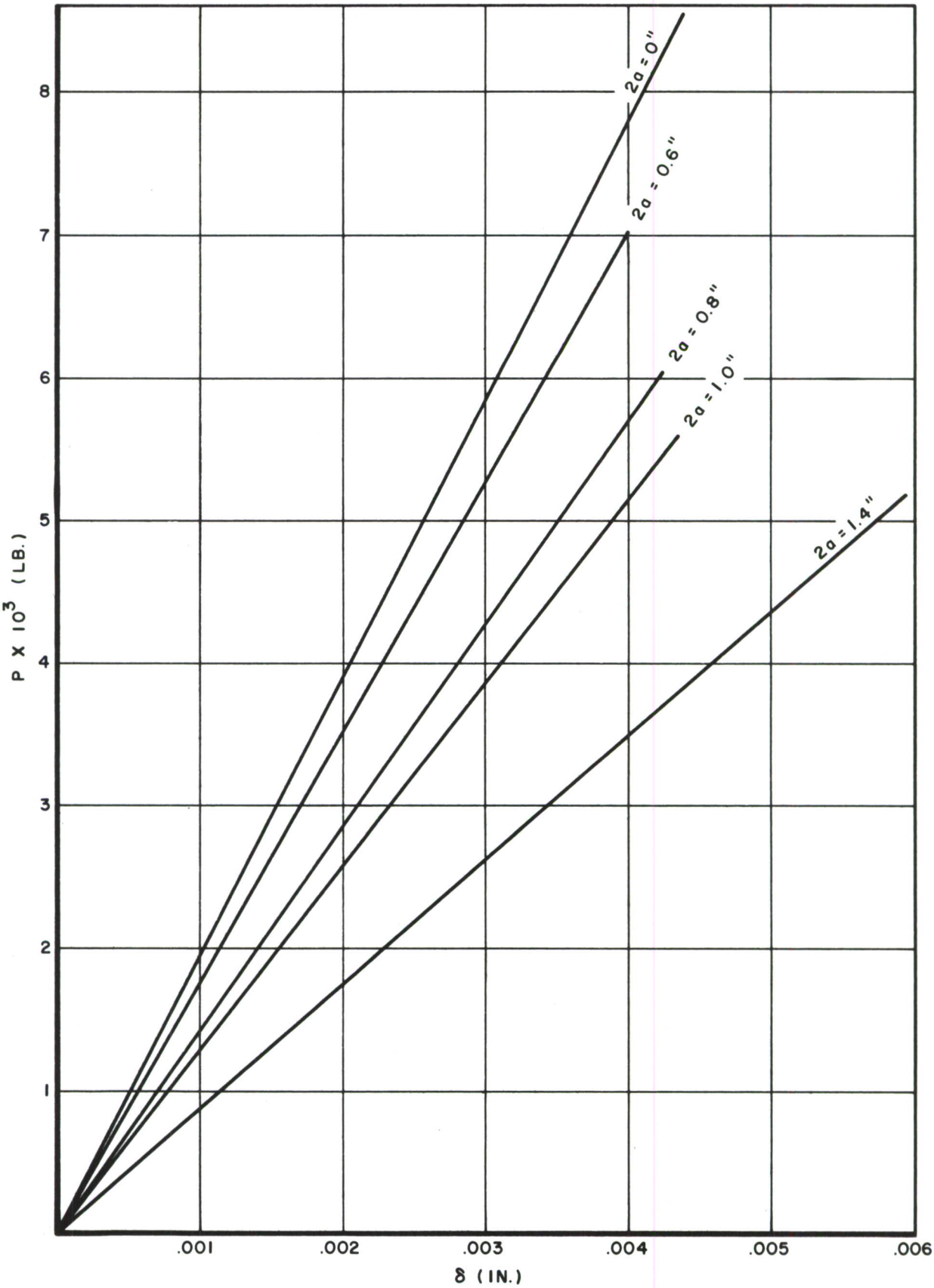


Figure 29. Derived Load-Deflection Curves for Centrally Notched Specimens, 75°F, Longitudinal

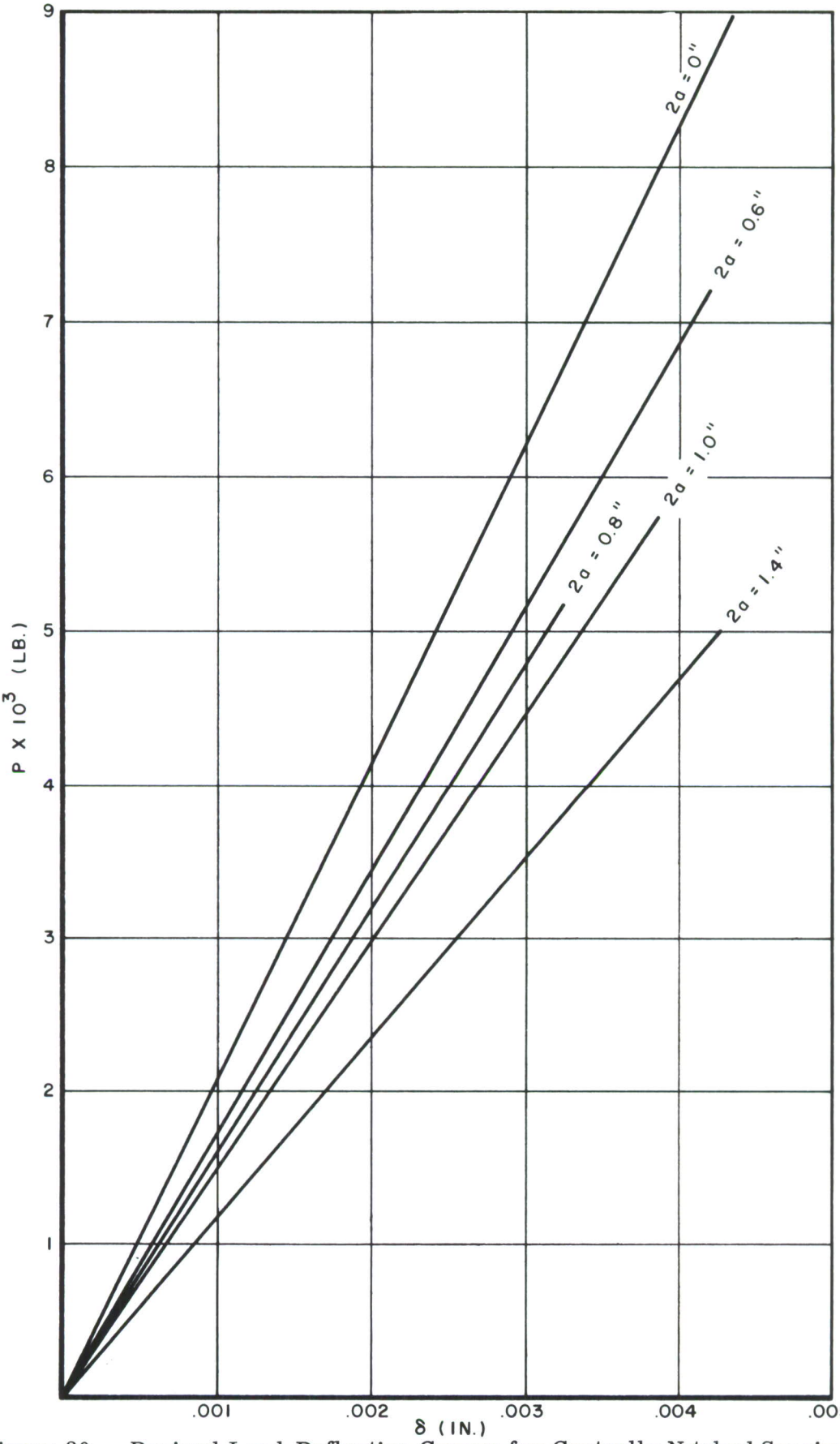


Figure 30. Derived Load-Deflection Curves for Centrally Notched Specimens, 75°F, Transverse

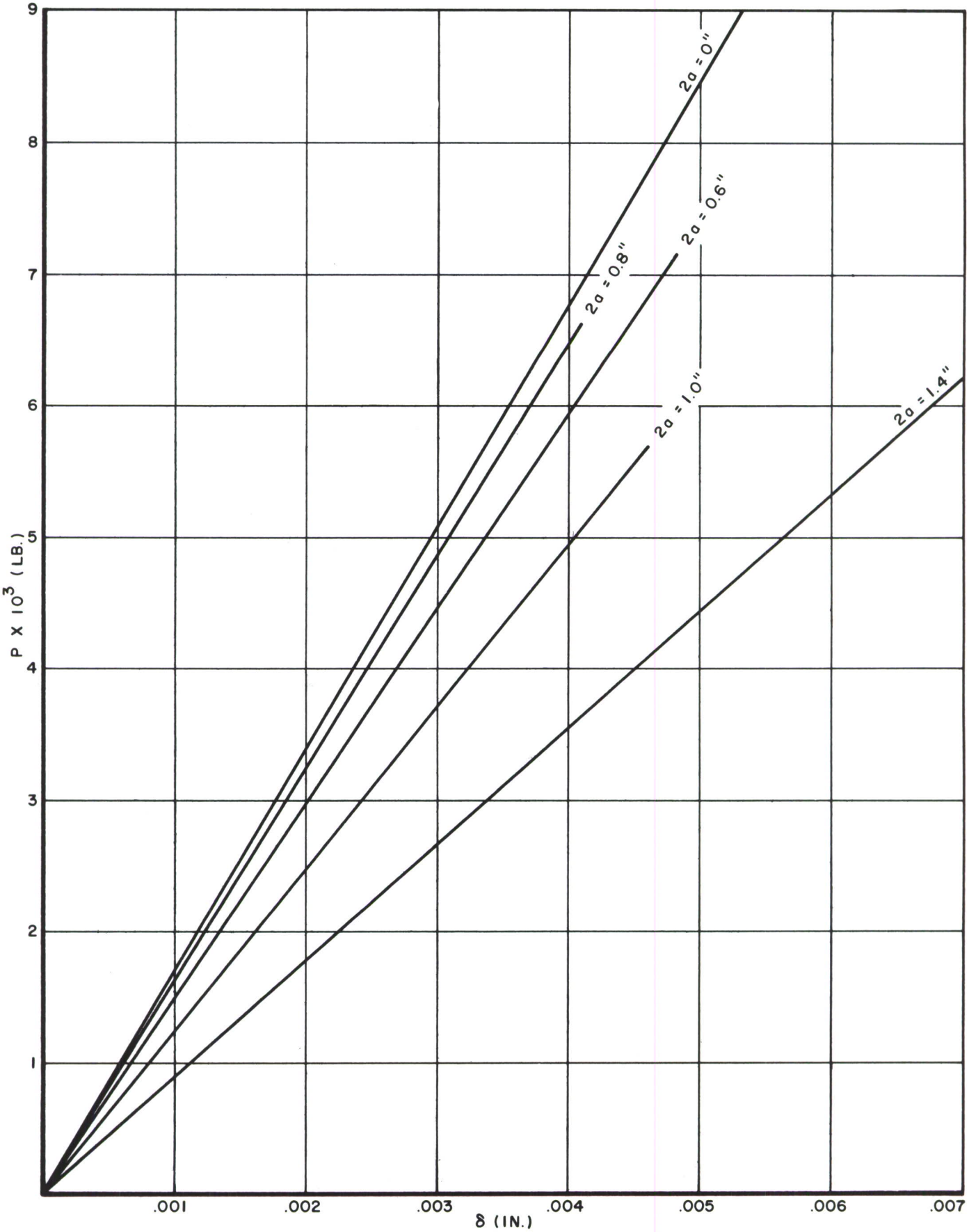


Figure 31. Derived Load-Deflection Curves for Centrally Notched Specimens, 350°F, Longitudinal

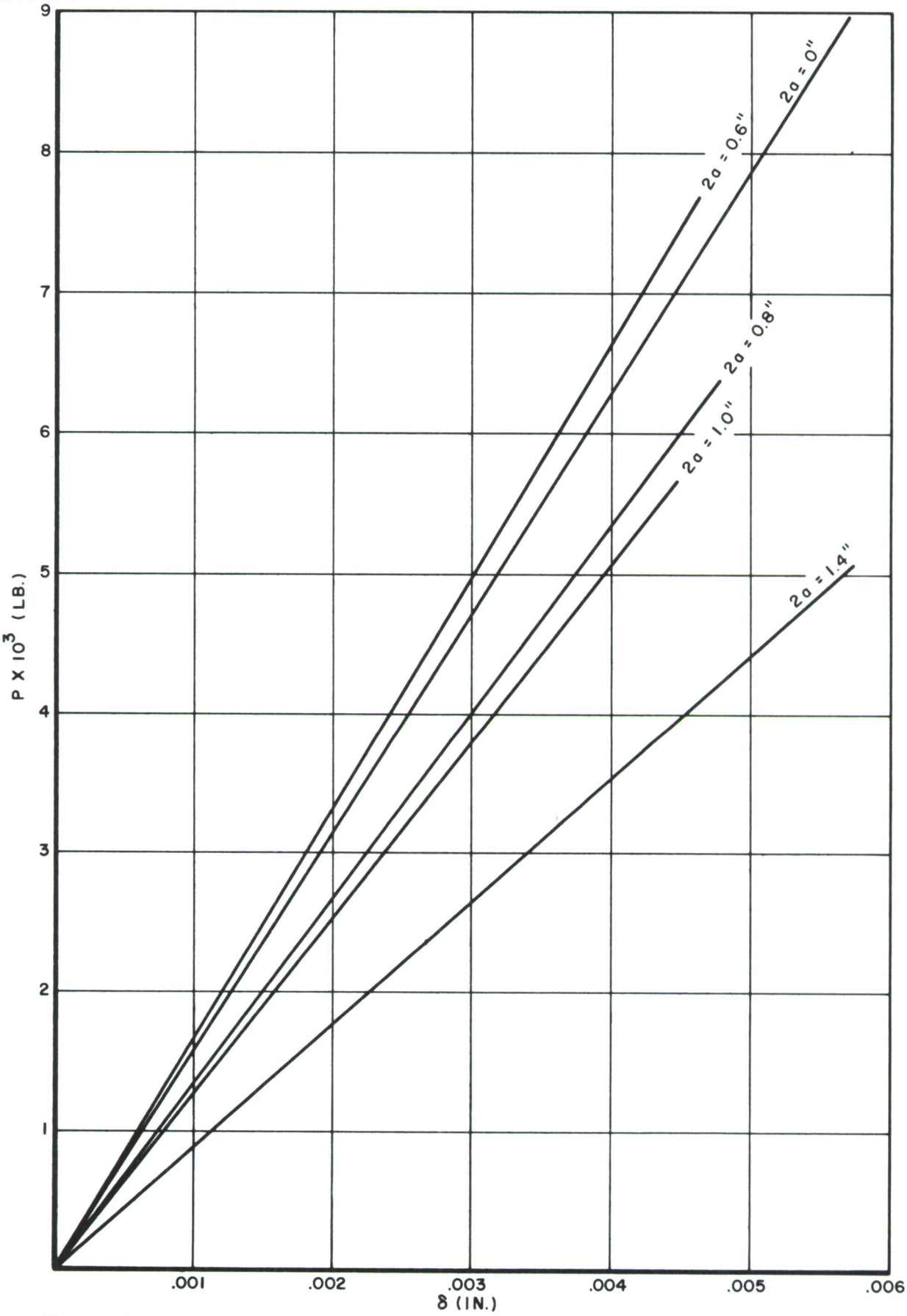


Figure 32. Derived Load-Deflection Curves for Centrally Notched Specimens, 350°F, Transverse

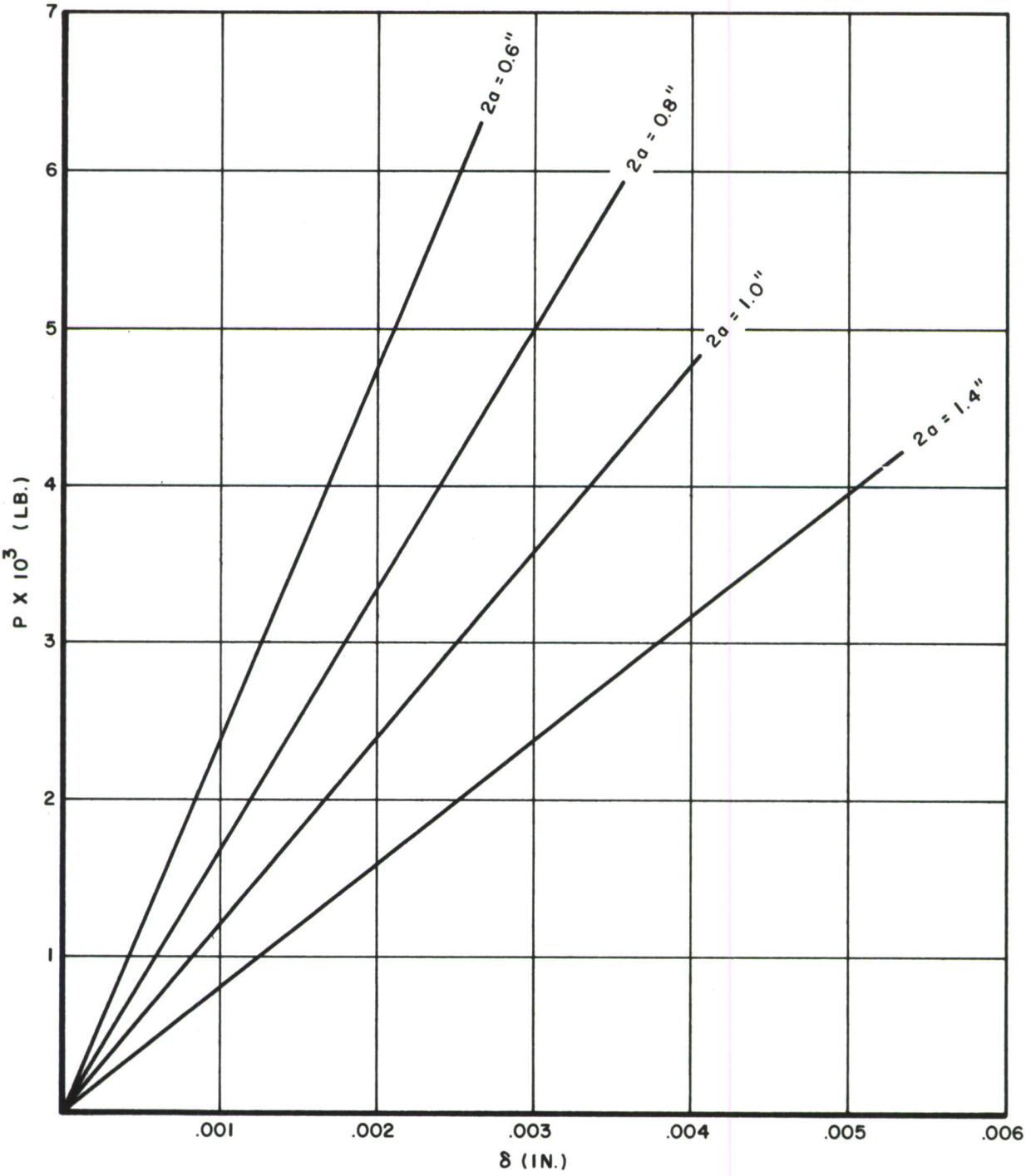


Figure 33. Averaged Transverse and Longitudinal Load-Deflection Curves for Centrally Notched Specimens, -320°F

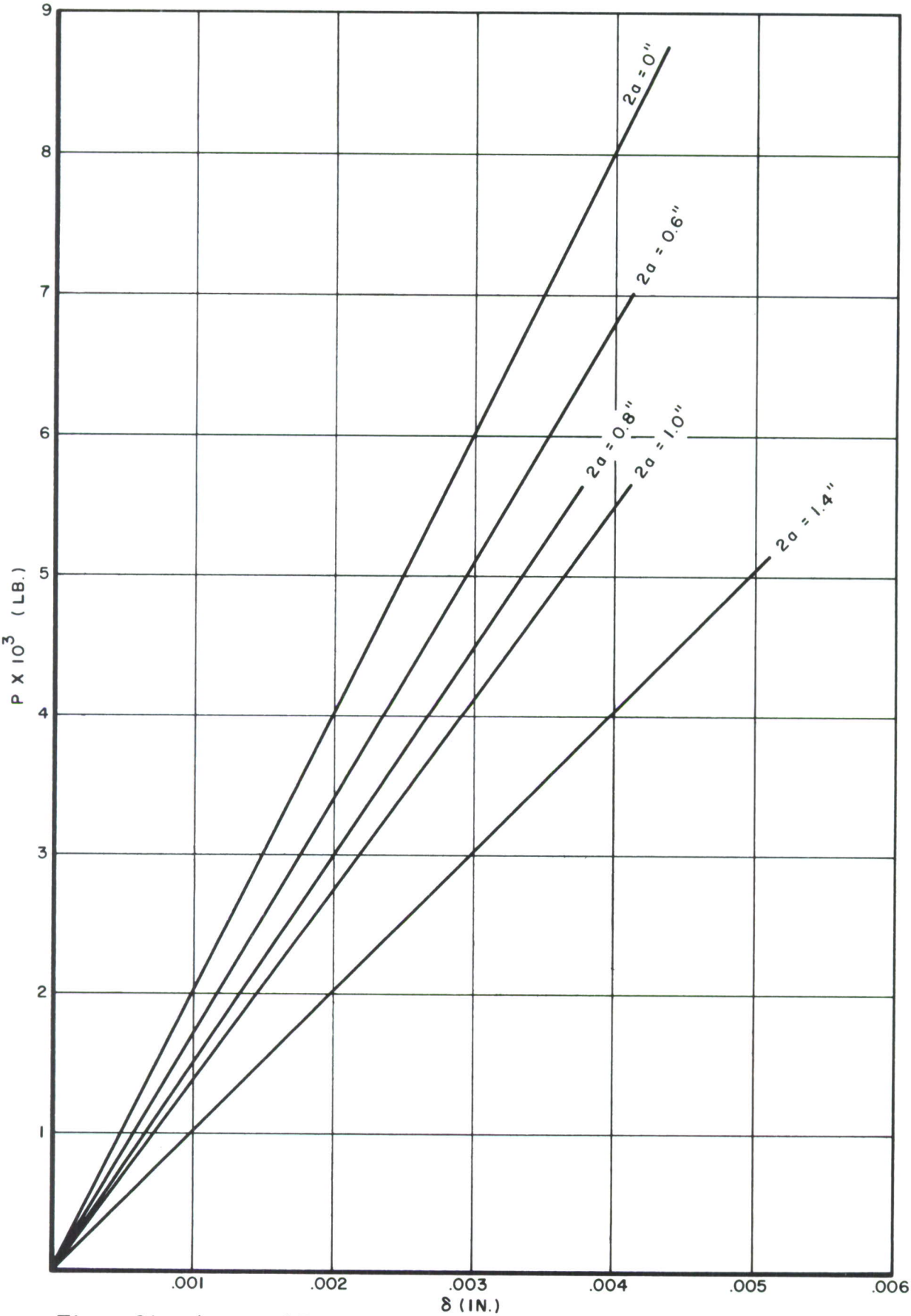


Figure 34. Averaged Transverse and Longitudinal Load-Deflection Curves for Centrally Notched Specimens, 75°F

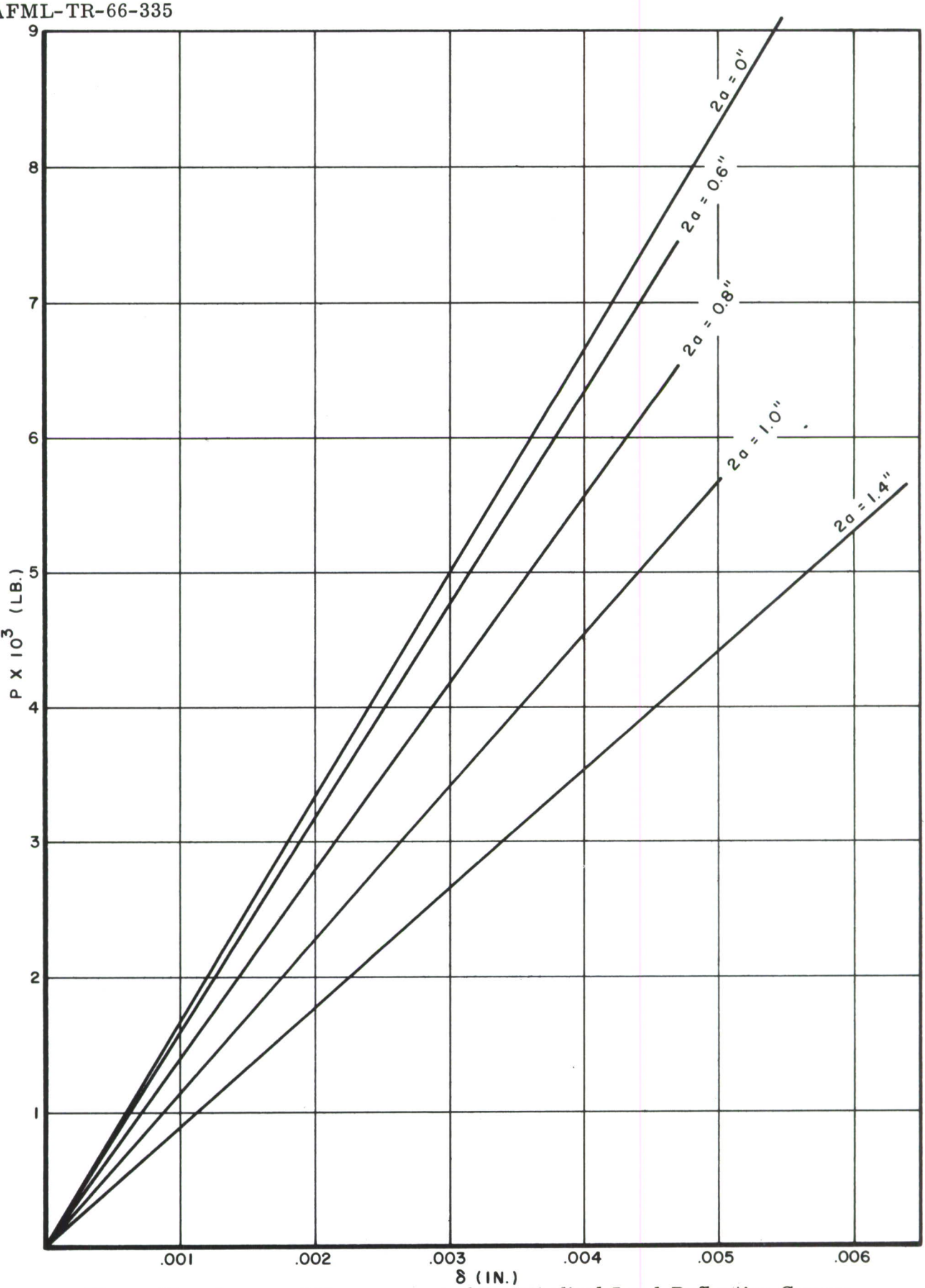


Figure 35. Averaged Transverse and Longitudinal Load-Deflection Curves for Centrally Notched Specimens, 350°F

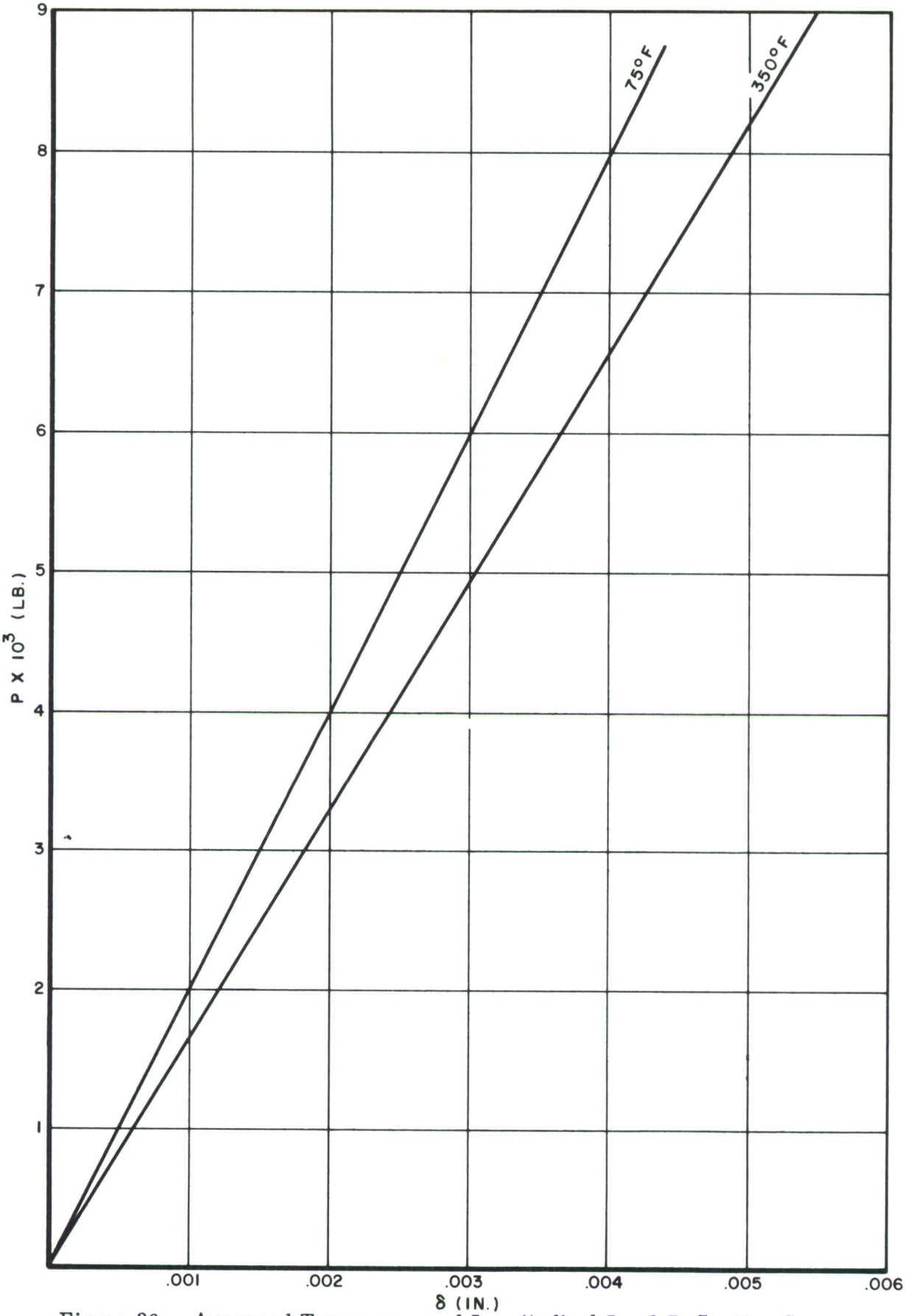


Figure 36. Averaged Transverse and Longitudinal Load-Deflection Curves for Centrally Notched Specimens, 2a = 0

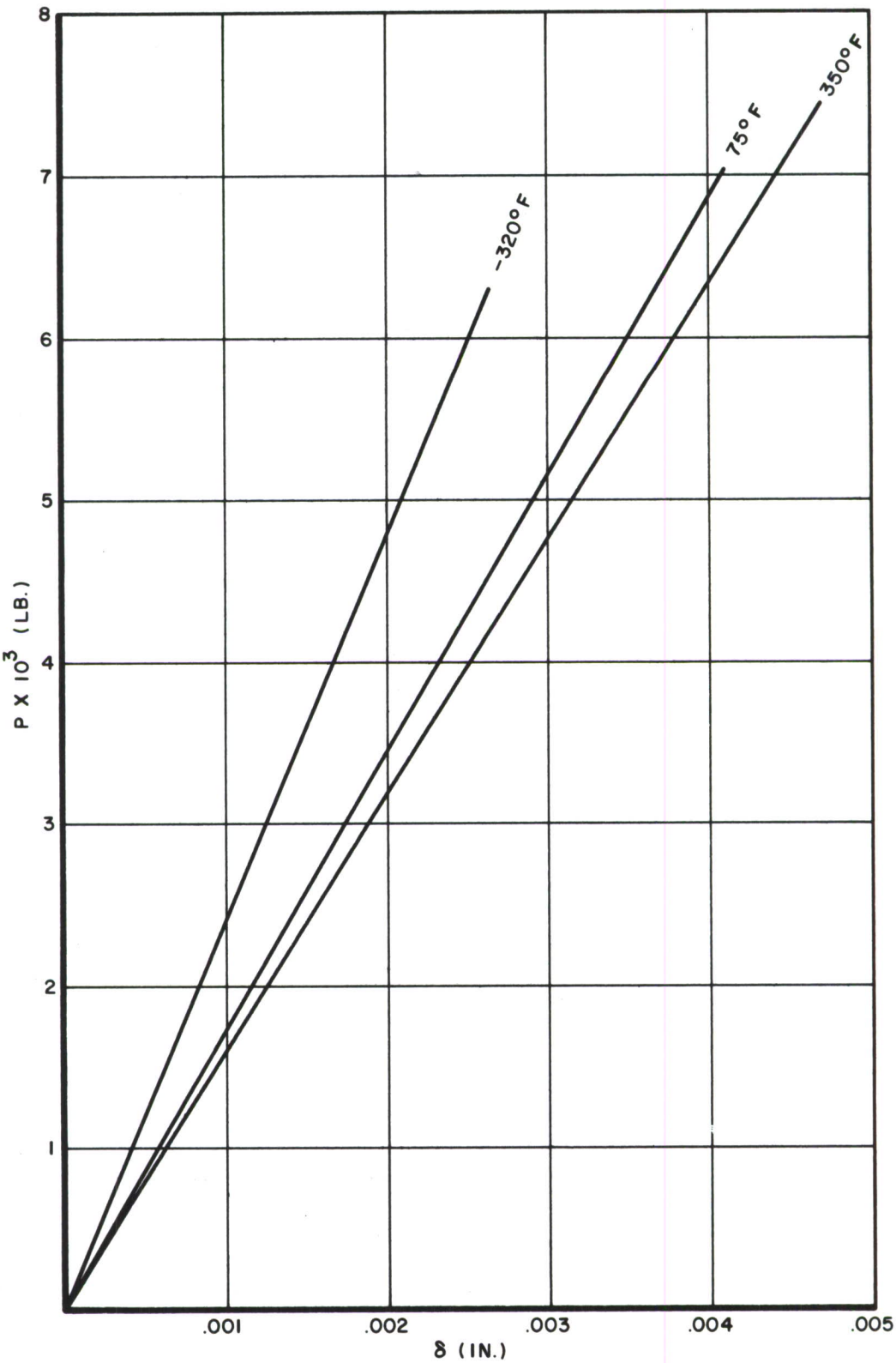


Figure 37. Averaged Transverse and Longitudinal Load-Deflection Curves for Centrally Notched Specimens, 2a = 0.6

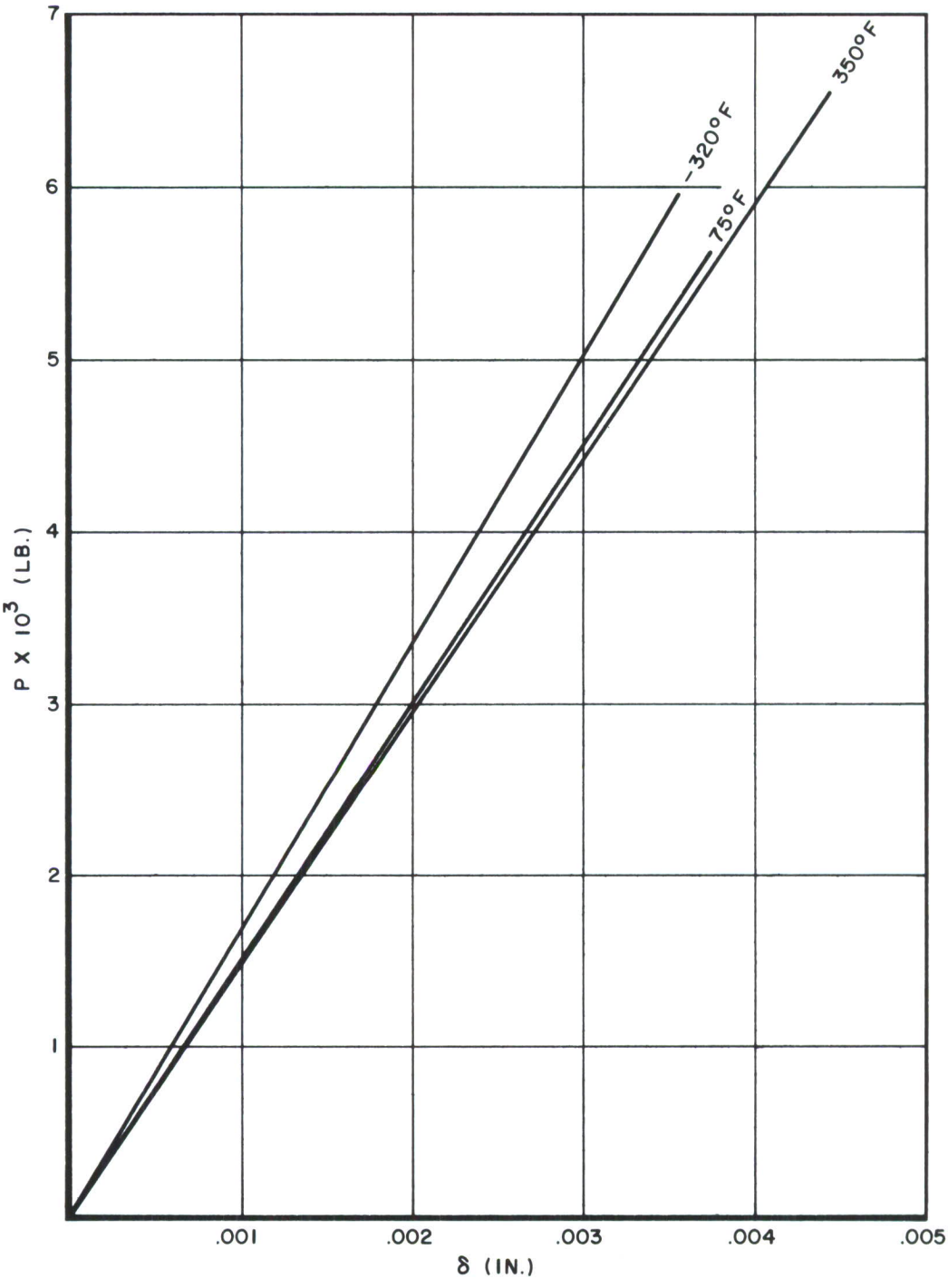


Figure 38. Averaged Transverse and Longitudinal Load-Deflection Curves for Centrally Notched Specimens, 2a = 0.8

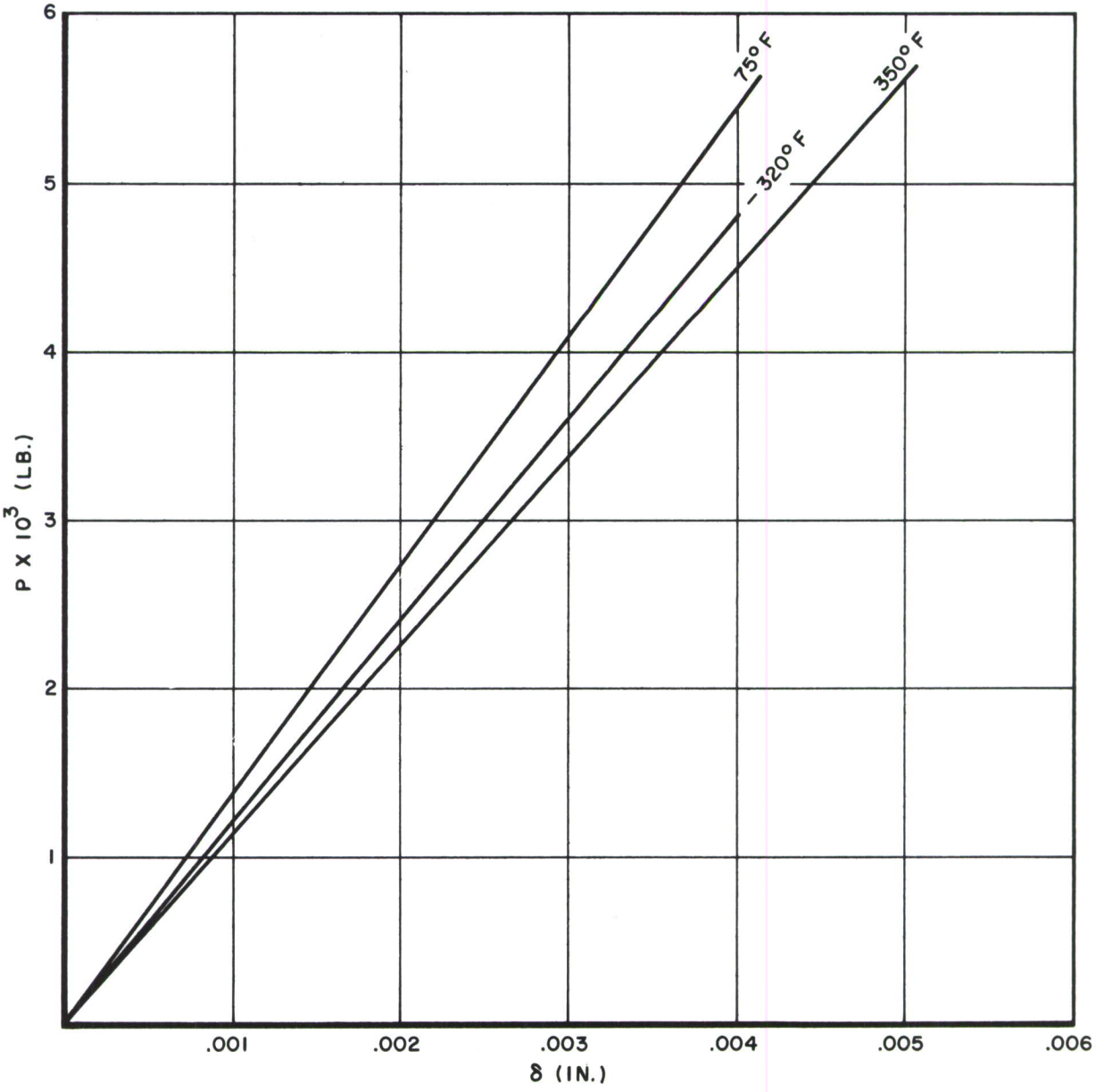


Figure 39. Averaged Transverse and Longitudinal Load-Deflection Curves for Centrally Notched Specimens, 2a = 1.0

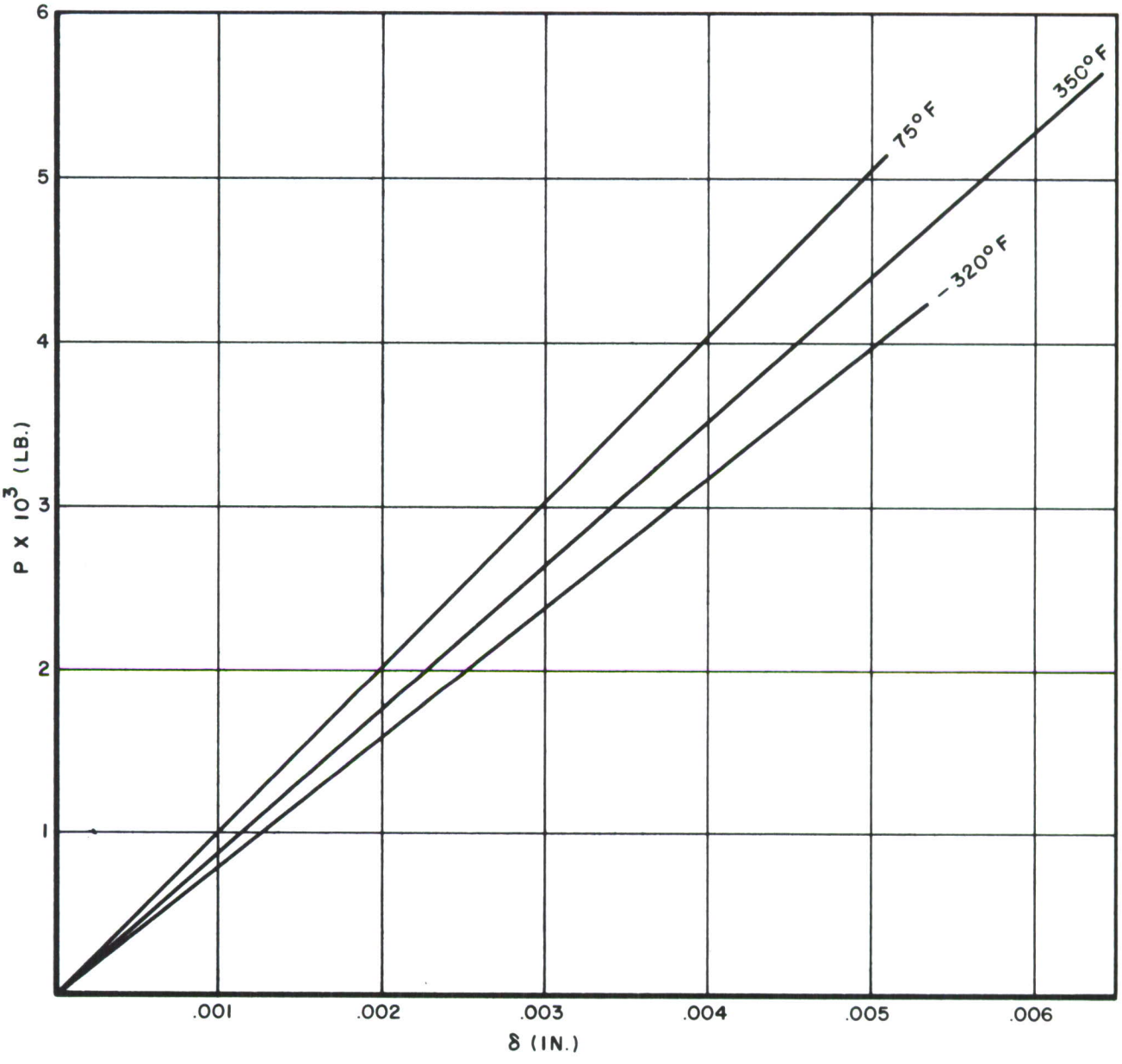


Figure 40. Averaged Transverse and Longitudinal Load-Deflection Curves for Centrally Notched Specimens, 2a = 1.4

TABLE IX

COMPLIANCE GAGE EXPERIMENTAL DATA*

SPECIMEN NO.	2a	E	W	V	σ	$\frac{Ev}{\sigma W}$	$\frac{\pi a}{W}$
LC-1-75	0	10.6×10^6	3	.002	22,890	.31	0
LC-2-75	.6	10.6×10^6	3	.002	18,700	.38	.314
LC-3-75	.8	10.6×10^6	3	.002	16,040	.439	.418
LC-4-75	1.0	10.6×10^6	3	.002	14,360	.492	.524
LC-5-75	1.4	10.6×10^6	3	.0026	14,100	.628	.732
TC-1-75	0	10.6×10^6	3	.0021	23,890	.3105	0
TC-2-75	.6	10.6×10^6	3	.002	18,720	.377	.314
TC-3-75	.8	10.6×10^6	3	.002	16,100	.438	.418
TC-4-75	1.0	10.6×10^6	3	.0021	15,150	.486	.524
TC-5-75	1.4	10.6×10^6	3	.00224	13,380	.596	.732
LC-1-350	0	10.6×10^6	3	.00272	24,000	.329	0
LC-21350	.6	10.6×10^6	3	.0024	20,600	.338	.314
LC-3-350	.8	10.6×10^6	3	.0023	17,190	.388	.418
LC-4-350	1.0	10.6×10^6	3	.0023	15,100	.442	.524
LC-5-350	1.4	10.6×10^6	3	.0028	13,550	.599	.732
TC-1-350	0	10.6×10^6	3	.00250	24,100	.322	0
TC-2-350	.6	10.6×10^6	3	.00230	19,100	.373	.314
TC-3-350	.8	10.6×10^6	3	.002	17,550	.353	.418
TC-4-350	1.0	10.6×10^6	3	.0028	15,280	.568	.524
TC-5-350	1.4	10.6×10^6	3	.0035	16,550	.656	.732

*NOTE: See Table X for definition of terms. Tabulated data plotted in Figure 41.

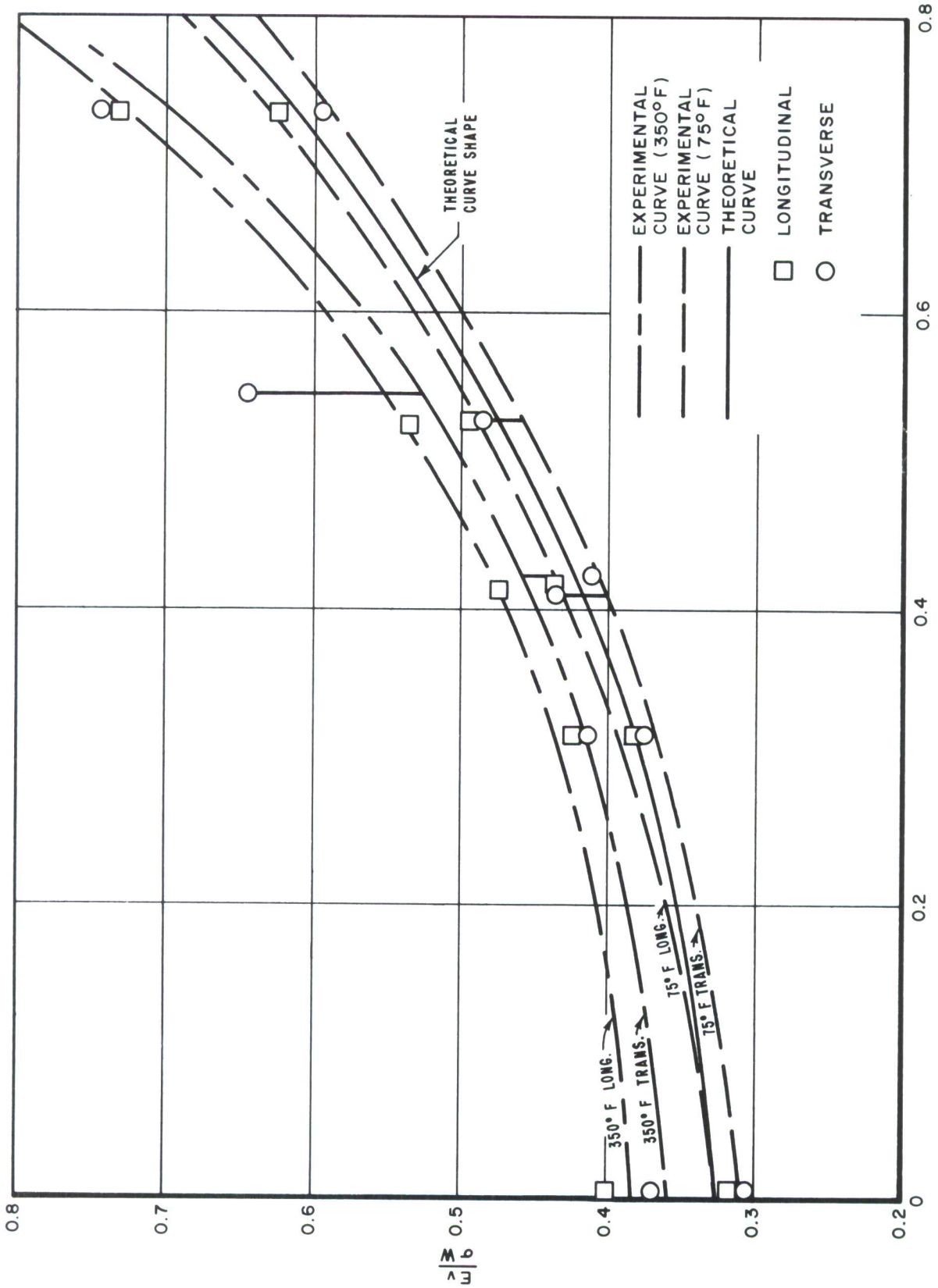


Figure 41. Theoretical and Experimental Compliance as a Function of Crack Length

TABLE X

ELASTIC COMPLIANCE GAGE EXPERIMENDTAL DATA

SPECIMEN NO.	2a	E	W NOMINAL	V	σ	$\frac{Ev}{\sigma W}$	$\frac{\pi a}{W}$
Cryogenic							
LC-1-320	0	11×10^6	3				
LC-2-320	.6	11×10^6	3	.00164	16,800	.365	.324
LC-3-320	.8	11×10^6	3	.00174	15,813	.403	.418
LC-4-320	1.0	11×10^6	3	.0024	12,560	.700	.524
LC-5-320	1.4	11×10^6	3	.00336	11,333	1.087	.732
Cryogenic							
TC-1-320	0	11×10^6	3				
TC-2-320	.6	11×10^6	3	.0010	16,800	.218	.314
TC-3-320	.8	11×10^6	3	.0018	15,733	.419	.418
TC-4-320	1.0	11×10^6	3	.00164	13,067	.460	.524
TC-5-320	1.4	11×10^6	3	.00196	11,200	.642	.732
Room Temp.							
LC-1-75	0	10.2×10^6	3	.0022	22,880	.327	0
LC-2-75	.6	10.2×10^6	3	.002	18,720	.363	.314
LC-3-75	.8	10.2×10^6	3	.00212	16,160	.446	.418
LC-4-75	1.0	10.2×10^6	3	.00216	14,933	.492	.524
LC-5-75	1.4	10.2×10^6	3	.00296	14,080	.715	.732
Room Temp.							
TC-1-75	0	10.2×10^6	3	.00216	23,867	.307	0
TC-2-75	.6	10.2×10^6	3	.0021	18,720	.381	.314
TC-3-75	.8	10.2×10^6	3	.00162	13.840	.398	.418
TC-4-75	1.0	10.2×10^6	3	.00194	15,180	.431	.524
TC-5-75	1.4	10.2×10^6	3	.00214	13,360	.544	.732

TABLE X (CONT'D)

ELASTIC COMPLIANCE GAGE EXPERIMENTAL DATA

SPECIMEN NO.	2a	E	W NOMINAL	V	σ	$\frac{Ev}{\sigma W}$	$\frac{\pi a}{W}$
Elevated Temp.							
LC-1-350	0	8.7×10^6	3	.00266	24,053	.320	0
LC-2-350	.6	8.7×10^6	3	.0024	19,067	.365	.314
LC-3-350	.8	8.7×10^6	3	.00204	17,733	.334	.418
LC-4-350	1.0	8.7×10^6	3	.0028	15,227	.533	.524
LC-5-350	1.4	8.7×10^6	3	.00354	16,533	.621	.732
Elevated Temp.							
TC-1-350	0	9.3×10^6	3	.0028	24,000	.361	0
TC-2-350	.6	9.3×10^6	3	.0023	20,533	.347	.314
TC-3-350	.8	9.3×10^6	3	.00238	17,173	.429	.418
TC-4-350	1.0	9.3×10^6	3	.00224	15,173	.457	.524
TC-5-350	1.4	9.3×10^6	3	.00286	13,547	.654	.732

NOTE: E = Young's Modulus
V = Deflection of a point 1 inch above or below the crack initiating slot that is ½ measured specimen deflection.
σ = Gross stress on specimen
W = Specimen width
A = ½ initial slot length
Tabulated data for Figures 42, 43 and 44.

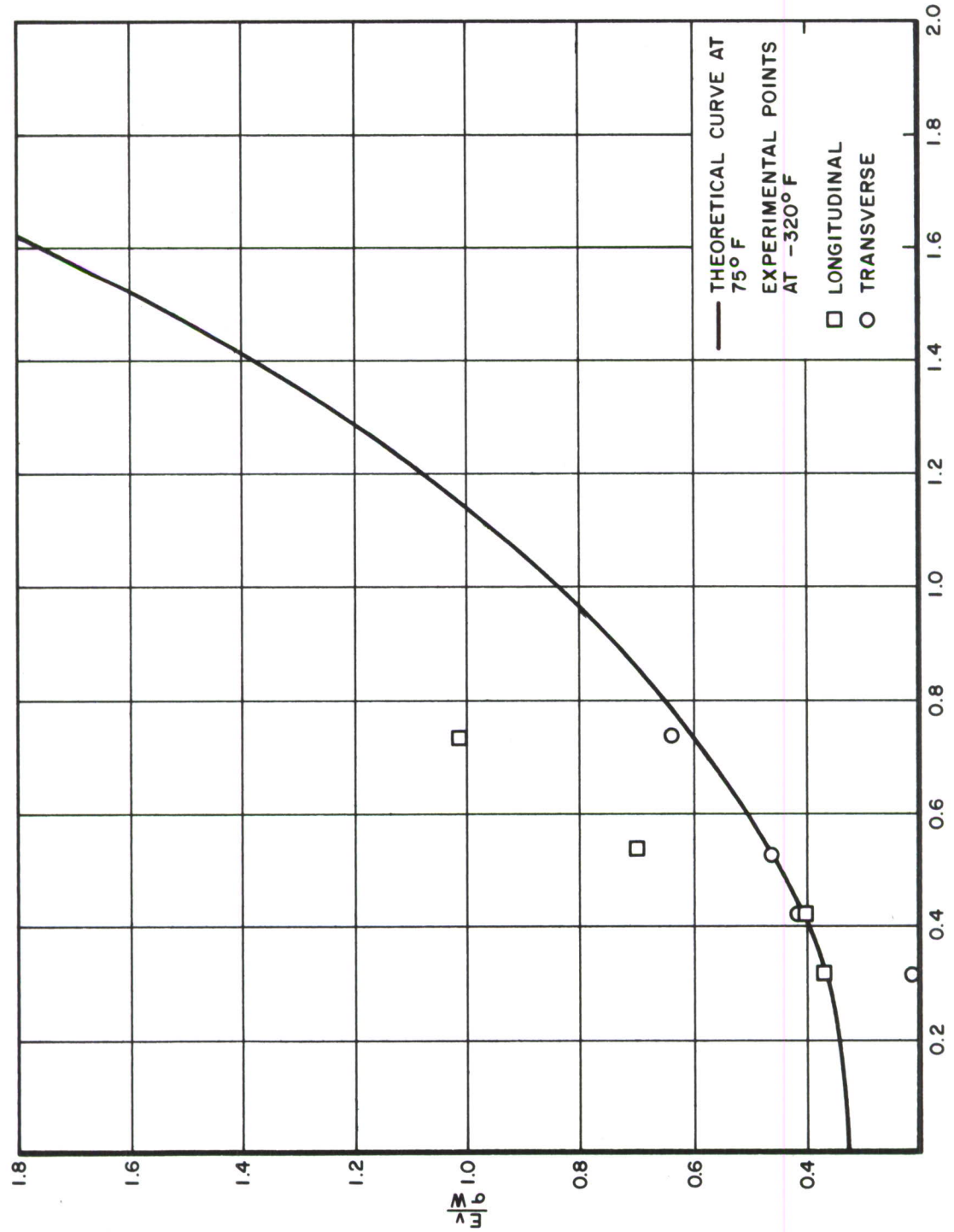


Figure 42. Example Theoretical and Experimental (-320°F) Compliance as a Function of Crack Length

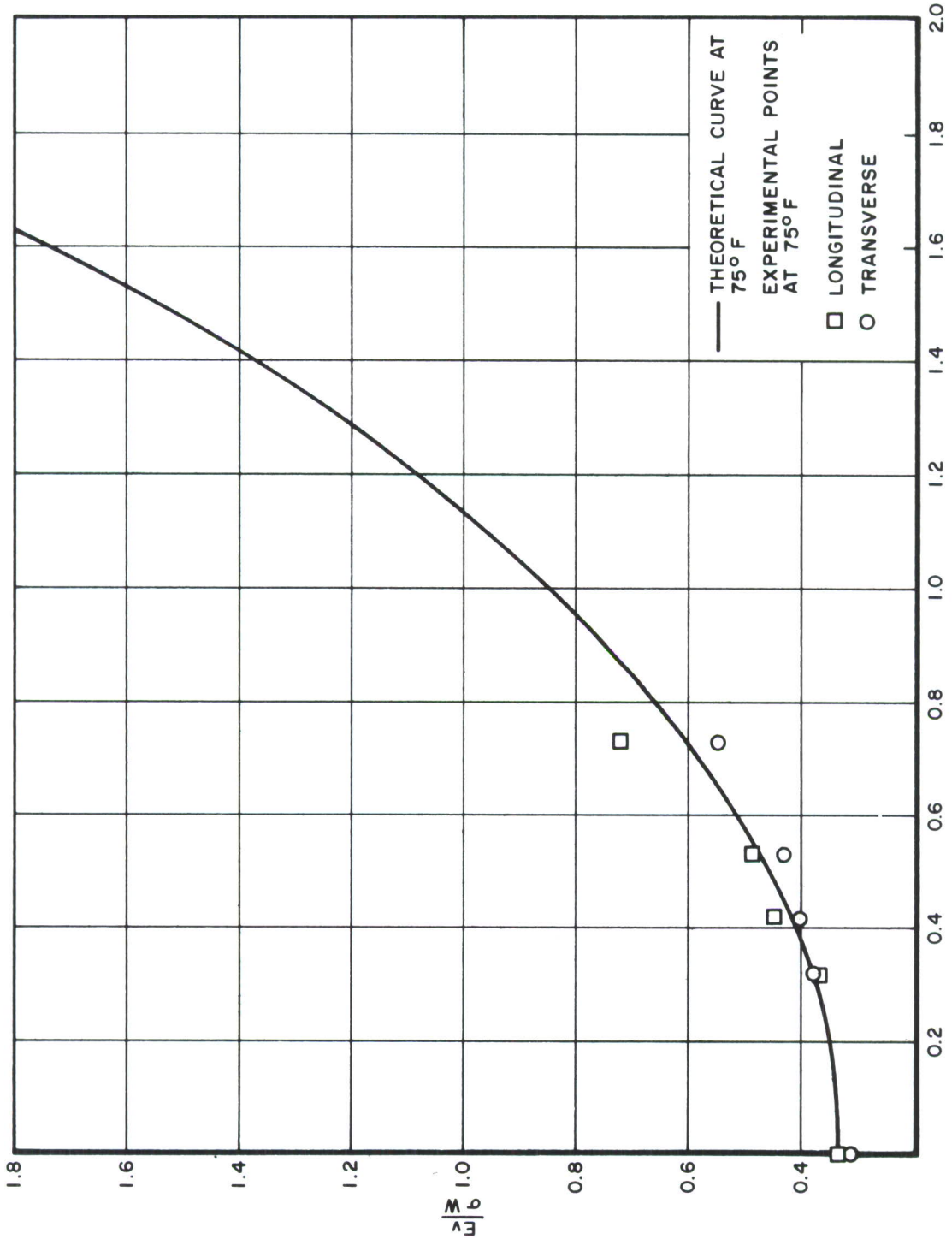


Figure 43. Example Theoretical and Experimental (75°F) Compliance as a Function of Crack Length

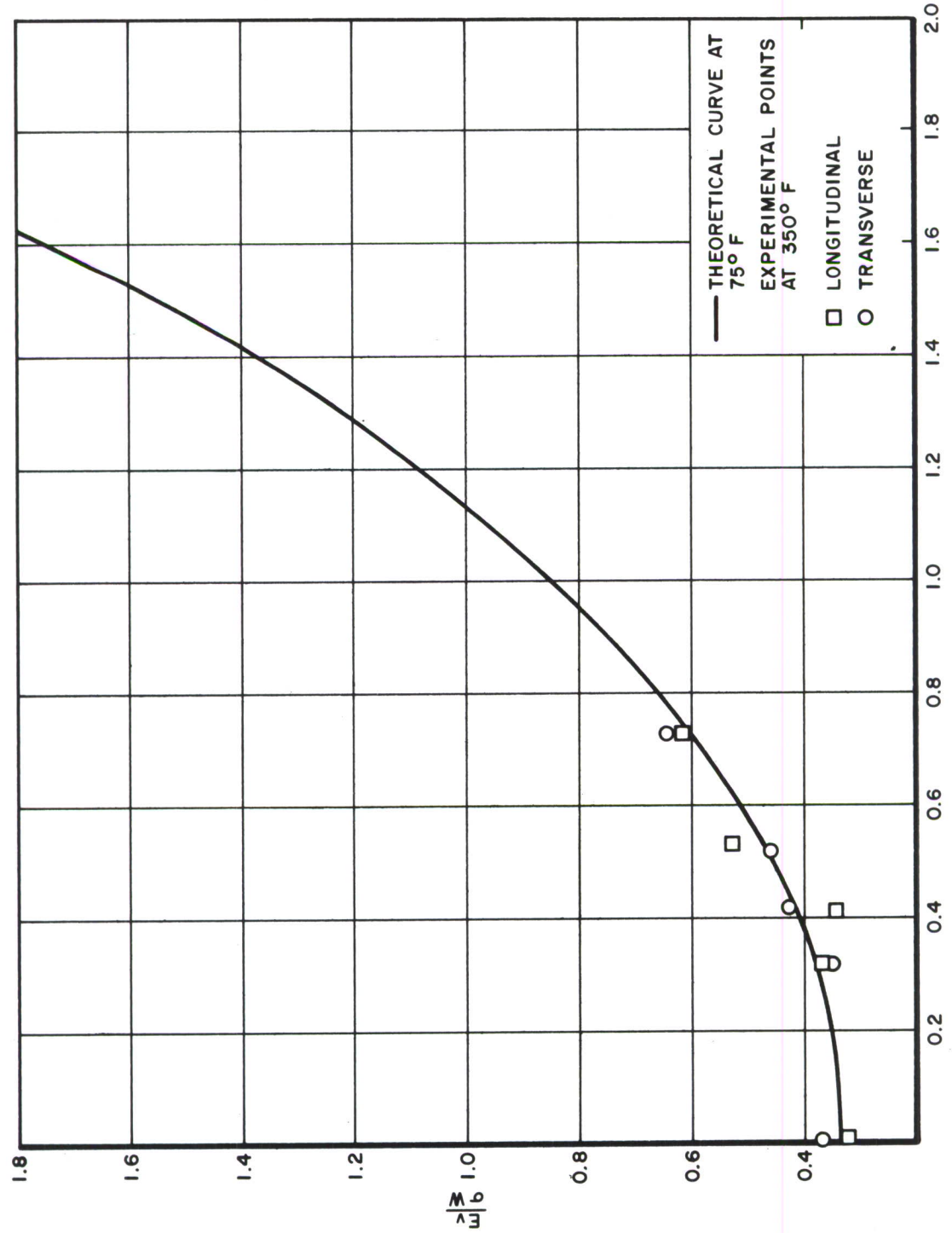


Figure 44. Example Theoretical and Experimental (350°F) Compliance as a Function of Crack Length

At least four thermocouples should be used. Preferably two thermocouples should be placed at the tip of the crack along the remaining area and near the side edges of the specimen. The other two should be placed at the outer edges of the gage length. These thermocouples should be calibrated in liquid N_2 before using. To obtain valid test information, the temperature of all test apparatus inside and outside of the cold-box (Figure 26D) must be allowed to stabilize. This stabilization will occur in approximately 15 to 20 minutes with a constant flow mist of cryogenic fluid sprayed directly on both sides of the test specimen.

Spring plunger loading screws on compliance gage should be tightened before beginning test after obtaining equilibrium test temperature to avoid surface contact between the rods and tubes of the compliance gage. The extensometer and the legs of the compliance gage outside of the cold chamber must be kept at a constant and equal temperature, preferably ambient. If this is not accomplished, one leg of the compliance gage will become longer than the other due to differential contraction of the two legs. As a consequence, the heads of the compliance gage will become cocked and will shift the zero of the extensometer attached to one of the legs of the gage (Figure 21A and B plus Figure 26D). Also, the resistance of the extensometer coil shown in Figure 21B will change causing an incorrect output. This problem was solved by blowing room temperature air over the legs of the compliance gage and the electrical extensometer located outside of the cryogenic cold-box shown in Figure 26D.

There appears to be wider scatter in compliance data at -320° than at 75° and 350°F when comparing Figures 41 through 44 with respect to the experimental points plotted in comparison with the theoretical compliance curve. Experimental scatter exists in Figure 41 through 44. The compliance of the specimens was measured under stresses 40 to 60 percent of that required to produce crack extension.

The compliance measured at lower stresses should give much better agreement with the theoretical curve than the compliances measured at the higher stresses. This is rationalized to be expected since the stress analysis is valid only for very small strains. The difference in compliance measured for the low and high stress with respect to the stress required to produce crack extension demonstrates that the "elastic region" of a load-extension curve for a centrally cracked specimen is not linear but curved as shown in Figures 59 through 64 in the Appendix. One may rationalize two distinct compliances: one the limit of compliance as stress approaches zero (which is compliance described in the stress analysis) and the other a practical compliance taken as the average compliance over the so-called elastic region. Figures 42 through 44 are the curves that were used subsequently for the determination of K_{Ic} (where applicable) and K_c stress intensity factors and critical crack lengths at -320°, 75°, and 350°F.

The calibration curves should be valid for other materials and at other temperatures. All that is required is that Young's modulus of elasticity be known for the material at the desired temperature plus the σ, v, and W parameters.

SECTION VII

CRYOGENIC, ELEVATED TEMPERATURE EXPERIMENTAL FRACTURE TOUGHNESS RESULTS AND DISCUSSION

RESULTS

The original load-deflection curves to fracture of the centrally notched test specimens at -320°, 75°, and 350°F are shown in Figure 65 through 70. The curves are shown collectively in Figure 45. Fractographs of the centrally notched specimens tested for fracture toughness at -320°, 75°, and 350°F are depicted in Figure 46. Tabulated results are shown in Table XI and are summarized in Table XII.

DISCUSSION

Figures 65 through 70 were used to determine the pop-in load under plane strain of the 2024-T3 aluminum specimens at -320°, 75°, and 350°F to calculate the K_{Ic} plane strain stress intensity factor. However, a pop-in load was only evident at -320°F on the longitudinal test specimen, where the crack was perpendicular to the longitudinal fibers of the specimen. In the -320°F transverse specimen test, (where the crack was parallel to the longitudinal fibers of the specimen) there was no evidence of pop-in. However deviation from linearity load versus pop-in load was 12,000 and 11,600 pounds, respectively. The mode of fracture of the -320°F fractured centerally notched specimens shown in Figure 46A and B was cleavage which indicated a brittle response. On the other hand, the 75° and 350°F test specimens mode of fracture was single shear which exhibited a ductile response. This was also quite evident in the tensile tests. The load-deflection curves at 75° and 350°F showed no signs of a pop-in load. The fractured surfaces as shown in Figure 46A and B exhibited 100 percent shear. The net fracture stress to yield stress ratio for all of the tests collectively varied between 0.9 and 1.0.

As discussed under Section II, the net stress at failure of a specimen under test for fracture toughness is a relative good measure of resistance to fracture. In Figure 2, the ratio σ_{net}/σ_{YS} is plotted versus σ_{YS}/E for aluminum and other metals with gage sections from 0.06 to 0.130 inch thick. It was stipulated that two types of information be extracted from this plot. First, there was a change in slope for each particular class of alloys at different values of σ_{YS}/E. This occurred at a σ_{net}/σ_{YS} value of about 0.75 for aluminum alloys. It was further stated that these transition points suggest that for values of σ_{YS}/E greater than those indicated, the K_c value obtained is probably good quantitative information. However, it was further stated that σ_{net}/σ_{YS} less than approximately 0.75 for aluminum alloys, 0.90 for steels, and 1.0 for titanium makes the fracture toughness approach very useful. However, based upon the data obtained for 2024-T3 aluminum alloy, this material can be designed into a structure incorporating the design criteria of gross plastic flow before failure at 75° and 350°F. However at -320°F much safer and more reliable design criteria would be fracture toughness and severity of defects, because the increased strength at -320°F increases the probability that the material will fail from a severe defect rather than from gross plastic flow as it would at 75° or 350°F. This is assuming that the material would remain metallurgically stable at 350°F for times under this environment. The curves in Figures 42 through 44 were used in actual practice for the determination of critical crack length for K_c plane stress intensity fracture toughness calculations. Figures 65 through 70 were used to determine maximum load for calculation of fracture stresses.

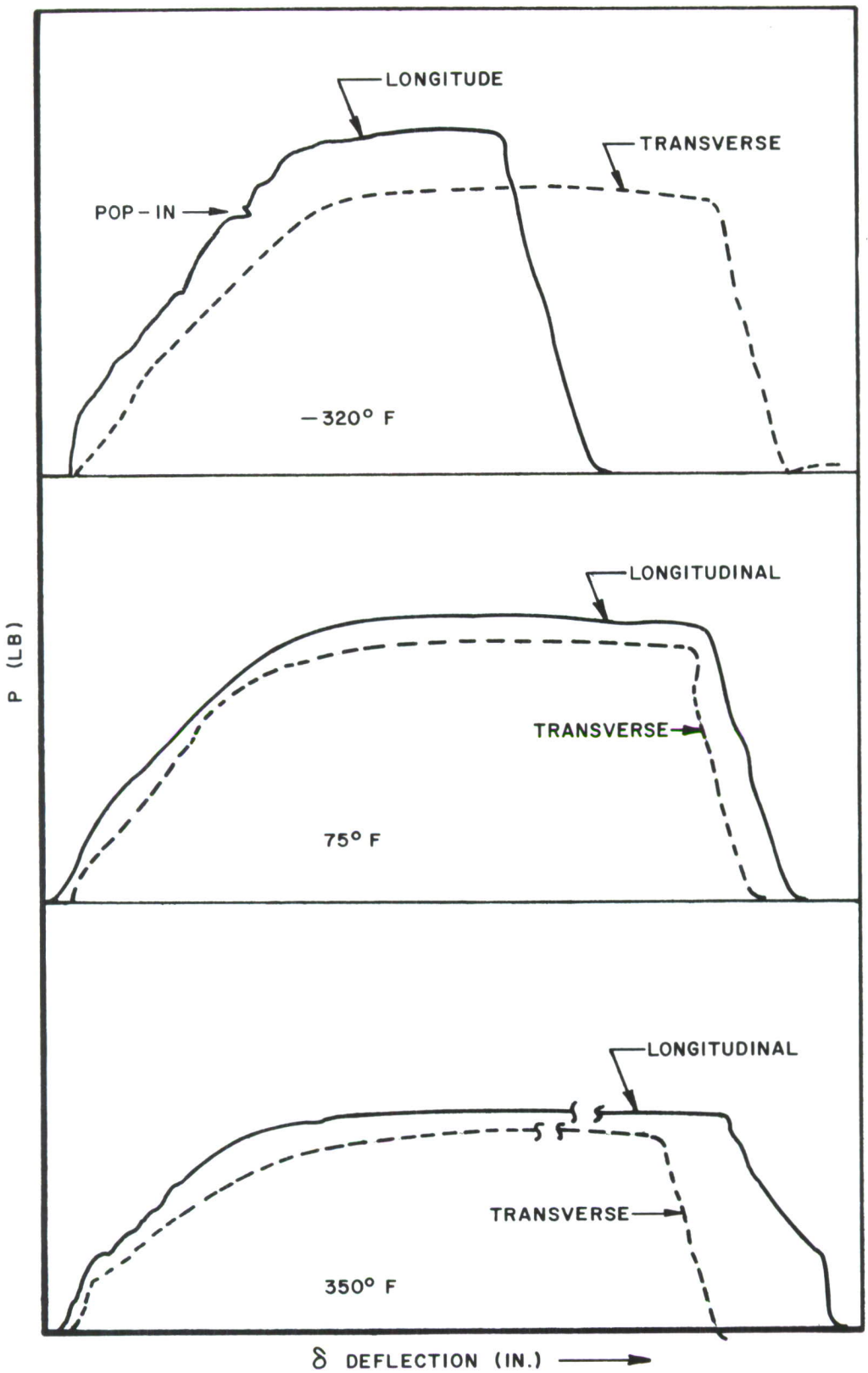
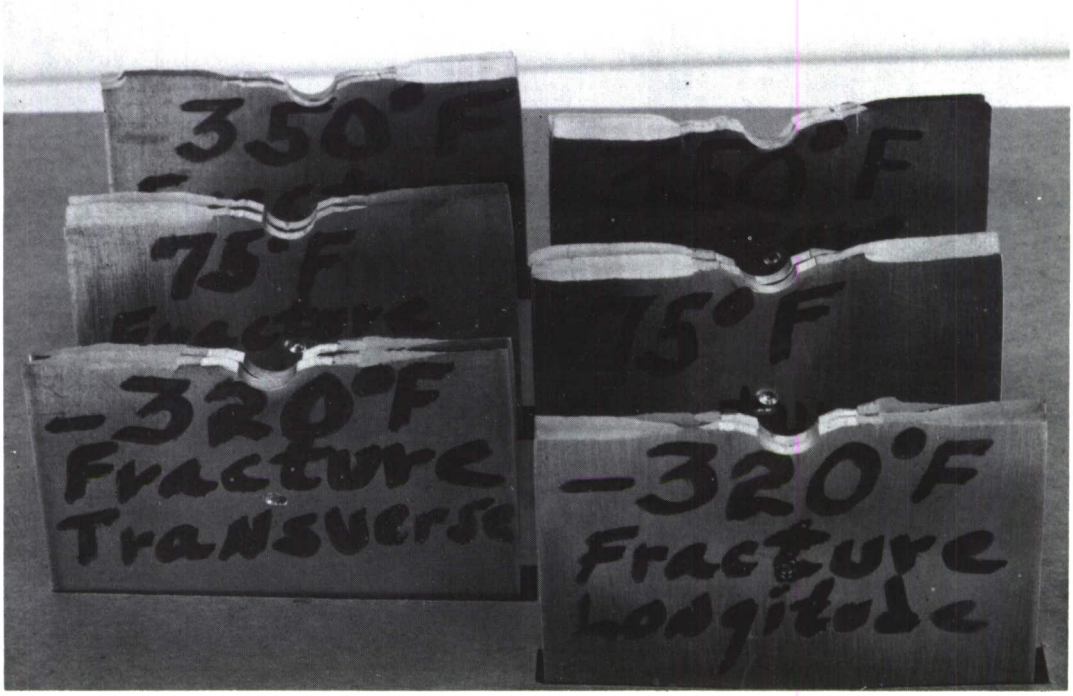
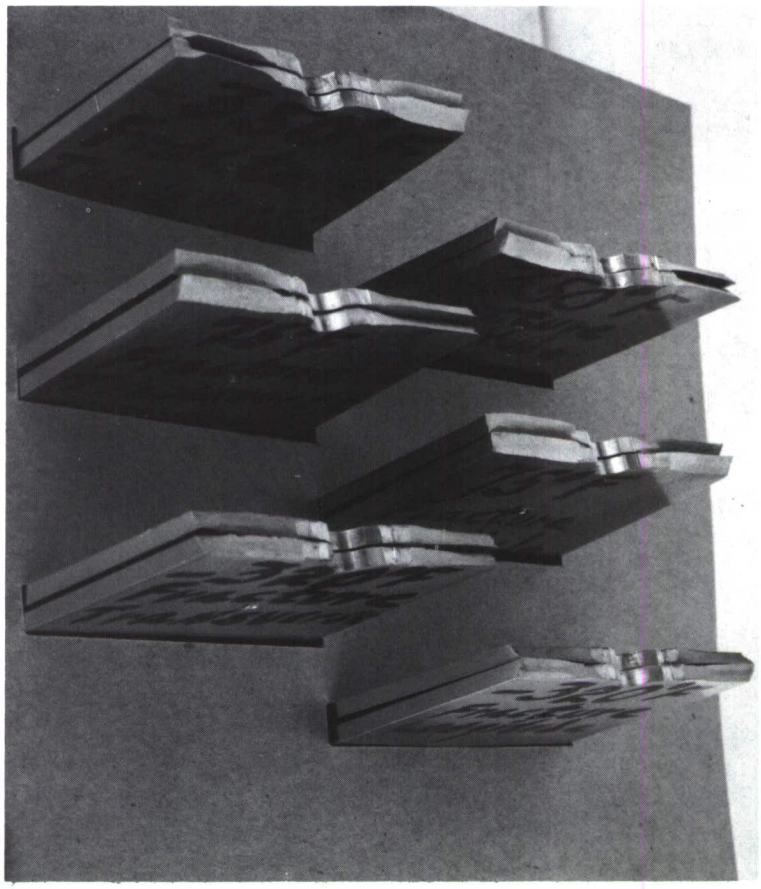


Figure 45. Summary of Load-Deflection Curves



(A)



(B)

Figure 46. Fractographs of Fractured Surfaces of 2024-T3 Centrally Notched Fracture Toughness Specimens

TABLE XI

TABULATED RESULTS* FROM FRACTURE TOUGHNESS TESTS
OF 2024 - T3 Al ALLOY

Specimen No.** and Temp.	Nominal Width (W) In.	Nominal Thickness (B) In.	W/B	a/W	2a	$2a_f$	Pop-In Load, Lb (P_{Ic})	Stress at Pop-In σg PSI	V	σ_{net} (Pop-In)
L[1]5, -320°F	3	.125	24	0.177	1.06	1.08	11,600	30,933	.008	64,583
T[2]3, -320°F	3	.125	-24	0.183	1.10	1.13	12,000	32,000	.012	55,793
L[1]4, 75°F	3	.125	24	0.162	.975	1.02	--	--	.0128	52,631
T[2]2, 75° F	3	.125	24	0.169	1.015	1.038	--	--	.0116	50,000
L[1]6, 350°F	3	.125	24	0.2	1.20	1.24	--	--	.017	46,818
T[2]7, 350°F	3	.125	24	0.2	1.235	1.24	--	--	.016	43,182

*Equations (Reference 36) used to calculate results:

(1.) $K_{Ic} = \sigma g \sqrt{W (\tan \frac{\pi a}{W})}$

(2.) $K_c = \sigma g \sqrt{W (\tan \frac{a}{W})}$

(3.) $a_c = \frac{1}{\pi} \frac{(Kc)^2}{\sigma g} - \frac{1}{2\pi} \frac{(Kc)^2}{\sigma YS}$

(4.) $\sigma g = \frac{P}{Wt}$

(5.) $\sigma_{net} = \frac{P}{(W - 2a_f)t}$

**L indicates longitudinal; T indicates transverse.

TABLE XI (Cont'd)

Specimen No. and Temp.	σ_y	σ_{net}/σ_y	Fracture Load, lb (P)	(d) σ_g	σ_g/σ_y	(a) K_{Ic}	(b) Kc	(c)Critical Flaw Size (a_c)	E 10^6	$\frac{Ev}{\sigma_g W}$	$\frac{\pi a}{W}$
K[1]5, -320°F	68,577	.942	15,500	41,333	.603	44,640	67,042	.685	11	0.71	.72
T[2]3, -320°F	59,200	.942	13,000	34,666	.585	44,662	129,796	3.69	11	1.27	1.36
L[1]4, 75°F	53,950	.975	13,000	34,666	.642	---	100,808	2.14	10.2	1.18	1.23
T[2]2, 75°F	45,250	1.105	12,250	32,666	.722	---	101,590	2.27	10.2	1.14	1.27
L[1]6, 350°F	51,500	.909	10,300	27,466	.533	---	---	---	8.7	1.79	1.62
T[2]7, 350°F	43,900	.984	9,500	25,333	.577	---	---	---	8.7	1.83	1.64

TABLE XII

TABULATED COMPARATIVE DATA FROM FRACTURE TESTS OF 2024-T3 A1 ALLOY

Temp. (°F)	Long. K_{Ic} $lb/in^2 - \sqrt{in.}$	B In.	Long. Kc $lb/in - \sqrt{in.}$	Trans. K_{Ic} $lb/in^2 - \sqrt{in.}$	Trans. Kc $lb/in2 - \sqrt{in.}$	Critical Flaw Size Ac, in.
-320	44,640	.125	67,042	44,642	129,796	2.19 (Av.)
75	No Pop-In	.125	100,808		101,590	2.15 (Av.)
350		.125		100% Plastic Flow		

SECTION VIII

CONCLUSIONS

1. The developed 304 stainless steel compliance gage can be used from cryogenic temperatures (down to -320°F) up to 800°F (for short times) without deleterious metallurgical effects to the structural integrity of the gage.

2. The strength, modulus, and toughness of 304 stainless steel is sufficient to withstand the designed cryogenic and elevated temperature environments without embrittling based upon Air Force Materials Laboratory Cryogenic Materials Data Handbook and Aerospace Structural Metals Handbook values.

3. The compliance gage can be used with any commercially available tensile testing machine and electrical post yield extensometer system.

4. The experimental results obtained on 2024-T3 aluminum alloy agree with Boyle's experimental calibration on 7075-T6 aluminum alloy and calculated results obtained from the Westergaard-Irwin equation for a centrally notched finite plate as shown in Figures 41 through 44.

5. Since the compliance parameter $\left(\frac{Ev}{\sigma W}\right)$ as a function of crack length expression $\left(\frac{\pi a}{W}\right)$ is dimensionless, the compliance gage can be used at cryogenic temperatures by shifting the compliance curve on the ordinate of the X-Y axes. This can be accomplished by determining the modulus of elasticity (E), one-half of the deflection ($\delta/2 = v$), and the gross stress σ at the cryogenic temperature of interest. The width (W) would be a constant which would be the specimen width. The crack length (a) would be of a known length machined into the specimen. Therefore, it is obvious from the parameters that the temperature environment of the gage is only limited by the materials of construction and not by the theory and fundamental principles upon which the development of the gage is based.

6. K_{Ic} (plane strain) and K_c (plane stress) fracture toughness data can be generated with the developed gage under cryogenic and elevated temperature environments on aluminum, titanium, and steel alloys without affecting the accuracy of the readout system, providing the alloys σ_{net}/σ_{YS} ratio are less than approximately 0.75, 1.0, and 0.9, respectively. Below these ratios for the various alloys, the evaluation approach in estimating the fracture toughness and severity of defect is very useful relative to selecting materials for the design of reliable engineering structures.

7. The lower section of the compliance gage near the deflection measurement extensometer should be kept at a constant ambient temperature to eliminate change in resistance of the coil of the extensometer and in turn reduce the possibility of zero shift. The electrical extensometer should be calibrated at the same temperature at which it will be used during the test.

8. The compliance gage is capable of following slow crack extension under plane stress conditions as well as possessing the sensitivity to detect pop-in under plane strain where applicable with respect to flaw sensitive materials

9. When using load-deflection curves to determine pop-in loads for K_{Ic} calculation and maximum loads and critical crack lengths for K_c determination, one should analyze the fractured surfaces of the specimen to determine whether a cleavage of shear mode of

fracture predominated. This information should be used with the load-deflection curves to arrive at rational conclusions concerning toughness and severity of defects in conjunction with K_{Ic} and K_c quantitative information of high strength materials.

10. At 75° and 350°F, design with the 2024-T3 aluminum alloy can be based on gross plastic flow design criteria. However, at -320°F temperature environment, design with this alloy should be based upon critical stress and severity of defects as a function of operating stresses.

11. The fracture mechanics approach to testing and designing for thin (plane stress) and thick (plane strain) sections can be used in practice. However, fractography should also be applied with respect to materials selection.

12. Two limits for Irwin's plane stress, K_c, fracture toughness equations can be used, a yield limit where the net fracture stress is less than or equal to the yield strength, $\sigma_{net} \leq \sigma_{YS}$, and an upper theoretical limit where σ_{net} approximates 1.15 σ_{YS}.

13. For values of σ_{net}/σ_{YS} less than about 0.8, the fracture toughness equations give quantitatively correct results. For values of σ_{net}/σ_{YS} from 0.8 to 1.0, the fracture toughness values obtained may not be exact but the numbers are still useful. Values of K_c may be calculated for σ_{net}/σ_{YS} ratios up to about 1.15 but the numbers are only relative and notch strength ratios are as good a method for evaluating notch toughness.

14. Experimental stress analysis determination of plastic energy release rates indicates that the Griffith-Irwin approach is not realistic for σ_{net}/σ_{YS} values much greater than 1.0.

15. Formulas for several types of plane strain, K_{Ic}, fracture toughness tests can be used. However, the σ_{net}/σ_{YS} ratio criteria has to be realized by the user.

16. Fracture mechanics concepts appear to be applicable to ultra-high strength metallic materials with $(\sigma tu/\rho) \geq 700,000$ inches. However, for extremely tough materials conventional design concepts seem to be appropriate with respect to increased reliability against catastrophic failures of structures.

REFERENCES

1. Sidney O. Davis, "Elevated Temperature Fatigue Properties of D6AC High Strength Steel," ASD-TDR-63-645, October 1963.

2. "Fracture Testing of High-Strength Sheet Materials," A Report of a Special ASTM Committee, January 1960.

3. W. W. Gerberich, "Current Trends In Testing Methods, Design, and Materials for Fracture Toughness," Publication No. U-2518, Philco Research Laboratories, Newport Beach, California, March 1964.

4. W. W. Gerberich, "Theoretical and Practical Aspects of Correlating Percent Shear-Lip to Relative Plastic Zone Size in Brittle Fracture," T.R. 32-112, Jet Propulsion Laboratory, Pasadena, California, September 1962.

5. "Fracture Testing of High-Strength Sheet Materials," A Report of a Special ASTM Committee, ASTM Bulletin, November 1961.

6. W.W. Gerberich, "Plastic Strains and Energy Density in Cracked Plates, I. Experimental Technique and Results," California Institute of Tech. Report GALCIT SM 63-23, June 1963, to be Presented, Soc. Exp. Stress Anal.

7. J. G. Sessler, "Behavior of a Brittle Metal," Proc. of the Seventh Sagamore Conf., Syracuse University, August 1960.

8. W. F. Brown, Jr., "Mechanical Screening Tests for Sheet Alloy," Proc. of the Seventh Sagamore Conf., Syracuse University, August 1960.

9. D. A. Corrigan, "The Effect of Heat Treatment Upon the Notch Toughness of High Strength Titanium Alloy Sheet," Proc. of the Seventh Sagamore Conf., Syracuse University, August 1960.

10. A. H. Knoll, "Tension Tests of Wide Slotted Sheet Specimens of Aluminum Alloys," Report 12-60-2, Alcoa Research Labs, New Kensington, Pa., February 1960.

11. J. E. Srawley and C. D. Beachem, "Resistance to Crack Propagation of High-Strength Sheet Materials for Rocket Motor Casings," NRL Report 5771, U.S. Naval Research Laboratory, May 1962.

12. J. E. Campbell, "Current Methods of Fracture-Toughness Testing of High-Strength Alloys With Emphasis on Plane Strain,"DMIC Report 207, August 1964.

13. J. E. Srawley, "Fracture Appearance of High Strength Steels and Other Alloys," Proc. of the Seventh Sagamore Conf., Syracuse University, August 1960.

14. J. L. Swedlow and W. W. Gerberich, "Plastic Strains and Energy Density in Cracked Plates, II. Comparison with Elastic Theory," Calif. Inst. of Tech. Report GALCIT SM 63-24, June 1963.

15. J. G. Kaufman and E. W. Johnson, "The Use of Notch-Yield Ratio to Evaluate the Notch Sensitivity of Aluminum Alloy Sheet," Proc. ASTM, 1962.

16. R. W. Boyle, A. M. Sullivan and J. M. Krafft, "Determination of Plane Strain Fracture Toughness with Sharply Notched Sheets," Welding Res. Journal, September 1962.

REFERENCE (CONT'D)

17. B. B. Muvdi, G. Sachs, and E. P. Klier, "Design Properties of High Strength Steels in the Presence of Stress Concentrations," WADC-TR-56-395, December 1956.

18. V. Weiss, J. Sessler, P. Packman, and G. Sachs, "The Effect of Several Geometrical Variables on the Notch Tensile Strength of 4340 Steel Sheet Heat-Treated to Three Strength Levels," WADD-TR-60-310, June 1960.

19. J. D. Lubahn, "Experimental Determination of Energy Release Rate for Notch Bending and Notch Tension," ASTM Preprint 80, 1959.

20. G. Sachs, J. G. Sessler, R. F. Pray, and T. H. Yeh, "Relations Between the Notch Tensile Strength of Cylindrical and Prismatic Specimens of Titanium Alloys and Heat Treated Steels," Journal of Basic Engineering, June 1960.

21. Screening Tests for High-Strength Alloys Using Sharply Notched Cylindrical Specimens, A Report of a Special ASTM Committee, Materials Research and Standards, March 1962.

22. G. Sachs, J. D. Lubahn, and L. J. Ebert, "Notched Bar Tensile Test Characteristics of Heat Treated Low Alloy Steels," Trans. ASM, Vol. 33, 1944.

23. B. M. Wundt, "A Unified Interpretation of Room-Temperature Strength of Notched Specimens As Influenced by Their Size," ASME Preprint 59-MET-9, 1959.

24. H. F. Bueckner, "The Stress Concentration of a Notched Bar in Bending," General Electric Report 57 TG 153, June 1957.

25. P. C. Paris, F. Erdogan, G. C. Sih, O. Tuncel, L. Y. Bahar, F. B. Beer, "Fracture Mechanics Research At Lehigh University, 1960-1961," Boeing Report D6-7960, Renton, Washington.

26. J. E. Srawley and C. D. Beachem, "Fracture of High-Strength Sheet Steel Specimens Containing Small Cracks," ASTM Preprint 80a, 1961.

27. S. J. Matas, M. Hill, and H. P. Munger, "Current and Future Trends for Steels with High Strength and Toughness," Metals Eng. Quart., Vol. 3, No. 3, August 1963.

28. D. J. Schmatz and V. F. Zackay, "Mechanical Properties of Deformed Metastable Austenitic Ultra-High Strength Steel," Trans. ASM, Vol. 51, 1959.

29. R. F. Decker, J. T. Eash, and A. J. Goldman, "18% Nickel Maraging Steel," Trans. ASM, Vol. 55, 1962

30. G. Sachs, V. Weiss, and E. P. Klier, "Effects of A Number of Heat Treating and Testing Variables on the Notch Strength of 4340 Steel,"Proc. ASTM, Vol. 56, 1956

31. A. B. Smith, "Missile Motor Cases," Metals Eng. Quart., Vol. 3, No. 4, November 1963.

32. H. E. Romine, "Plane Strain Toughness Measurements of Solid Booster Case Materials," U. S. Naval Weapons Laboratory, Dahlgren, Virginia, 1963.

33. E. A. Steigerwald, Private Communication Reported in Interim Progress Report of RTD Project No. 7381, Wright-Patterson AFB, March 1965.

REFERENCE (CONT'D)

34. "Thick Section Fracture Toughness," ML-TDR-64-236, Air Force Materials Laboratory, October 1964, pp 15-17.

35. G. Murphy, "Advanced Mechanics of Materials," McGraw-Hill Book Co., 1946, p 61.

36. Fifth Report of a Special ASTM Committe, "Progress in Measuring Fracture Toughness and Using Fracture Mechanics," Materials Research and Standards, Vol. 4, No. 3, March 1964.

37. Morrison, Jenkins, and Kattus, "Summary Technical Report on an Investigation of the Crack-Propagation Resistance of High-Strength Alloys and Heat-Resistance Alloys, November 1962.

38. H. M. Westergaard, "Bearing Pressures and Cracks," J. Appl Mech., Vol. 6, 2A, June 1939.

39. G. R. Irwin, "Fracture Testing of High-Strength Sheet Materials Under Conditions Appropriate for Stress Analysis," NRL Report 5486, July 27, 1960.

40. R. W. Boyle, "An Instrument for Crack Growth Determinations from the Compliance of Notched Sheet Specimens," U. S. Naval Research Laboratory, Washington 25, D. C.

41. R. W. Boyle, "A Method for Determining Crack Growth in Notched Sheet Specimens," Materials Research and Standards, Vol 2, August 1962, p 646.

42. R. W. Boyle, "Progress in Determing K_{Ic} by the 'Pop-In' Technique," Presented at a Meeting of the ASTM Committe on Fracture Testing of High Strength Metallic Materials, NASA Lewis Research Center, August 29 and 30, 1961.

43. J. E. Srawley, and W. F. Brown, Jr., "Fracture Toughness Testing," NASA Technical Memorandum, TM-X-52030, Technical Preprint prepared for Symposium on Fracture Toughness Testing and Its Applications sponsored by the American Society for Testing and Materials at the Annual Meeting in Chicago, Illinois (June 23-24, 1964).

44. R. W. Boyle, "A Method For Determing Crack Growth in Notched Sheet Specimens," Materials Research and Standards, Vol. 2 (8), pp 646-651 (August, 1962).

45. E. A. Steigerwald and G. L. Hanna, "Initiation of Slow Crack Propagation in High-Strength Materials," Proc. ASTM Vol. 62, pp 885-904 (1962).

46. A. A. Anctil, E. B. Kula, and E. DiCesare, "Electric Potential Technique for Determining Slow Crack Growth," Proc. ASTM Vol. 63, pp 799-808 (1963).

47. C. S. Yen and S. L. Pendleberry, "Technique for Making Shallow Cracks in Sheet Metals," Materials Research and Standards, Vol. 2 (11), pp 913-916 (November, 1962).

48. C. F. Tiffany and J. N. Masters, "Applied Fracture Mechanics," Preprint prepared for Symposium on Fracture Toughness Testing and Its Applications by the American Society for Testing and Materials at the Annual Meeting in Chicago, Illinois (June 23-24, 1964).

REFERENCE (CONT'D)

49. J. A. Kies, H. L. Smith, H. E. Romine, and H. Berstein, "Fracture Testing of Weldments," Preprint prepared for Symposium on Fracture Toughness Testing and Its Applications by the American Society for Testing and Materials at the Annual Meeting in Chicago, Illinois (June 23-24, 1964).

50. A. M. Sullivan, "New Specimen Design for Plane-Strain Fracture Toughness Tests," Materials Research and Standards, Vol. 4 (1), pp 20-24 (January, 1964).

51. G. M. Orner, and C. E. Hartbower, "Precracked Charpy Fracture Toughness Correlations," Preprint prepared for Symposium on Fracture Toughness Testing and Its Applications sponsored by the American Society for Testing and Materials at the Annual Meeting in Chicago, Illinois (June 23-24, 1964).

52. G. L. Hanna, and E. A. Steigerwald, "Fracture Characteristics of Structural Metals", Final Summary Technical Report ER-5426, TAPCO, a division of Thompson Ramo Wooldridge, Inc., Cleveland, Ohio, Bureau of Naval Weapons Contract No. N 600(19)-58831 (June 30, 1963).

53. J. L. Christian, "Physical and Mechanical Properties of Pressure Vessel Materials for Application in a Cryogenic Environment," ASD-TDR-62-258, General Dynamics/Astronautics, San Diego, California, U. S. Air Force Contract No. AF 33(616)-7719 (March, 1962).

54. J. L. Christian and A. Hurlich, "Physical and Mechanical Properties of Pressure Vessel Materials For Application in a Cryogenic Environment," ASD-TDR-62-258, Part II, General Dynamics/Astronautics, San Diego, California, U. S. Air Force Contract No. AF 33(616)-7719 (April, 1963).

55. G. R. Irwin, "Relation of Crack Toughness Measurements to Practical Applications," Welding J., Research Supplement, Vol. 41 (11), pp 519-s-528-s (November, 1962).

56. C. F. Tiffany and P. M. Lorenz, "An Investigation of Low-Cycle Fatigue Failures Using Applied Fracture Mechanics," Technical Documentary Report ML-TDR-64-53, The Boeing Company, Aero-Space Division, Seattle, Washington, U. S. Air Force Contract No. AF 33(657)-10251 (May, 1964).

57. J. W. Spretnak, A Summary of the Theory of Fracture In Metals, DMIC Report 157, August 1961.

58. Lauta, Hanna, and Steigerwald, Development of Standardized Test Methods to Determine Plane Strain Fracture Toughness, Contract No. AF 33(615)-1611, December 1964.

APPENDIX

CURVE-PLOTTED DATA

A. TENSILE TEST CURVES OF RAW DATA

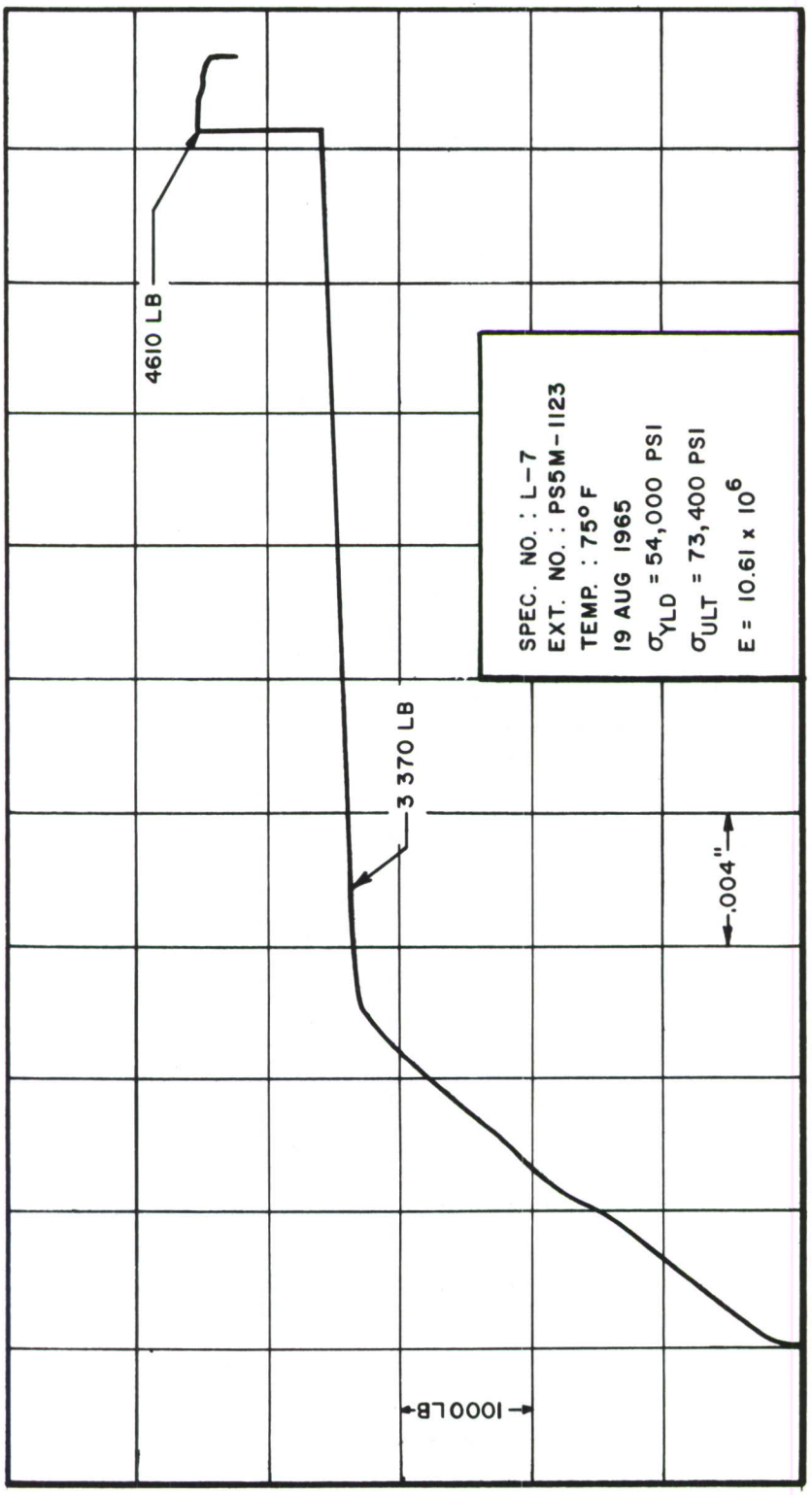


Figure 47. Tensile Test Data at Room Temperature, Specimen Number L-7

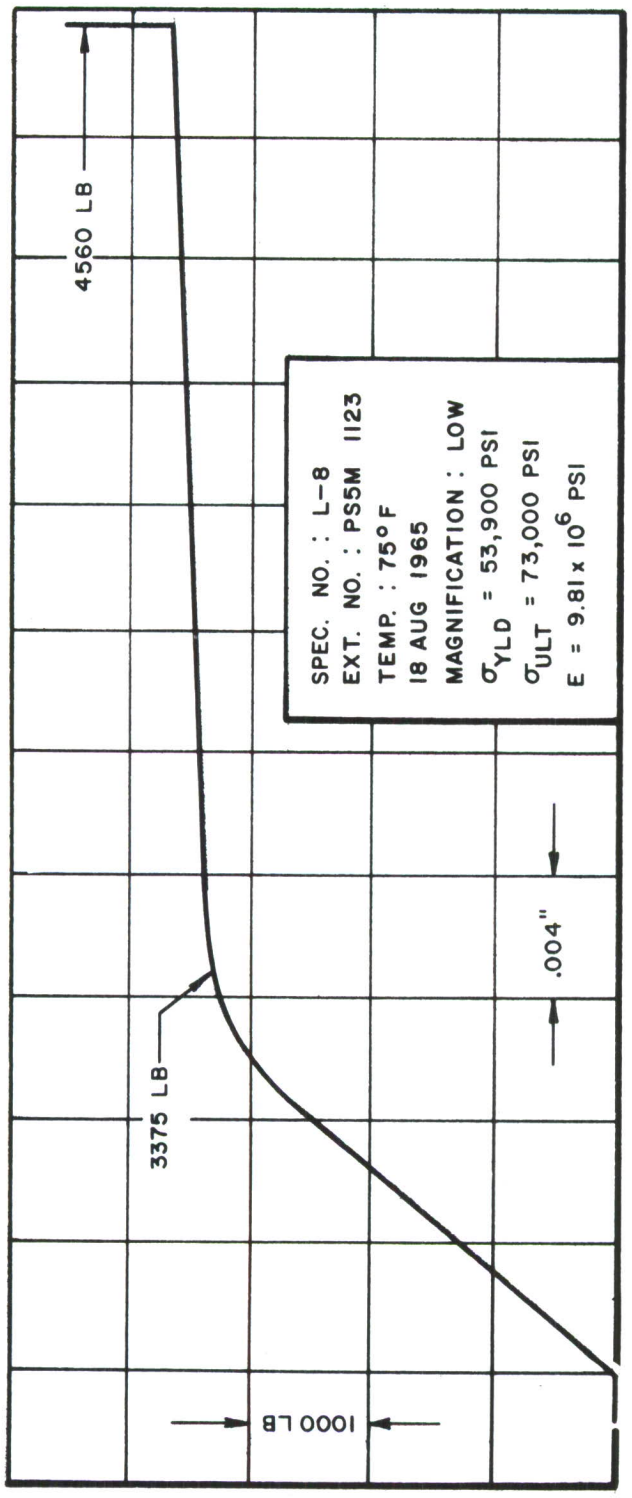


Figure 48. Tensile Test Data at Room Temperature, Specimen Number L-8

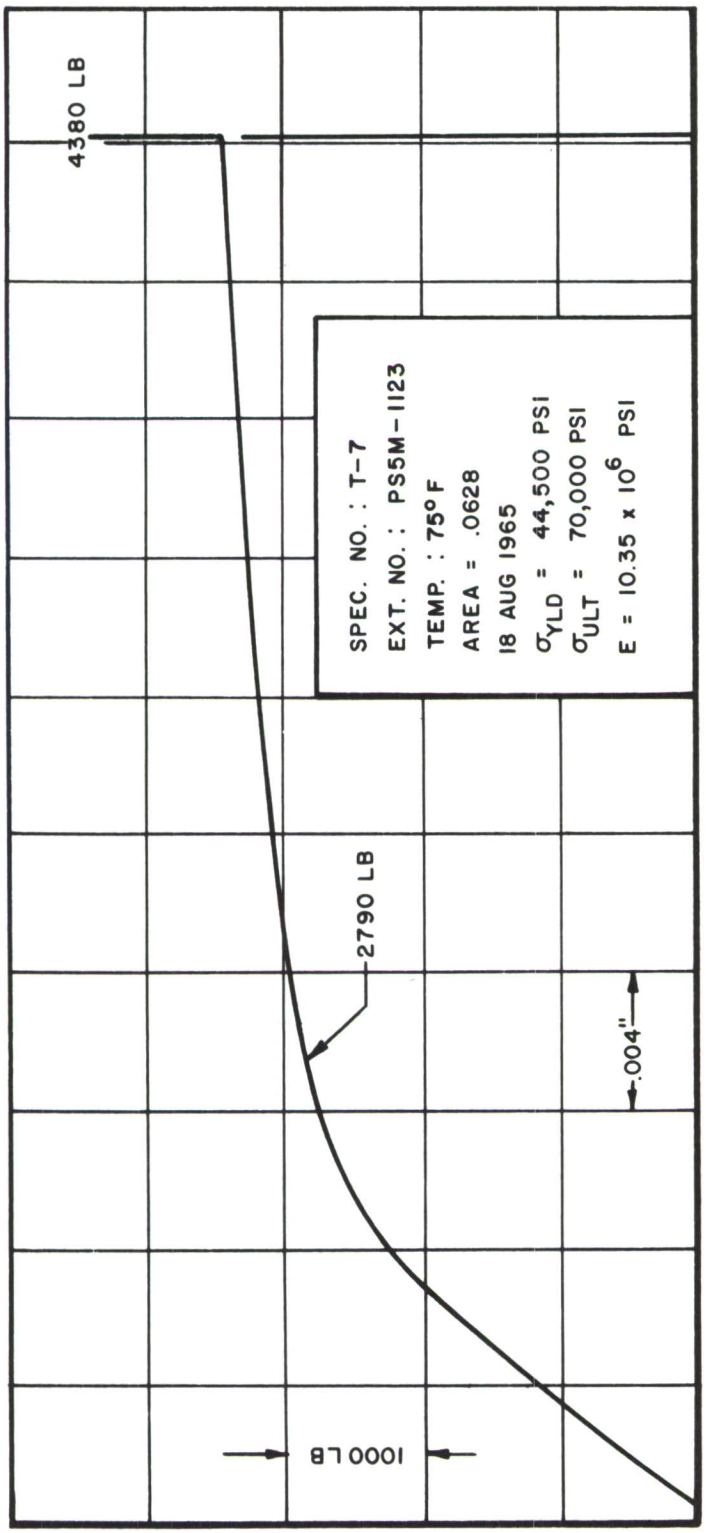


Figure 49. Tensile Test Data at Room Temperature, Specimen Number T-7

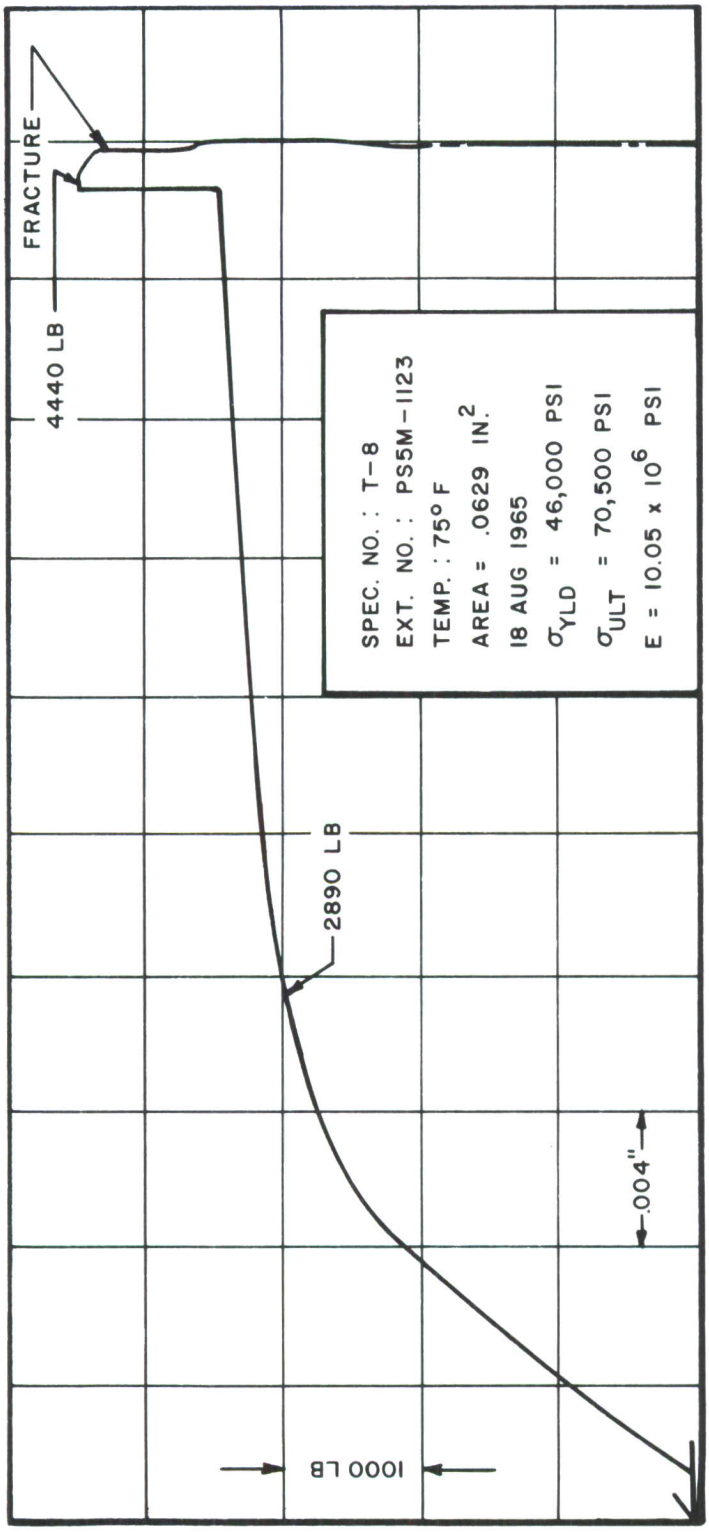


Figure 50. Tensile Test Data at Room Temperature, Specimen Number T-8

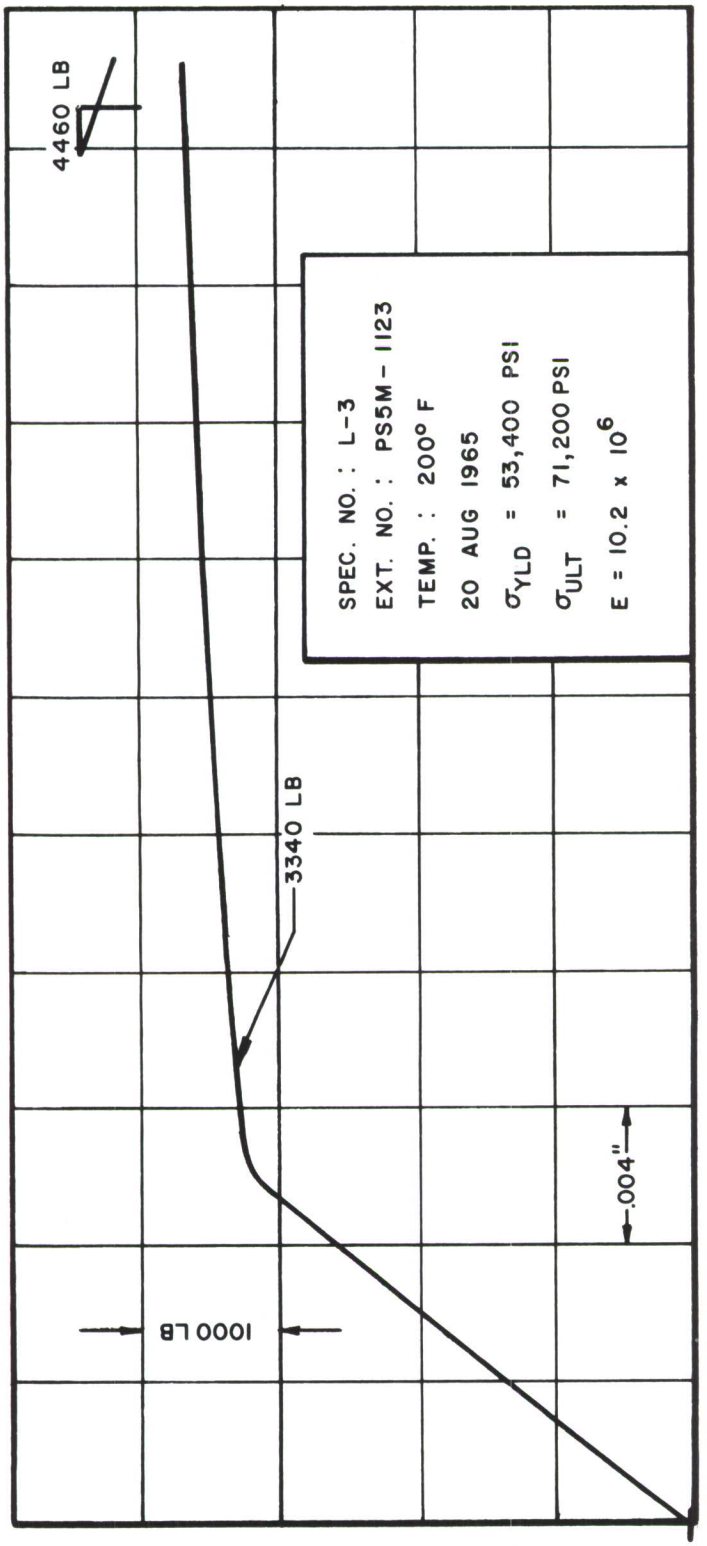


Figure 51. Tensile Test Data at 200°F, Specimen Number L-3

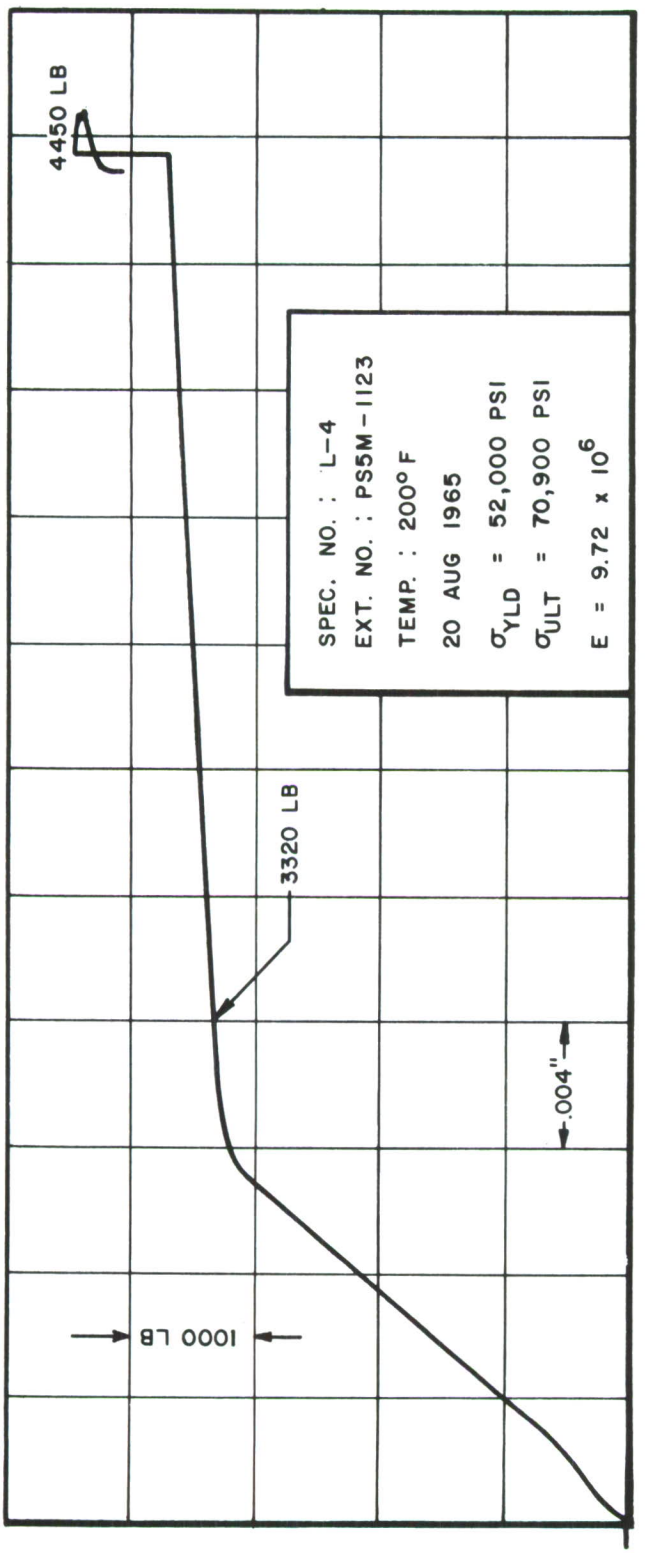


Figure 52. Tensile Test Data at 200°F, Specimen Number L-4

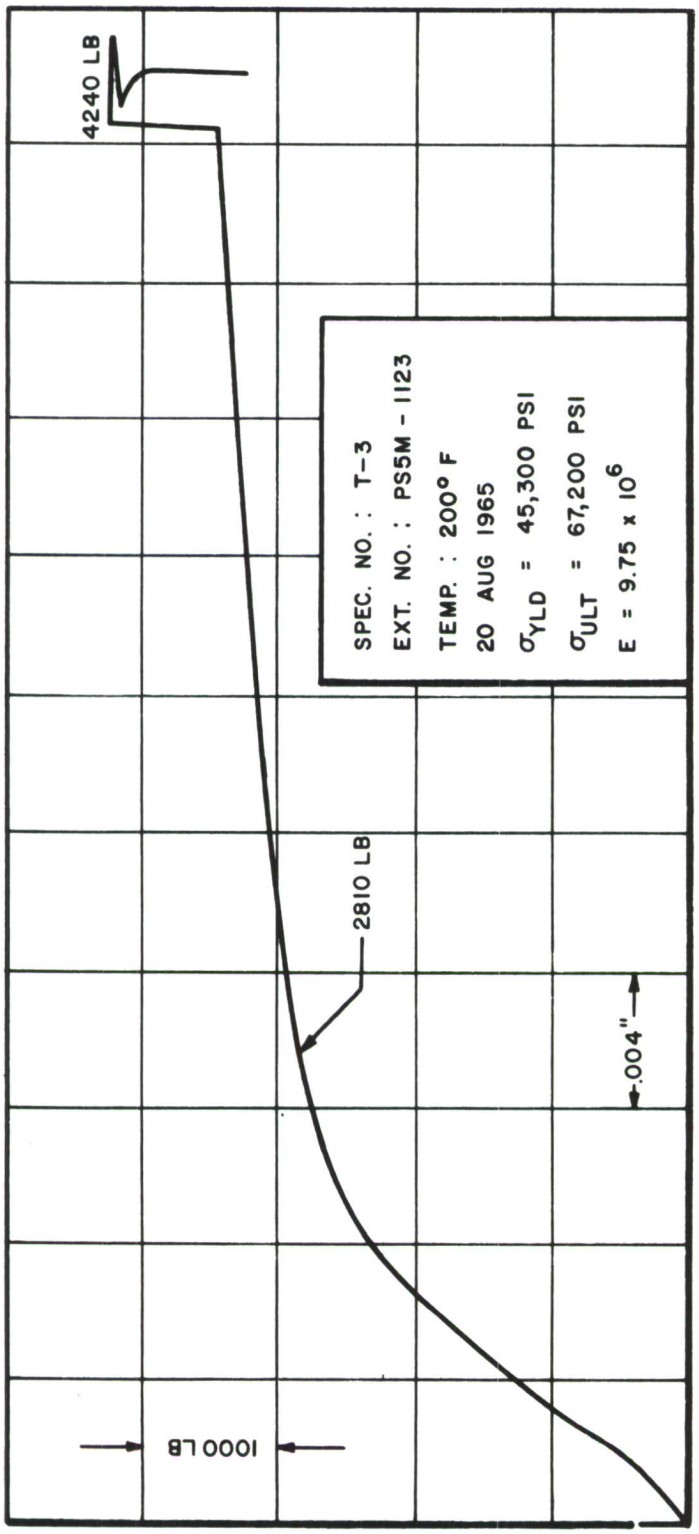


Figure 53. Tensile Test Data at 200°F, Specimen Number T-3

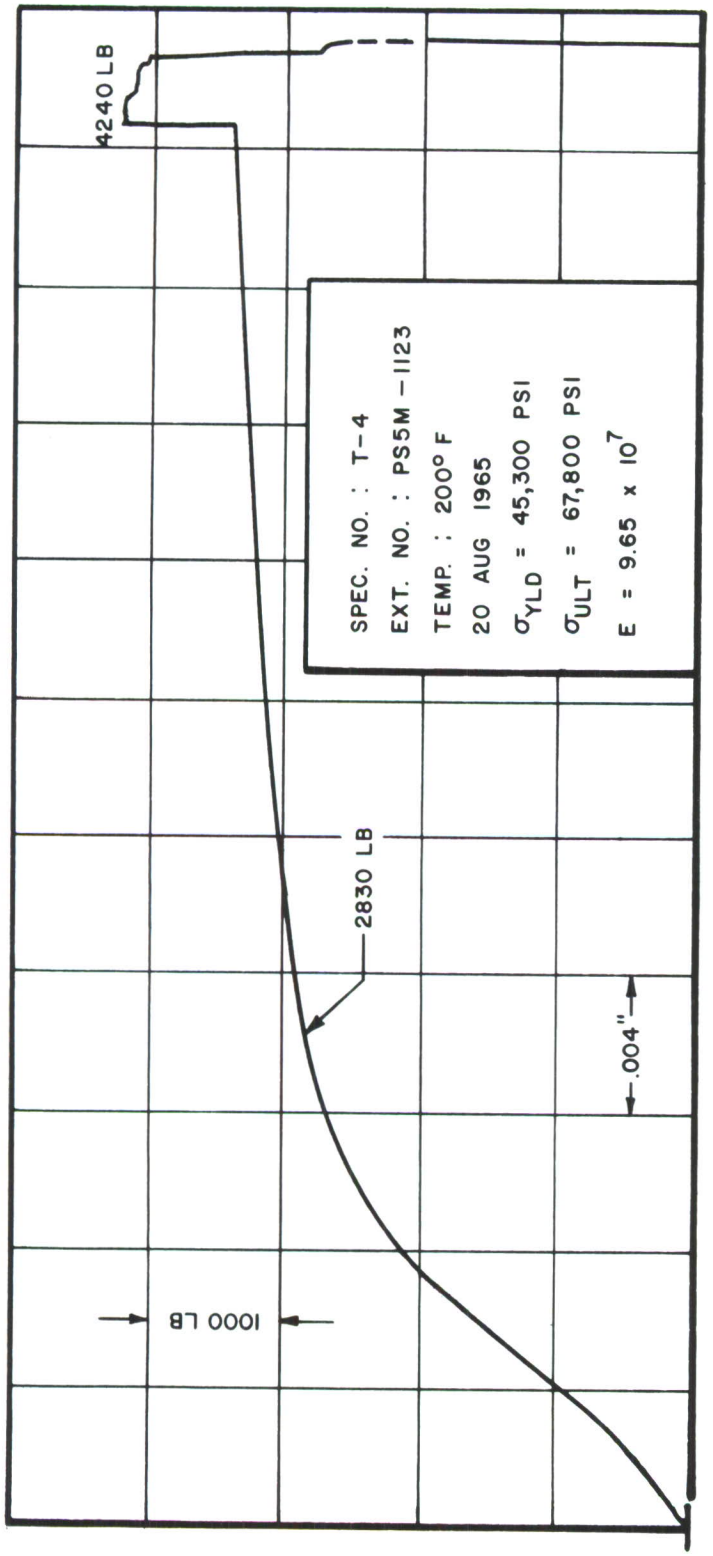


Figure 54. Tensile Test Data at 200°F, Specimen Number T-4

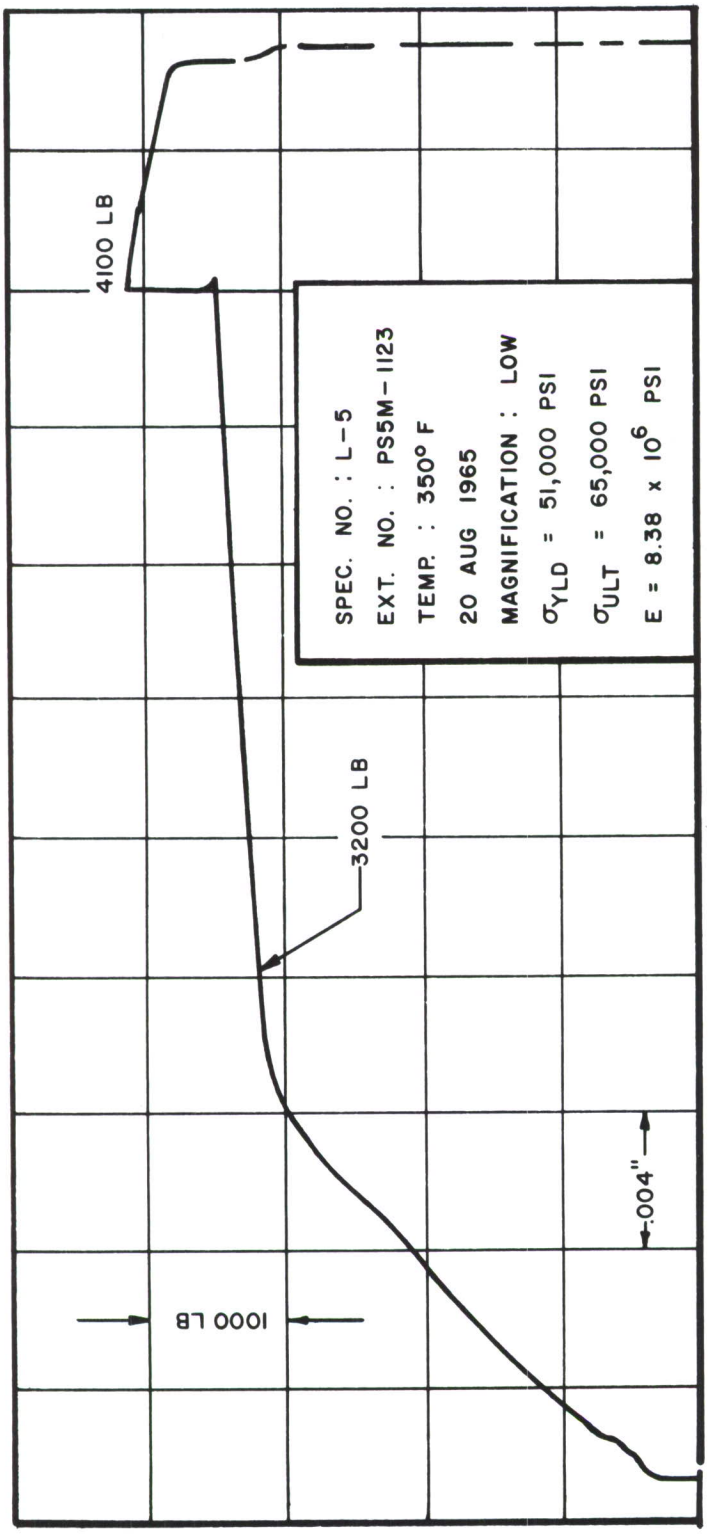


Figure 55. Tensile Test Data at 350°F, Specimen Number L-5

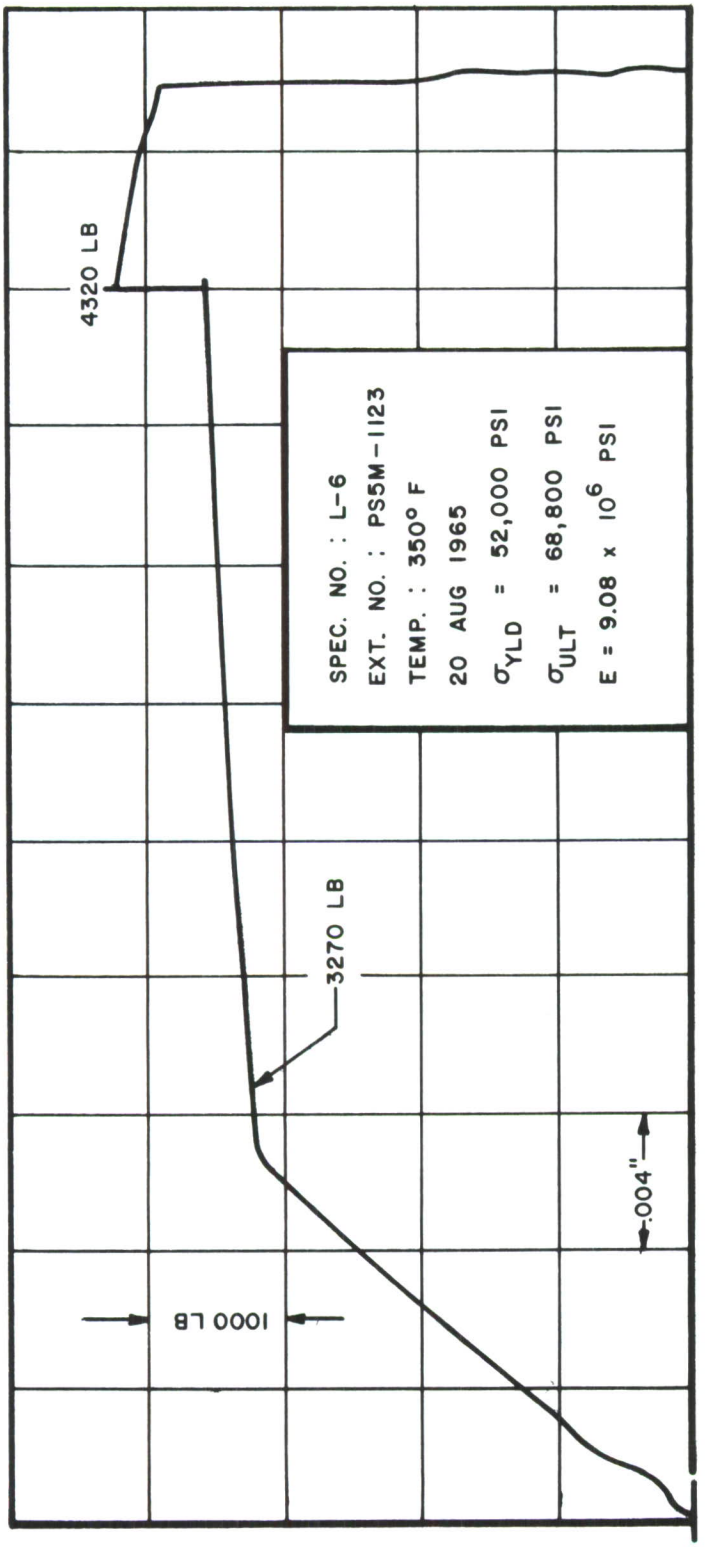


Figure 56. Tensile Test Data at 350°F, Specimen Number L-6

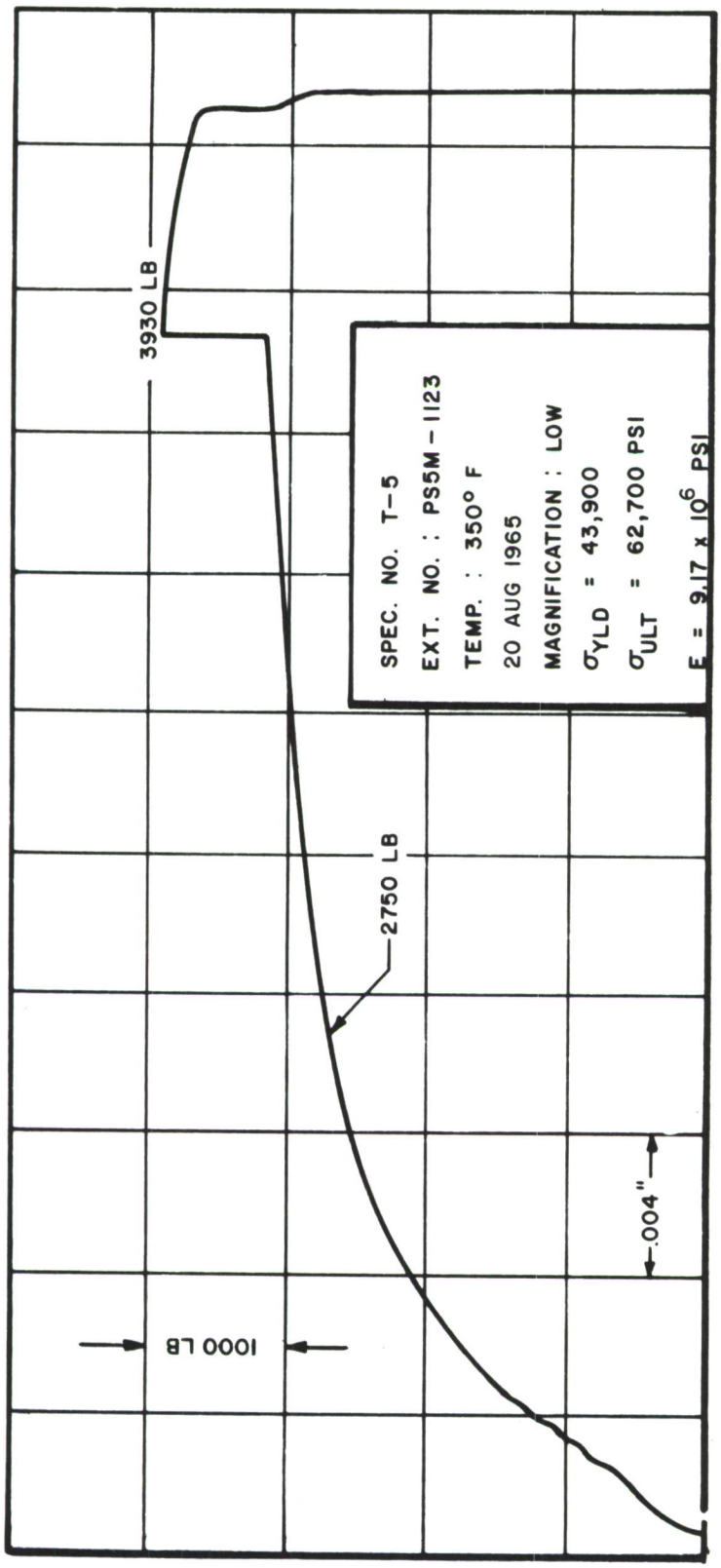


Figure 57. Tensile Test Data at 350°F, Specimen Number T-5

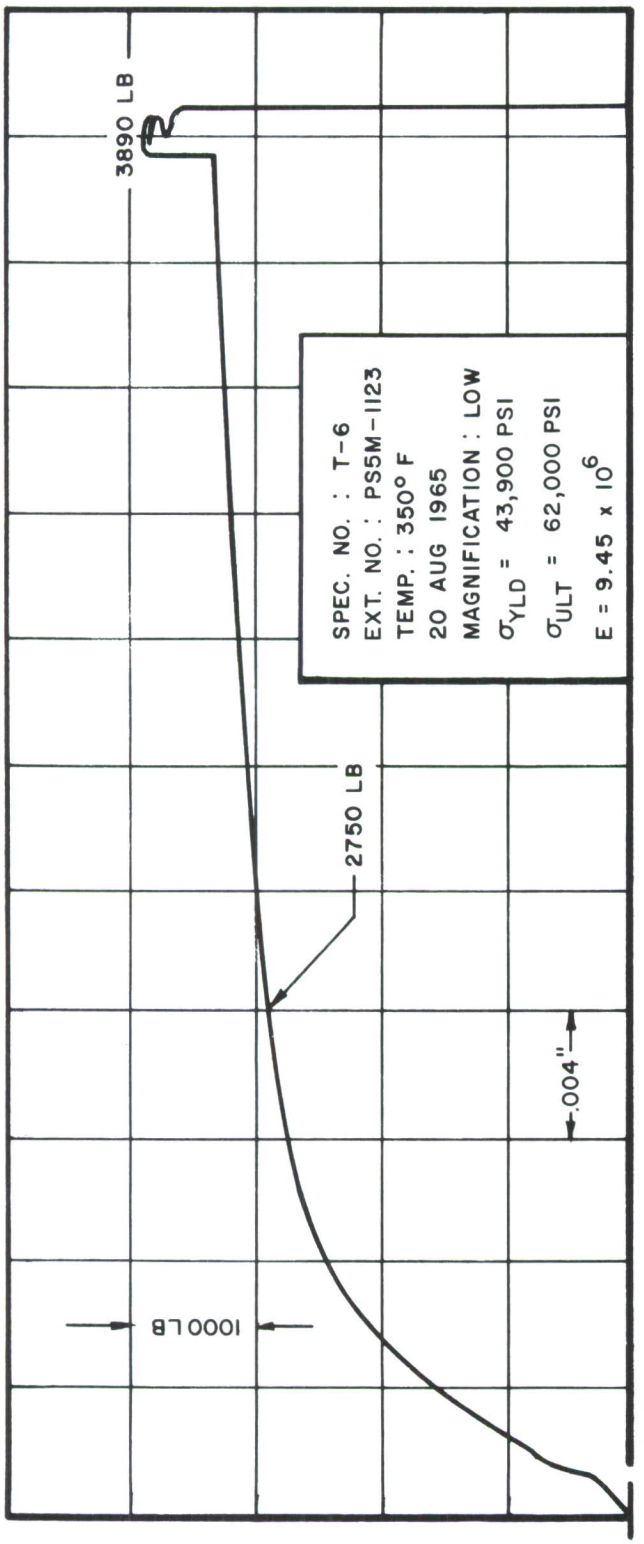


Figure 58. Tensile Test Data at 350°F, Specimen Number T-6

B. CALIBRATION LOAD-DEFLECTION CURVES OF RAW DATA FOR VARIABLE-CRACK-LENGTH CENTRALLY NOTCHED SPECIMENS

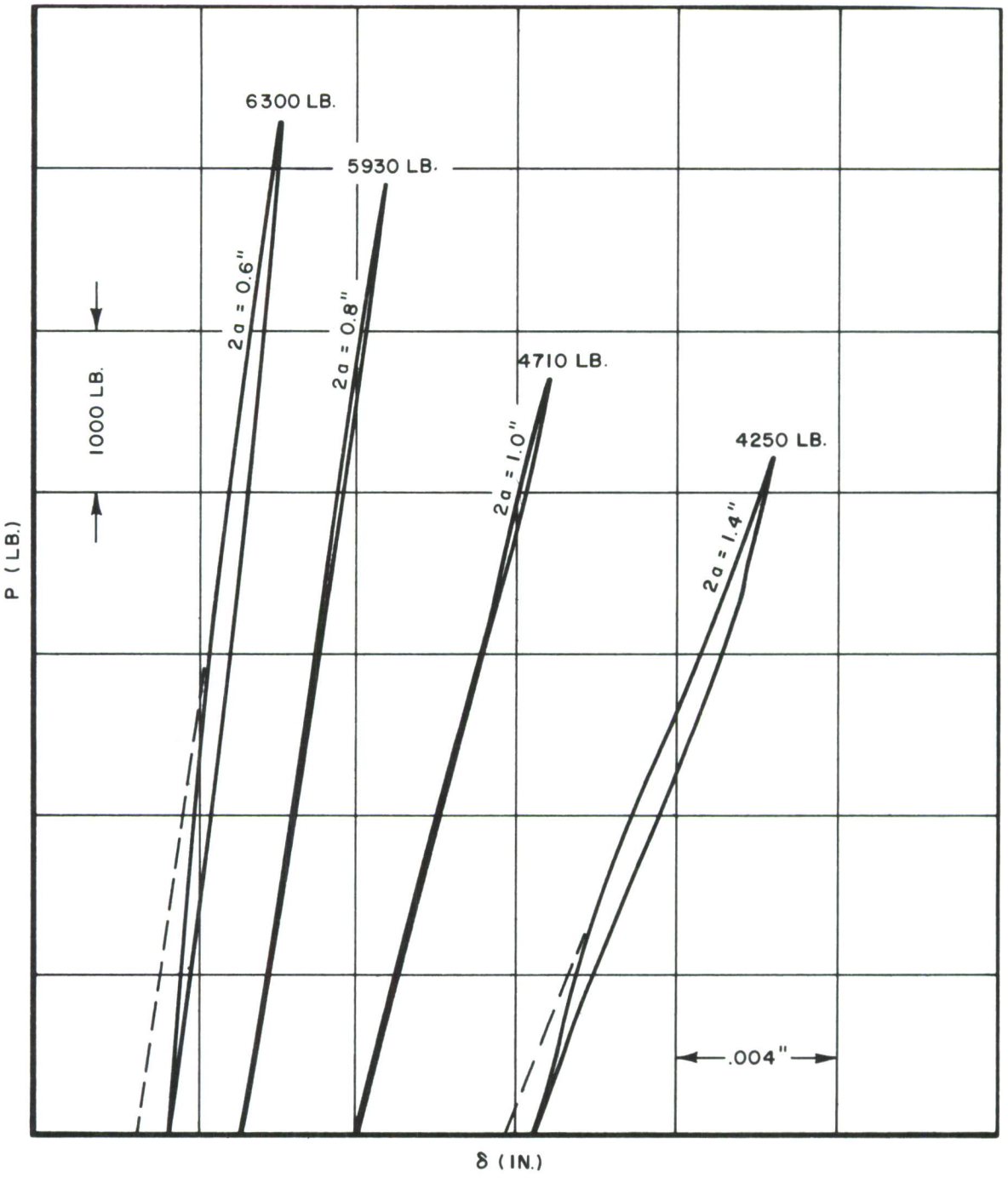


Figure 59. Load-Deflection Curves for Centrally Notched Specimens -320°F (Longitudinal)

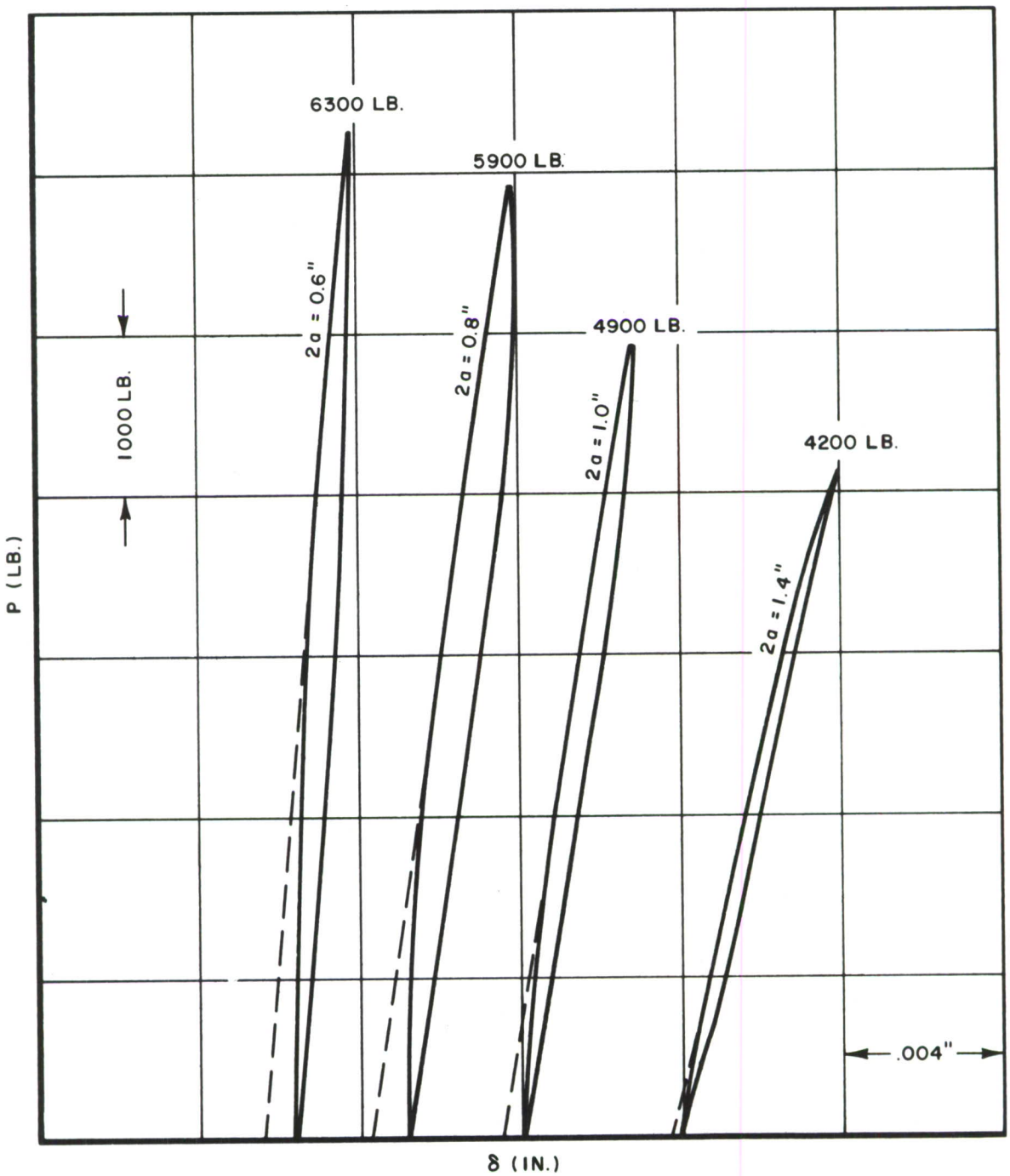


Figure 60. Load-Deflection Curves for Centrally Notched Specimens -320°F (Transverse)

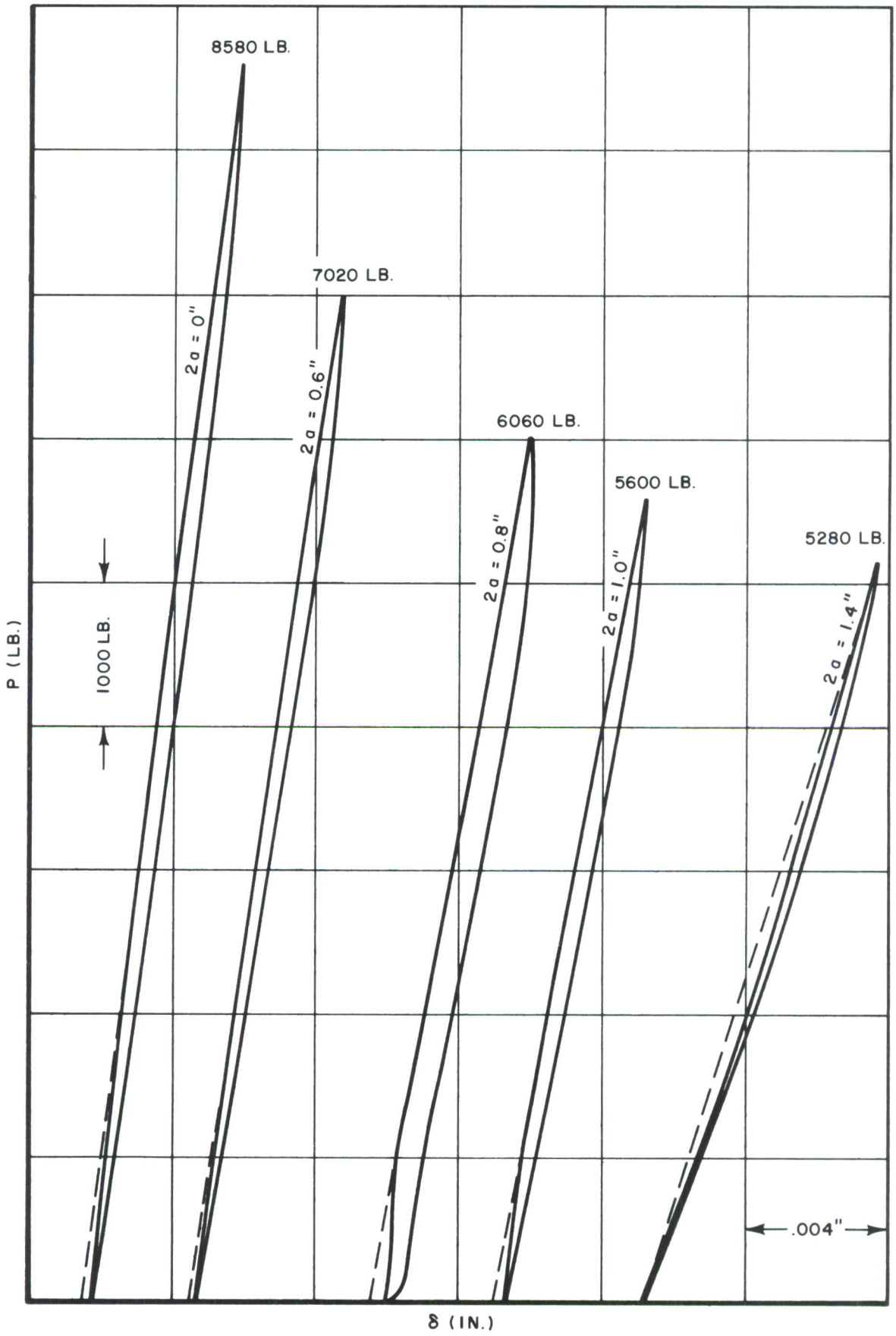


Figure 61. Load-Deflection Curves for Centrally Notched Fracture Specimens, 75°F, (Longitudinal)

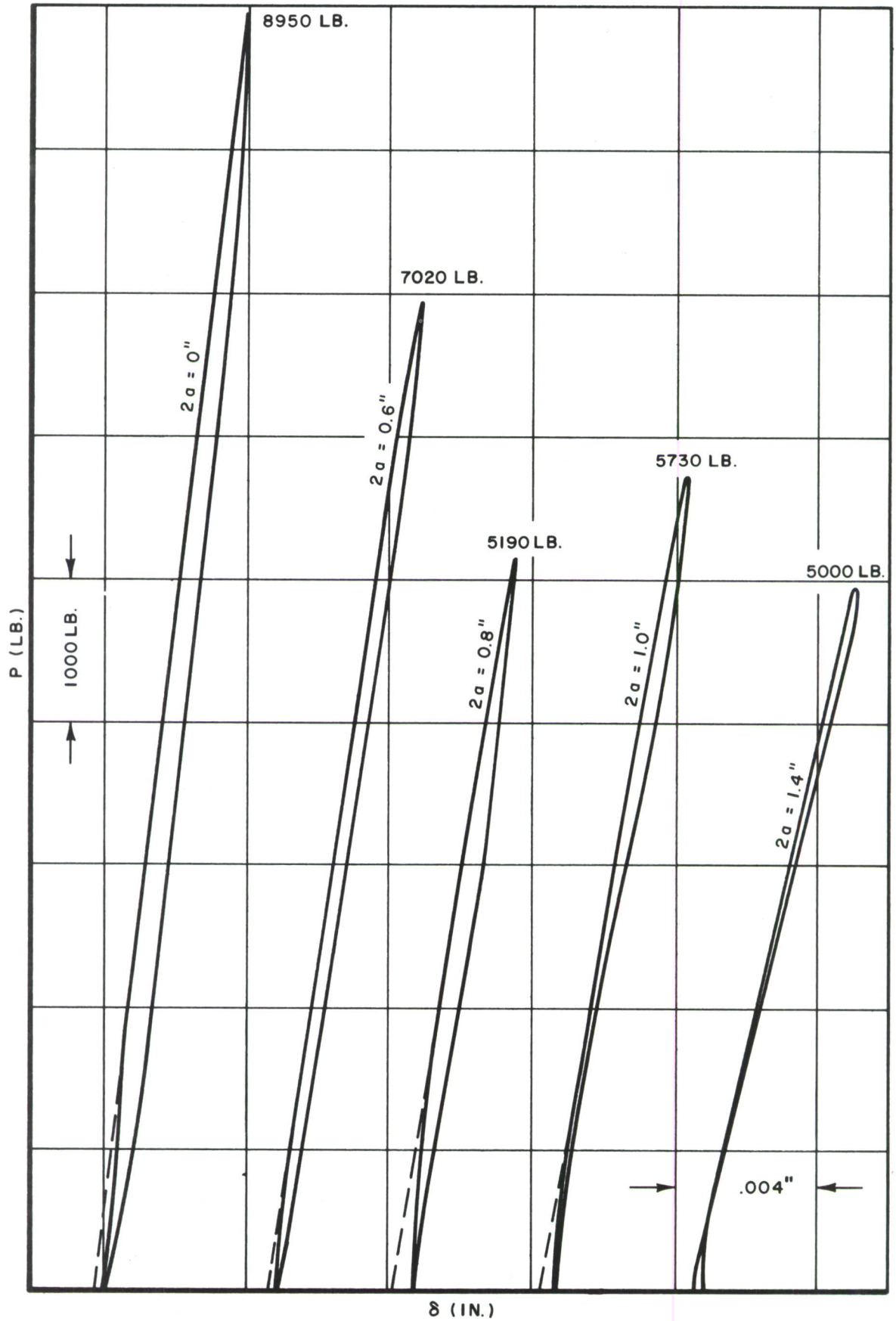


Figure 62. Load-Deflection Curves for Centrally Notched Fracture Specimens, 75°F, (Transverse)

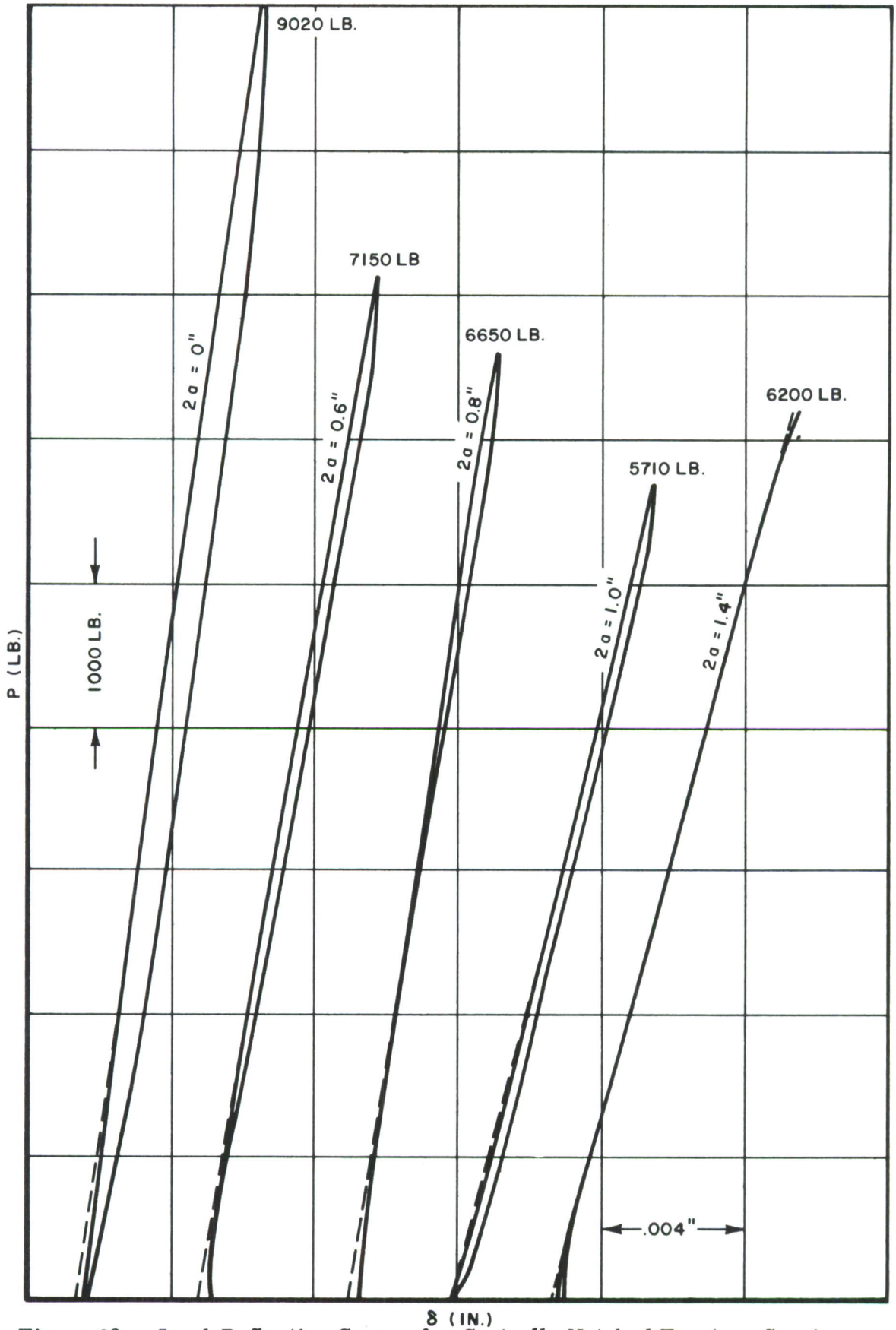


Figure 63. Load-Deflection Curves for Centrally Notched Fracture Specimens, 350°F, (Longitudinal)

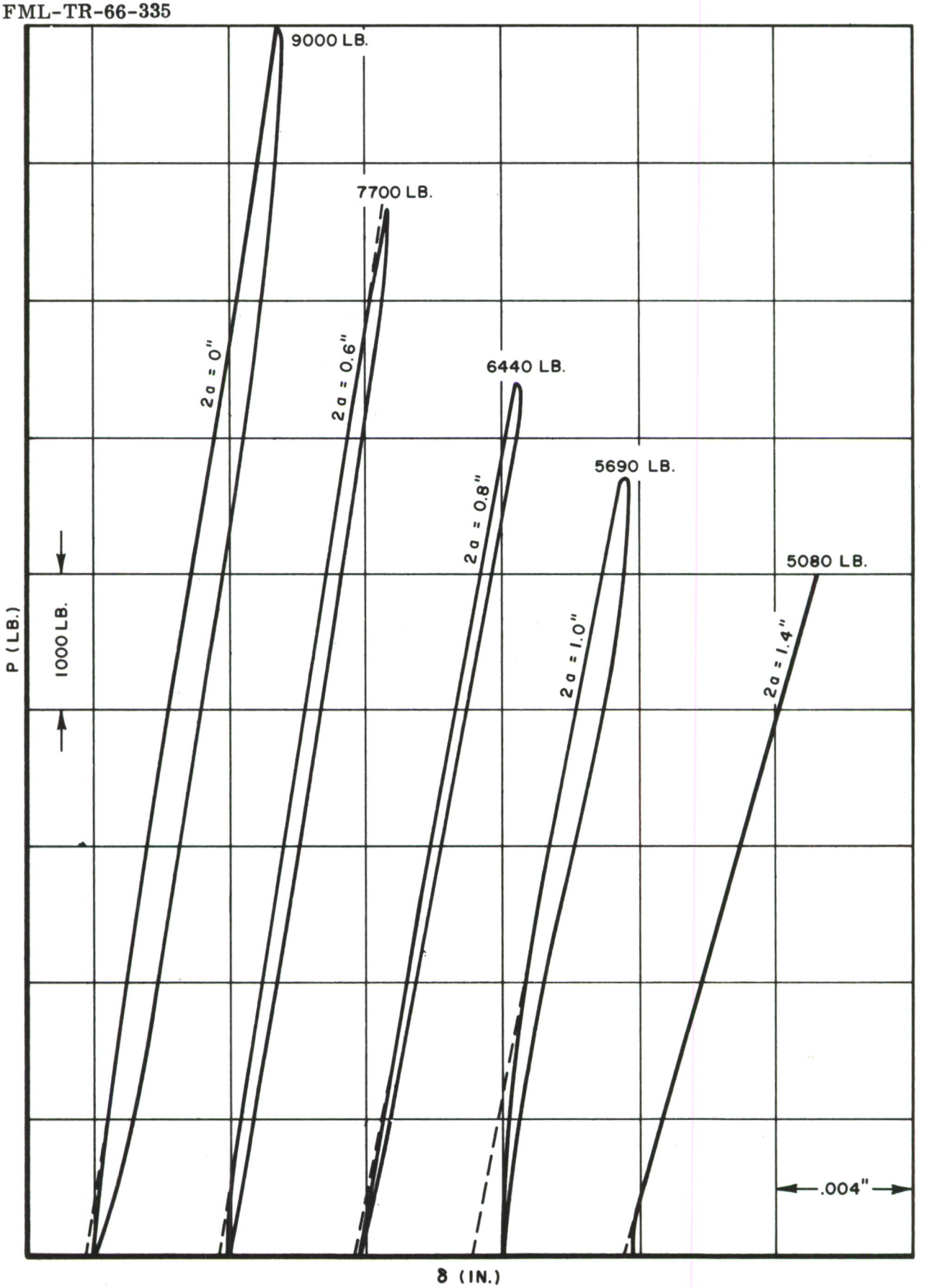


Figure 64. Load-Deflection Curves for Centrally Notched Specimens, 350°F, (Transverse)

C. LOAD-DEFLECTION CURVES OF RAW DATA FOR FRACTURED CENTRALLY NOTCHED SPECIMENS

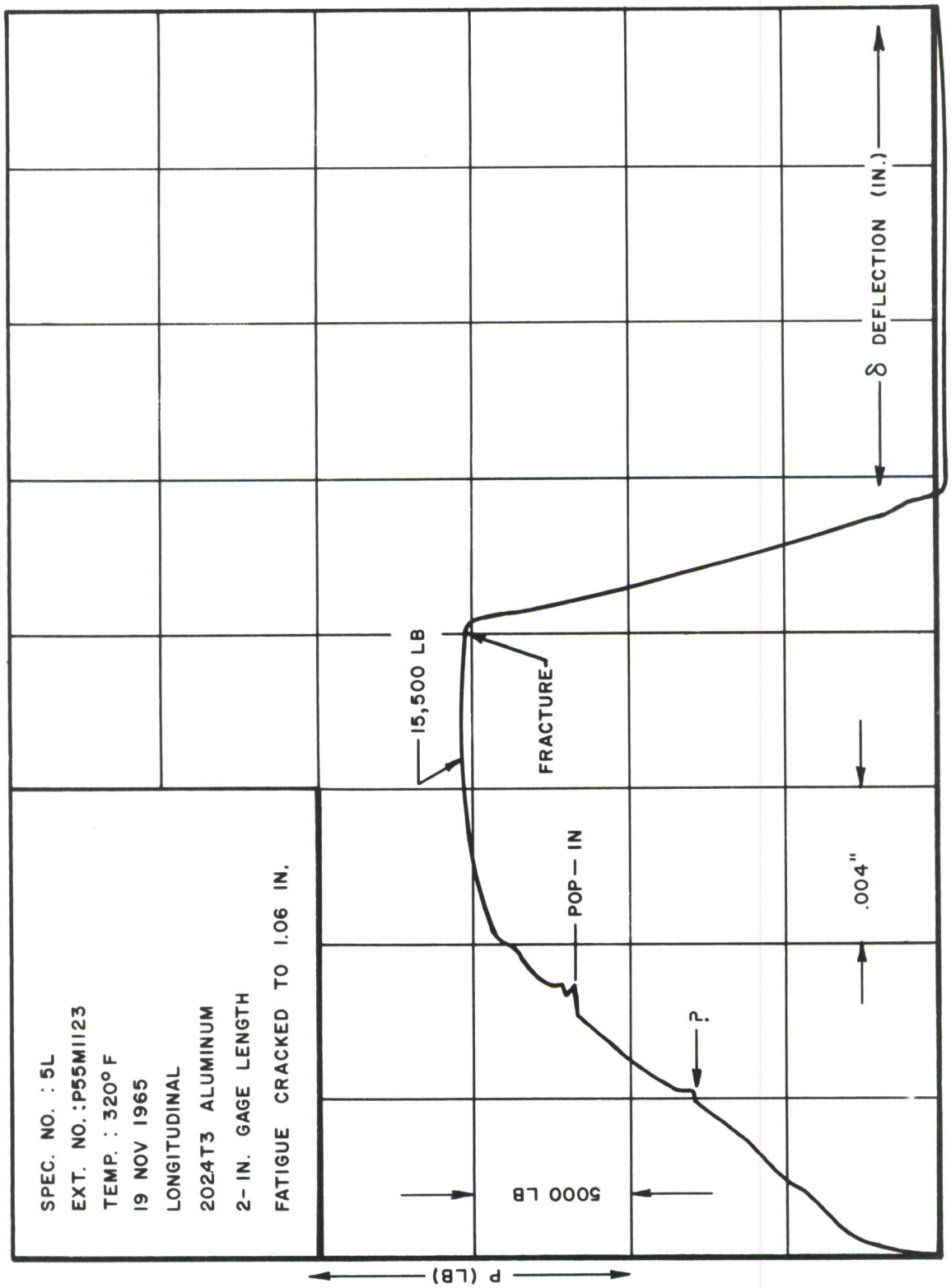


Figure 65. Original Load-Deflection Curve to Fracture, Longitudinal Centrally Notched Specimen at -320°F

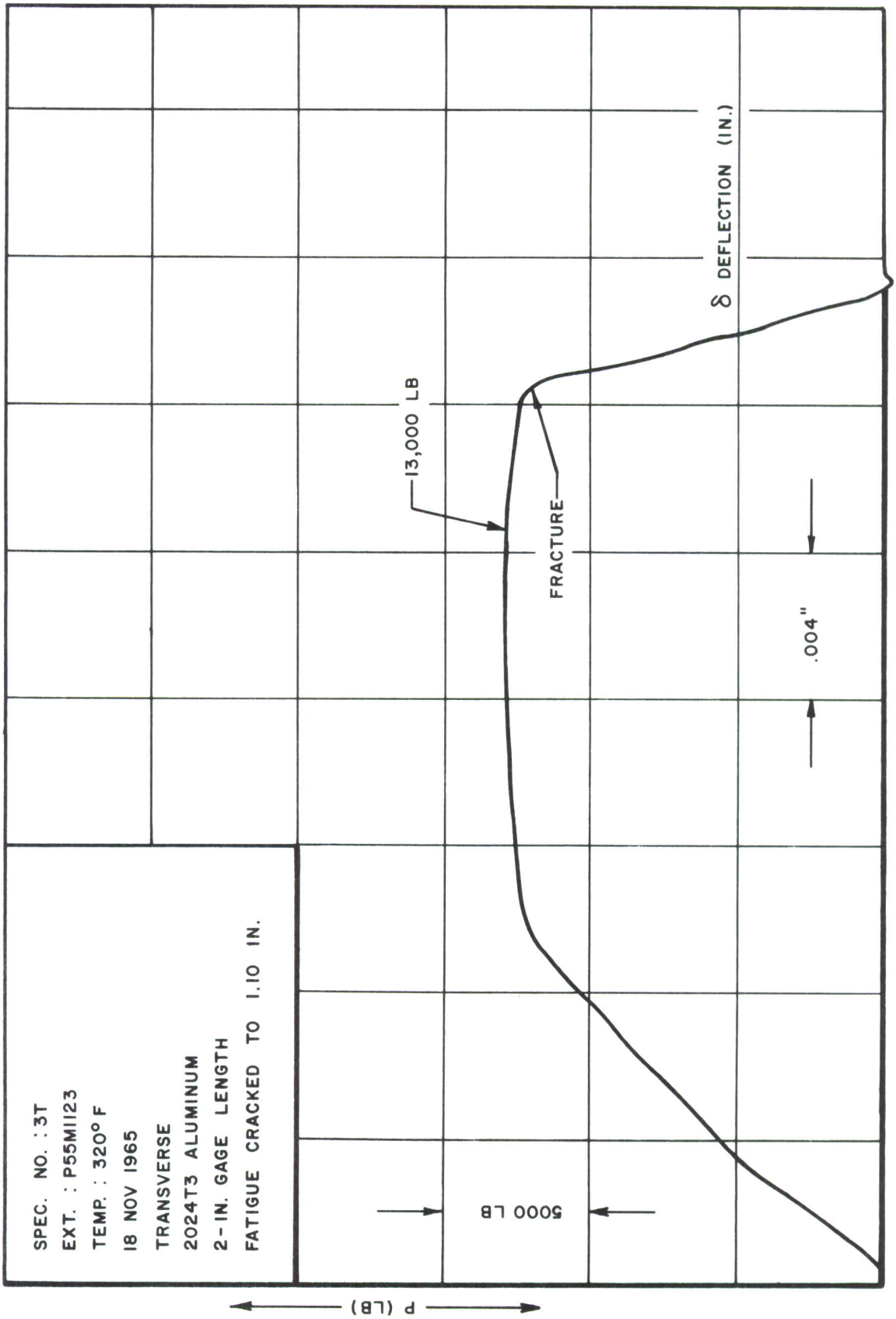


Figure 66. Original Load-Deflection Curve to Fracture, Transverse Centrally Notched Specimen at -320°F

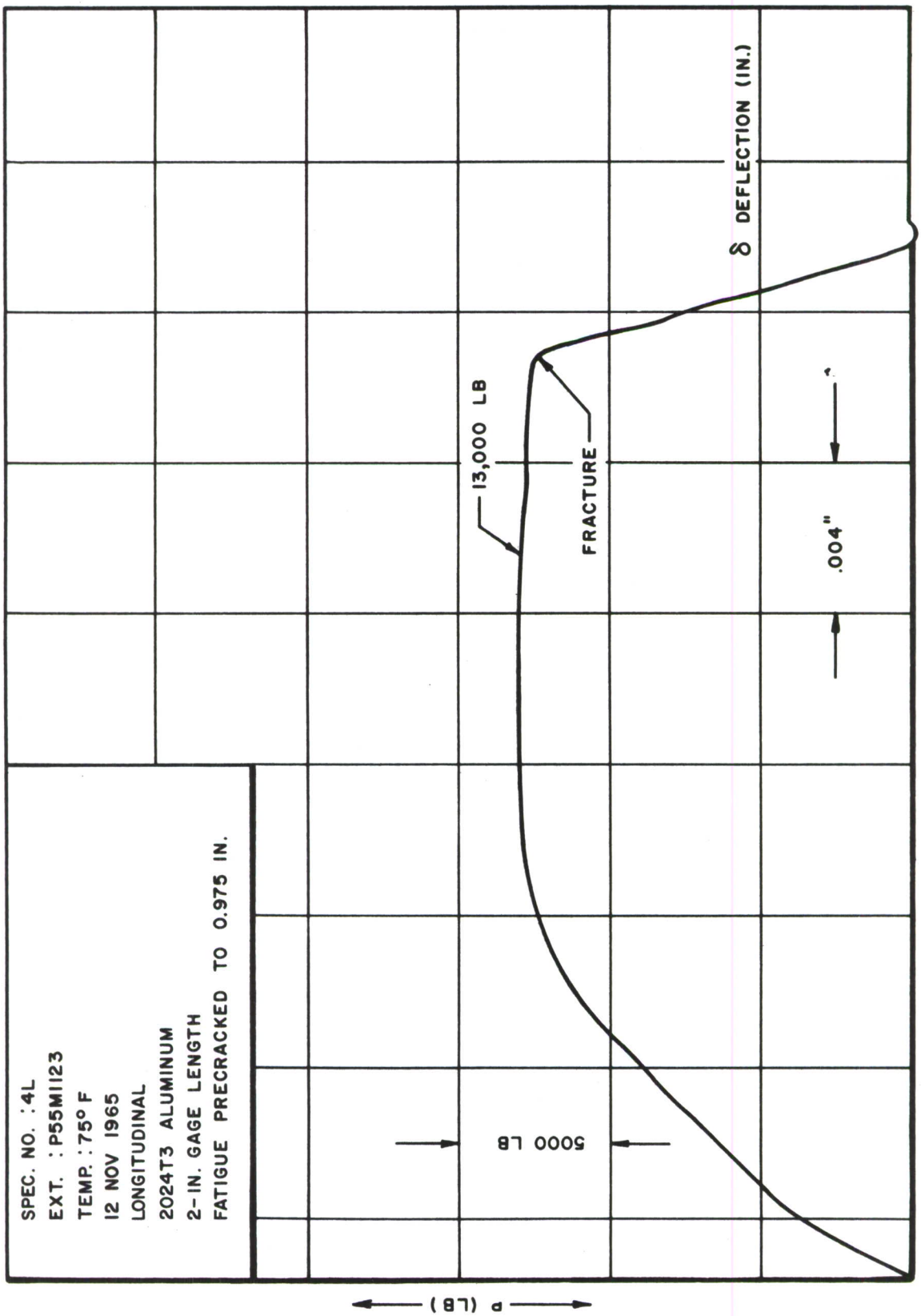


Figure 67. Original Load-Deflection Curve to Fracture, Longitudinal Centrally Notched Specimen at 75°F

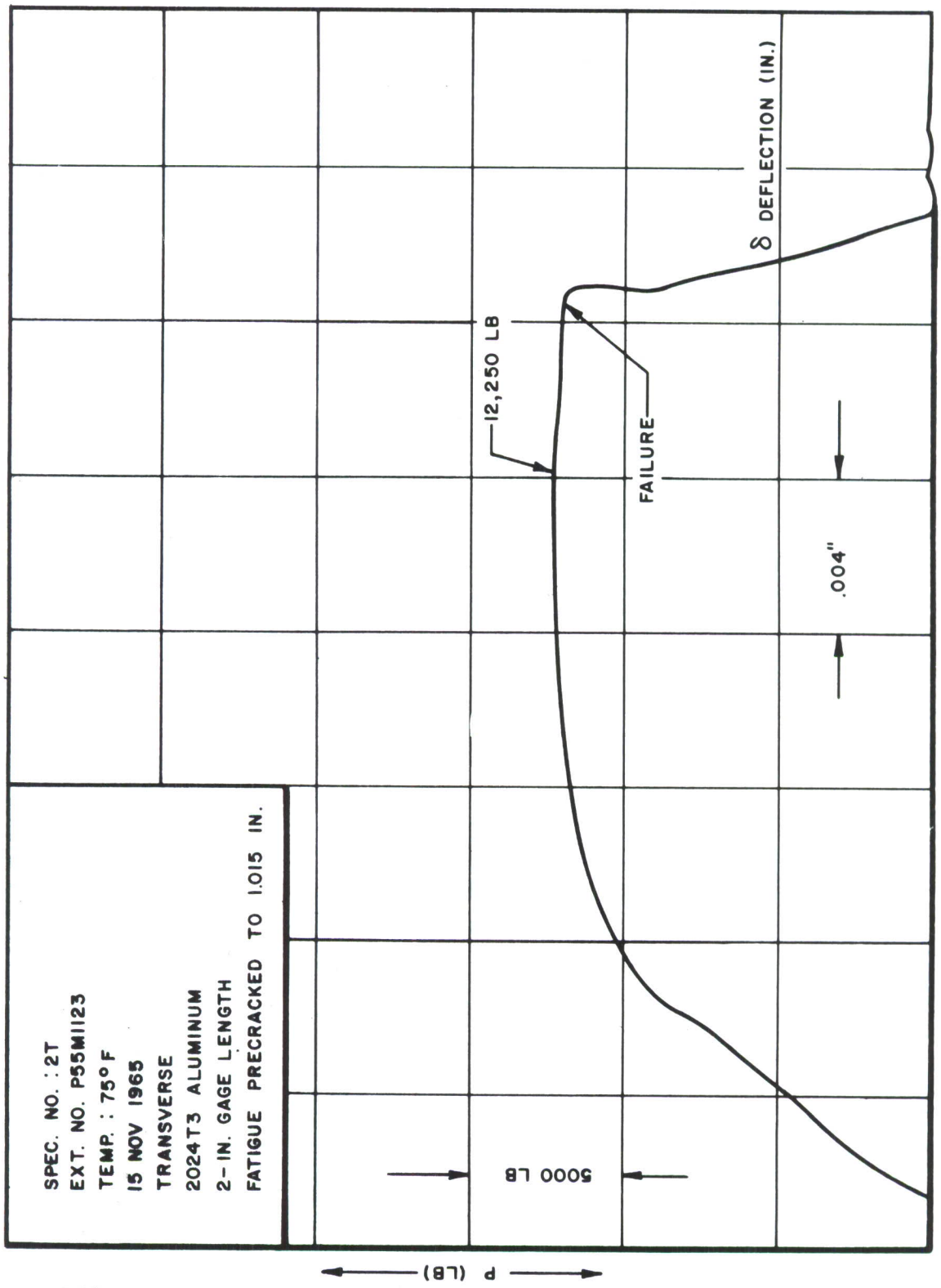


Figure 68. Original Load-Deflection Curve to Fracture, Transverse Centrally Notched Specimen at 75°F

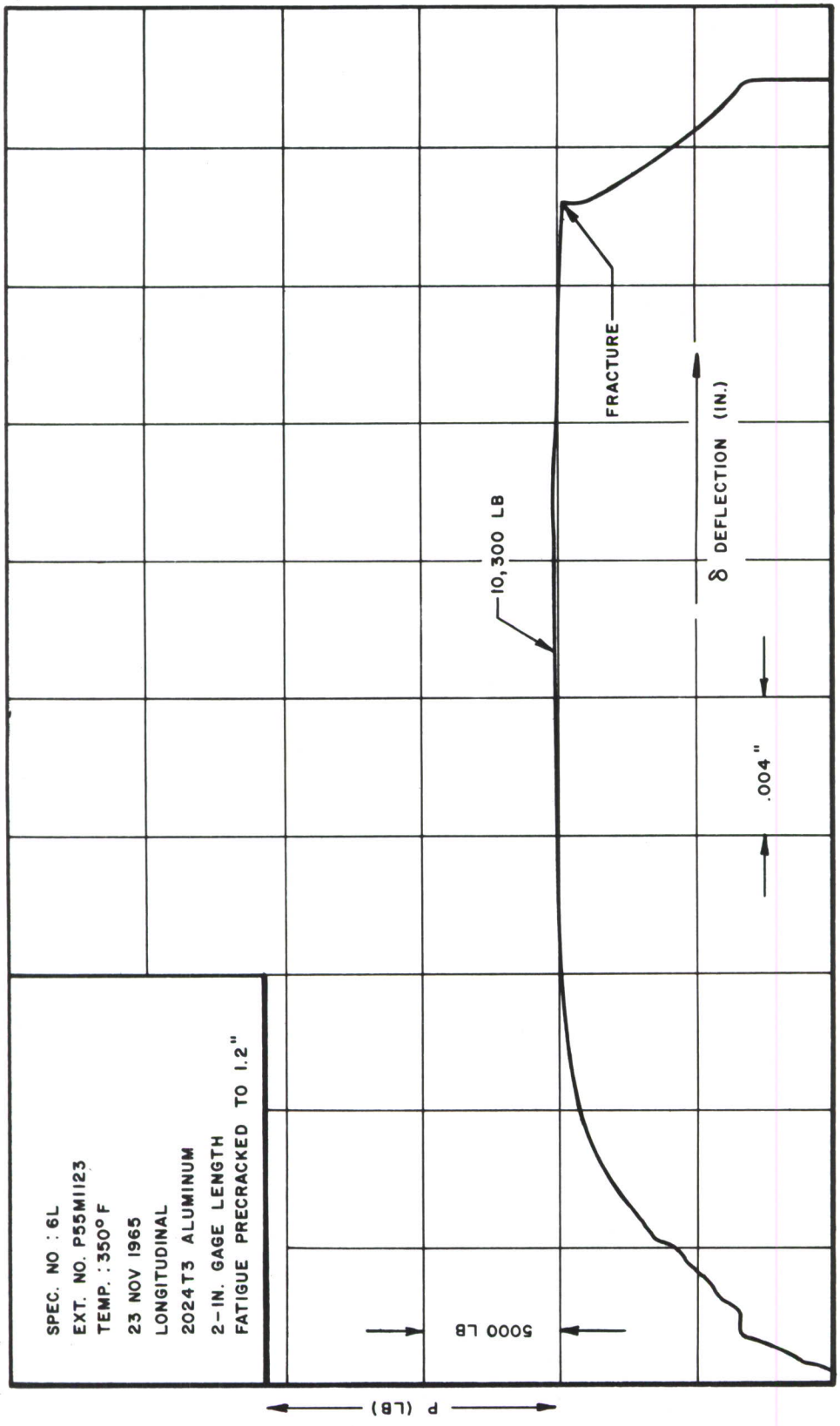


Figure 69. Original Load-Deflection Curve to Fracture, Longitudinal Centrally Notched Specimen at 350°F

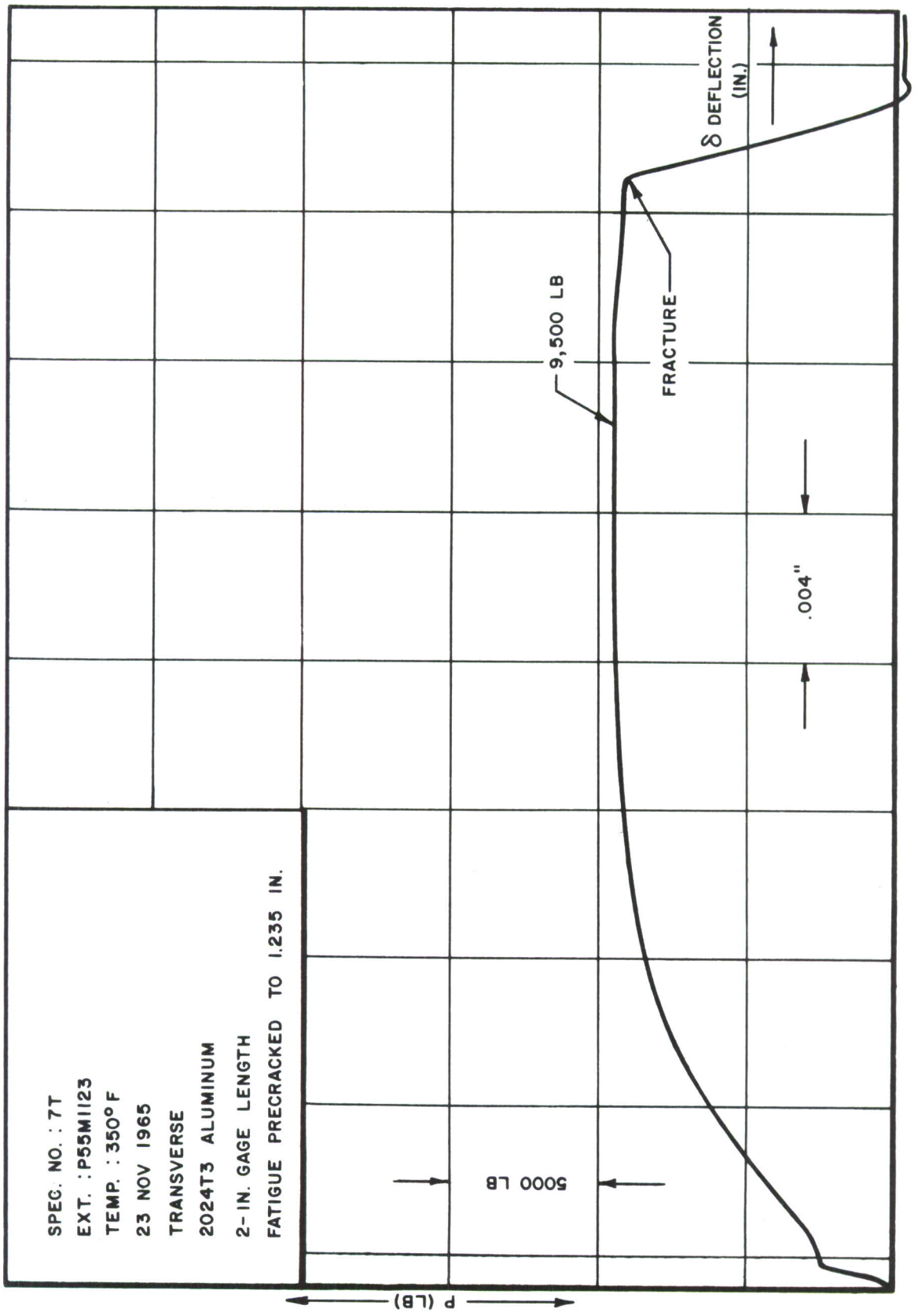


Figure 70. Original Load-Deflection Curve to Fracture, Transverse Centrally Notched Specimen at 350°F

UNCLASSIFIED

Security Classification

DOCUMENT CONTROL DATA - R&D

(Security classification of title, body of abstract and indexing annotation must be entered when the overall report is classified)

1. ORIGINATING ACTIVITY *(Corporate author)*
Air Force Materials Laboratory
Directorate of Laboratories
Wright-Patterson AFB, Ohio 45433

2a. REPORT SECURITY CLASSIFICATION
Unclassified

2b GROUP

3. REPORT TITLE
Development and Utilization of a Combination Cryogenic and Elevated Temperature Compliance Gage for Determination of Fracture Toughness of High Strength Metallic Materials

4. DESCRIPTIVE NOTES *(Type of report and inclusive dates)*
Technical Report - 21 June to 14 December 1965

5. AUTHOR(S) *(Last name, first name, initial)*
Davis, Sidney O.

6. REPORT DATE	7a. TOTAL NO. OF PAGES	7b. NO. OF REFS
July 1967	125	58

8a. CONTRACT OR GRANT NO.	9a. ORIGINATOR'S REPORT NUMBER(S)
b. PROJECT NO. 7381	AFML-TR-66-335
c. Task 738106	9b. OTHER REPORT NO(S) *(Any other numbers that may be assigned this report)*
d.	

10. AVAILABILITY/LIMITATION NOTICES
This document is subject to special export controls and each transmittal to foreign governments or foreign nationals may be made only with prior approval of MAAM, Air Force Materials Laboratory. In DDC.

11. SUPPLEMENTARY NOTES

12. SPONSORING MILITARY ACTIVITY
Air Force Materials Laboratory
Directorate of Laboratories
Wright-Patterson AFB, Ohio 45433

13. ABSTRACT

The Fracture Mechanics approach and its limitations are discussed based upon a literature survey. A workable compliance gage enabling the measurement of plane strain K_{IC} pop-in stress or load level and plane stress K_c failure load as a function of compliance (deflection) from -320° to 600°F in an air environment has been developed, designed, and constructed. The load-deflection readout instrumentation is compatible with commercially available X-Y recorders. The gage was calibrated at -320°, 75°, and 350°F in an air environment. This was performed and accomplished by comparing experimentally determined results on 2024-T3 aluminum alloy with the Westergaard-Irwin theoretically derived compliance parameters that reflect compliance at the edges of a centrally cracked sheet or plate specimen. The compliance gage was used to determine the fracture toughness of 2024-T3 aluminum alloy at -320°, 75°, and 350°F.

The experimentally obtained compliance results were in agreement with the Westergaard-Irwin theoretically derived hypothesis involving a mathematical model and general theory of elasticity (Reference 2). It was also established from experimental test data and fracture mechanics analytical concepts that 2024-T3 aluminum alloy data at 75° and 350°F (short time) use can be based on the evidences of gross plastic flow before failure. However, at -320°F and below the design criteria with this alloy should be based upon the fracture thoughness of the material and the severity of defects to avoid catastrophic failure under cryogenic service conditions.

(Over)

DD FORM 1 JAN 64 1473

UNCLASSIFIED

Security Classification

14. KEY WORDS	LINK A		LINK B		LINK C	
	ROLE	WT	ROLE	WT	ROLE	WT
Compliance Gage Plane Stress Plane Strain Fracture Toughness High Strength Alloys Irwin-Westergaard Compliance Theoretical Compliance Experimental Compliance Boyle's Experimental Compliance Pryogenic and Elevated Temperature Compliance						

INSTRUCTIONS

1. ORIGINATING ACTIVITY: Enter the name and address of the contractor, subcontractor, grantee, Department of Defense activity or other organization *(corporate author)* issuing the report.

2*a*. REPORT SECURITY CLASSIFICATION: Enter the overall security classification of the report. Indicate whether "Restricted Data" is included. Marking is to be in accordance with appropriate security regulations.

2*b*. GROUP: Automatic downgrading is specified in DoD Directive 5200.10 and Armed Forces Industrial Manual. Enter the group number. Also, when applicable, show that optional markings have been used for Group 3 and Group 4 as authorized.

3. REPORT TITLE: Enter the complete report title in all capital letters. Titles in all cases should be unclassified. If a meaningful title cannot be selected without classification, show title classification in all capitals in parenthesis immediately following the title.

4. DESCRIPTIVE NOTES: If appropriate, enter the type of report, e.g., interim, progress, summary, annual, or final. Give the inclusive dates when a specific reporting period is covered.

5. AUTHOR(S): Enter the name(s) of author(s) as shown on or in the report. Enter last name, first name, middle initial. If military, show rank and branch of service. The name of the principal author is an absolute minimum requirement.

6. REPORT DATE: Enter the date of the report as day, month, year; or month, year. If more than one date appears on the report, use date of publication.

7*a*. TOTAL NUMBER OF PAGES: The total page count should follow normal pagination procedures, i.e., enter the number of pages containing information.

7*b*. NUMBER OF REFERENCES: Enter the total number of references cited in the report.

8*a*. CONTRACT OR GRANT NUMBER: If appropriate, enter the applicable number of the contract or grant under which the report was written.

8*b*, 8*c*, & 8*d*. PROJECT NUMBER: Enter the appropriate military department identification, such as project number, subproject number, system numbers, task number, etc.

9*a*. ORIGINATOR'S REPORT NUMBER(S): Enter the official report number by which the document will be identified and controlled by the originating activity. This number must be unique to this report.

9*b*. OTHER REPORT NUMBER(S): If the report has been assigned any other report numbers *(either by the originator or by the sponsor)*, also enter this number(s).

10. AVAILABILITY/LIMITATION NOTICES: Enter any limitations on further dissemination of the report, other than those imposed by security classification, using standard statements such as:

(1) "Qualified requesters may obtain copies of this report from DDC."

(2) "Foreign announcement and dissemination of this report by DDC is not authorized."

(3) "U. S. Government agencies may obtain copies of this report directly from DDC. Other qualified DDC users shall request through

_____."

(4) "U. S. military agencies may obtain copies of this report directly from DDC. Other qualified users shall request through

_____."

(5) "All distribution of this report is controlled. Qualified DDC users shall request through

_____."

If the report has been furnished to the Office of Technical Services, Department of Commerce, for sale to the public, indicate this fact and enter the price, if known.

11. SUPPLEMENTARY NOTES: Use for additional explanatory notes.

12. SPONSORING MILITARY ACTIVITY: Enter the name of the departmental project office or laboratory sponsoring *(paying for)* the research and development. Include address.

13. ABSTRACT: Enter an abstract giving a brief and factual summary of the document indicative of the report, even though it may also appear elsewhere in the body of the technical report. If additional space is required, a continuation sheet shall be attached.

It is highly desirable that the abstract of classified reports be unclassified. Each paragraph of the abstract shall end with an indication of the military security classification of the information in the paragraph, represented as *(TS), (S), (C), or (U)*.

There is no limitation on the length of the abstract. However, the suggested length is from 150 to 225 words.

14. KEY WORDS: Key words are technically meaningful terms or short phrases that characterize a report and may be used as index entries for cataloging the report. Key words must be selected so that no security classification is required. Identifiers, such as equipment model designation, trade name, military project code name, geographic location, may be used as key words but will be followed by an indication of technical context. The assignment of links, rules, and weights is optional.